Novel roles for peroxisome-linked genes in *Drosophila*

by

Conrad Pridie

A thesis submitted in partial fulfillment of the requirements for the degree of

Doctor of Philosophy

Department of Cell Biology
University of Alberta

Abstract

Peroxisomes are organelles responsible for processing lipids and managing reactive oxygen species. A conserved family of genes called peroxisome biogenesis factors (*Peroxin, Pex*) encode proteins necessary for peroxisome biogenesis and function. In yeast and mammals, PEROXIN7 (PEX7) acts as a cytosolic receptor protein that targets proteins containing a peroxisome targeting sequence 2 (PTS2) motif for peroxisome matrix import. The PTS2 motif is not present in the *Drosophila melanogaster* homologs of proteins that are trafficked by PEX7 in yeast or mammals. The fly genome does contain a *Pex7* gene (CG6486) that is very similar to yeast and human *PEX7*. My work (Chapter 3) showed that *Pex7* was expressed in tissue-specific patterns analogous to neurons in *Drosophila* embryos. I correlated this with a requirement for *Pex7* in that cell lineage, as targeted somatic *Pex7* knockout in embryonic neurons reduced survival. *Pex7* over-expression in neurons caused lethality during the larval stage. Targeted somatic over-expression of a *Pex7* transgene in neurons of *Pex7* homozygous mutants resulted in a semi-lethal phenotype similar to targeted *Pex7* knockout. These observations suggested tissue-specific requirements for *Pex7* during *Drosophila* development.

Prior studies of the interactions between peroxisomes and microtubules uncovered a role for genes outside the *Peroxin* gene family in the regulation of peroxisome import competence, morphology and abundance. A genome-wide RNA interference (RNAi) screen identified seventeen such genes that qualitatively altered the peroxisome marker GFP-PTS1 in Schneider 2 cells. My work (Chapter 4) showed that transient knockdown of eight of these genes resulted in altered peroxisome abundance. Transient over-expression of eleven of these genes also resulted in altered peroxisome abundance. Of thirteen total genes with a demonstrated effect, eight have canonical roles in mitosis and two are involved in the regulation of non-muscle myosin motors. The effects of three genes encoding parts of the chromosome passenger complex - *aurB*, *borr* and *Incenp* - suggest cytokinesis and abscission function as cues for peroxisome proliferation. My studies showed that while peroxisomes are largely conserved in *Drosophila*, and that flies represent an effective model for identifying new aspects of peroxisome biogenesis, there are also substantial differences in *Drosophila Peroxin* function compared to other models.

Preface

Material presented in Chapters One, Two, Three and Five was published previously as:

Pridie C, Simmonds AJ. 2020. The role of *Peroxin 7* during *Drosophila* embryonic development. Genome. 19 March 2020. https://doi.org/10.1139/gen-2019-0207.

Pridie C, Ueda K, Simmonds AJ. 2020. Rosy beginnings: studying peroxisomes in *Drosophila*. Front Cell Dev Biol. 25 August 2020. https://doi.org/10.3389/fcell.2020.00835.

The initial screens supporting the experiments presented in Chapter 4 were performed by Dr. Adam Magico (unpublished data), Dr. Joanne Lacey (Lacey, 2015) and Dr. Peter Drake (Drake, 2012).

Logic is the beginning of wisdom, not the end.

Acknowledgements

I am grateful to my supervisor Andrew Simmonds, PhD, for taking a chance on me.

Thanks to my graduate committee, John Locke, PhD and Paul LaPointe, PhD, for frank and meaningful discourse.

Thanks to my arm's-length examiner Qiumin Tan, PhD and my external examiner Elizabeth Rideout, PhD, for their timely assistance and flexibility.

Special thanks to Simmonds lab members Julie Haskins, Matt Anderson-Baron, PhD, and Virginia Pimmett, PhD, for sharing the good and bad times.

Very special thanks to:
Pliny Harold Hayes, PhD, for kindling my interest in the study of genetics.
John Parrish, PhD, for his irreverent perspectives on the institute of academia.
Adam Magico, PhD, for the cell screen that inspired me.

Hi Mum!

Table of Contents

List of Tables

List of Figures

List of Abbreviations

AAA: ATPases Associated with diverse cellular Activities

AEL: after egg laying

ALD: adrenoleukodystrophy

AMACR: α-methylacyl-CoA racemase

ACOX2: Acyl-CoA oxidase 2

ACSL4: Acyl-CoA Synthetase Long Chain Family Member 4

AGPS: Alkylglycerone phosphate synthase

AOx: Acyl-CoA oxidase

ATPase: adenosinetriphosphatase

BAAT: Bile acid-CoA:amino acid *N*-acyltransferase

CAAX: C-terminal Cysteine-Aliphatic-Aliphatic-Any residue protein motif

CerPE: phosphoethanolamine ceramide

CHO: Chinese hamster ovary, a mammalian cell line

CM: cardiomyocyte

CNS: central nervous system

CoA: Coenzyme A

DAB: 3,3'-diaminobenzidine

DBP: D-bifunctional protein

DGRC: Drosophila Genomics Resource Centre

DHAP: dihydroxyacetone phosphate

DHAP reductase: *see* GPD1

DMOG: Dimethyloxaloylglycine

DNASU: non-profit plasmid repository led by Arizona State University

DP: docking protein

DSHB: Developmental Studies Hybridoma Bank

dsRNA: double-stranded RNA

ECM: extra-cellular matrix

EMS: ethyl methanesulfonate

EPAS1: Endothelial PAS domain protein 1

ER: endoplasmic reticulum

ER-PPV: endoplasmic reticulum-derived pre-peroxisomal vesicle

FAO: fatty acid oxidation

FACL4: Fatty acid-CoA ligase 4

FAR1/2: Fatty acyl-CoA reductase 1/2

FAS: Fatty acid synthase

FFA: free fatty acid

FRET: fluorescence resonance energy transfer

Gal4: a positive regulation transcription factor native to *S. cerevisiae*

Gal4-UAS: two-part transgenic construct activation system

gDNA: genomic DNA

GNPAT: Glyceronephosphate O-acyltransferase

GPD1: Glycerol-3-phosphate dehydrogenase 1

GR: Glutathione reductase

HD: bifunctional enoyl-CoA hydratase-β-hydroxy acyl-CoA dehydrogenase

HETE: hydroxyeicosatetraenoic acid ($C_{20}H_{32}O_3$)

IP: Immunoprecipitation

IRD: infantile Refsum disease

ISH: *in situ* hybridization

LCFA: long-chain fatty acid

LSFM: light sheet fluorescent microscopy

MAPK: mitogen-activated protein kinase

MARCM: mosaic analysis with a repressible cell marker

MCFA: medium-chain fatty acid

Mtpα: Mitochondrial trifunctional protein α subunit

MZT: Maternal-zygotic transition (of gene expression)

NALD: neonatal adrenoleukodystrophy

NO: nitric oxide

OE: over-expression (of a protein or other gene product, usu. by transgenic construct)

P4HA1: Prolyl 4-hydroxylase, subunit α-1

PBD: peroxisome biogenesis disorder

PC: pericardial cell

PIM: Percent identity matrix

PMP: peroxisome membrane protein

PNS: peripheral nervous system

PPAR: peroxisome proliferator-activated receptor

PTS1: peroxisome targeting signal 1

PTS2: peroxisome targeting signal 2

RCDP: rhizomelic chondrodysplasia punctata

RhoGEF: Rho guanine nucleotide exchange factor

RING: Really Interesting New Gene; contains C_3HC_4 zinc finger domain

RNAi: RNA interference

RNS: reactive nitrogen species

ROS: reactive oxygen species

SCPx: Sterol carrier protein X, a class of Thiolase

SH3: SRC Homology 3 domain

SOD: Superoxide dismutase

TAG: triacylglycerol

THCA-CoA: 3α,7α,12α-trihydroxycholestanoic acid-Coenzyme A

TSA: tyramide signal amplification

UAS: upstream activating sequence for Gal4 transcription factor

VLCFA: very long-chain fatty acid

WD40: forty-reside domain ending in tryptophan-aspartic acid (WD), usually found in tandem

X-ALD: X-linked adrenoleukodystrophy

XDH: Xanthine dehydrogenase; encoded by *rosy* in *Drosophila*

ZSD: Zellweger spectrum disorder

Gene and Protein Nomenclature

Throughout the text, gene names are *italicized*, e.g. *Pex7* or *nmd*, unless that gene has no proper name in which case its placeholder is written in regular text, e.g. CG7627. Proteins are written in regular text, e.g. Pex7 or AGPS. *Drosophila* genes are written in italics per their accepted shorthand, e.g. *cat*, and *Drosophila* proteins are written in regular text using their accepted shorthand with the first letter capitalized, e.g. Cat. Human genes and proteins are written in capital letters, e.g. *PEX7* and ACSL4, respectively. Specific mutant alleles are written with their lesion, e.g. $Pex7^{MiMIC}$. A non-specific mutant allele is written per the gene convention outlined here, e.g. *nmd* or *DNM1L*. All mutant alleles have a nearby description of their effect such as "loss of function" or "null mutant". Genes and proteins from other species use their proper names and otherwise follow the *Drosophila* nomenclature conventions outlined here.

Chapter 1 Introduction

1.1. Peroxisomes

The cell is the smallest indivisible unit of life as we know it, with the possible exception of viruses which are not discussed further herein. The present form of the "tree of life" taxonomy model permits classification of cells into two categories: prokaryotes, comprised of the domains *Bacteria* and *Archaea*, and eukaryotes, comprised exclusively of the domain *Eukaryota* (Mindell, 2013). Prokaryotes (from Greek *pro*, 'before' and *karyon*, 'kernel') are unicellular micro-organisms that do not contain membranous internal compartments. Eukaryotes (from Greek *eu*, 'true' and *karyon*, 'kernel') may be unicellular or multicellular, and are defined by the presence of a membrane-bound nucleus and other specialized internal compartments collectively termed organelles. Some of the functions of a given organelle may vary by species, though each has a characteristic core function. For example, the nucleus is where chromosomes are stored, mitochondria are where macromolecules are oxidized to produce the proton motive force necessary for ATP production, and the endoplasmic reticulum (ER) is where many proteins are synthesized. Several smaller organelles, of various composition and function, were collectively termed microsomes by early research that first observed them in certain fractions of centrifuged rat liver homogenates (Palade and Siekevitz, 1956). One type of microsome, a single membrane-bound organelle with a specific enzymatic complement and consistent localization to non-mitochondrial fractions, is the peroxisome.

1.1.1 Discovery and classical characterization of the peroxisome

a. Ultrastructure

In 1954, Johannes Rhodin published electron micrographs detailing the ultrastructural organization of mouse kidney tubule cells. Rhodin identified novel organelles he termed "microbodies", round or ovoid structures bounded by a single membrane layer. They had ubiquitous distribution, a mean length of 0.3 μm and a mean width of 0.1 μm (Rhodin, 1954). Their apparent granularity, and by inference relative density, was similar to that of mitochondria. Rhodin's observations became the visual "gold standard" for qualitative microbody identification, and were used to find similar structures in tissue homogenates of other mammals. Rouiller and Bernhard (1956) observed the microbodies of rat liver cells were generally found

near the mitochondria and the ER. They proposed there may be a relationship between these presumptive organelles, citing similar observations for secretory vesicles. Later, Hruban and Swift (1964) observed structures within the microbodies of rat liver cells that matched the shape of crystallized urate oxidase (uricase) purified commercially from pig liver. This observation suggested microbodies were sites of enzymatic activity.

b. Specific enzymatic activity

Classical characterization of sub-cellular organelles involved differential centrifugation, correlating specific enzymatic activity to fractions isolated from various tissues. This was later coupled with electron microscopy of fraction samples to correlate enzymatic activity with cellular structures or organelles. Early studies of glucose-6-phosphatase in rat liver found acid phosphatase activity in both the mitochondrial fraction and an ER sub-fraction full of cytoplasmic granules termed "microsomes" (Berthet and de Duve, 1951). These granules were considered different from microbodies although they were both found in the same fractions. Rat and mouse liver fractions containing large, dense microsomes correlated with enriched specific activity of acid phosphatase and uricase (Novikoff *et al.*, 1952; Kuff and Schneider, 1954). Refinement of the differential sedimentation technique resolved these granules into particles of differing diameters (Thomson and Moss, 1955) suggesting microsomes were a heterogeneous population of vesicular organelles with specialized enzymatic functions. Acid phosphatase and other acid hydrolase enzymes co-localized to microsomes subsequently dubbed "lysosomes" (de Duve *et al*., 1960). The specific activities of two other enzymes, catalase and D-amino acid oxidase, were found to be enriched in non-lysosomal microsomes (de Duve *et al*., 1960). Both enzymes involved hydrogen peroxide, either as product or substrate, prompting speculation that non-lysosomal microsomes were the site of peroxide metabolism. Thus, their function was proposed to be protection of the cell from reactive oxygen species (de Duve *et al*., 1960).

Characterization of the intracellular enzyme distribution in mammalian tissues and single-cell eukaryotes revealed catalase was present in all microbodies, though urate oxidase was specific to the liver in rats (Baudhuin *et al.*, 1965a; Baudhuin *et al*., 1965b). This suggested microbody enzyme complement was both tissue- and species-specific. It also identified catalase as a non-lysosomal marker enzyme for both microsomes and microbodies, and strongly

suggested these two terms described the same organelle. de Duve made this assumption and proposed a name for the organelle at the fifth meeting of the American Society of Cell Biologists, coining the term “peroxisome”:

> *Peroxisomes contain 1) oxidases that reduce oxygen to hydrogen peroxide at the expense of the oxidation of a substrate RH_2 and 2) large amounts of catalase, an enzyme able to reduce hydrogen peroxide to water by two distinct mechanisms: a) the peroxidatic mechanism requiring an electron donor $R'H_2$; b) the catalytic mechanism in which a second molecule of hydrogen peroxide serves as electron donor. The peroxisome enzymes are therefore linked functionally…* (Baudhuin and de Duve, 1966).

c. Interspecies conservation

de Duve’s definition was initially rejected by those working on plant cell biology. In plants, the glyoxylate cycle converts lipids into sucrose during germination and is the functional equivalent of the citric acid cycle. Biochemical analysis of the compartmentalization of glyoxylate cycle enzymes, such as malate synthase and isocitrate lyase, determined some of them co-sedimented with high-density particulate other than mitochondria. This particulate was considered a microsome related to peroxisomes dubbed “glyoxysomes” (Breidenbach and Beevers, 1967). Interestingly, these enzymes were also found in catalase-positive organelles in the ciliate protozoan *T. pyriformis* (Müller and Hogg, 1967). Improved purification techniques revealed the same enzymes were found in rat liver peroxisomes (Leighton *et al*., 1968). Spinach leaf microbodies were enzymatically consistent with peroxisomes and contained glycolate oxidase, suggesting leaf microbodies were more “peroxisome-like” to handle the reactive by-products of photorespiration (Tolbert *et al*., 1968). Peroxisomes were later found in the leaves of non-photorespiring plants, albeit in lower abundance, ultimately disproving the glyoxysome hypothesis (Tolbert *et al*., 1969).

Catalase-positive particles were discovered in the epithelial cells of small intestine from guinea pigs fed the non-ionic detergent WR-1339, a peroxisome proliferation agent (Connock and Pover, 1970). A similar approach led to the discovery of large numbers of small, catalase-positive microbodies throughout the intestinal tract of guinea pigs and rats (Novikoff and

Novikoff, 1972). The innovation of peroxisome staining via detection of catalase activity with 3,3'-diaminobenzidine (DAB) permitted resolution of peroxisome adjacency to smooth ER, with a generally supra-nuclear localization and ubiquitous cytosolic presence (Novikoff and Novikoff, 1972). The differing size, clustering and staining reactivity of intestinal peroxisomes supported the hypothesis that animal peroxisomes had tissue-specific functions (Novikoff and Novikoff, 1972). A similar cytochemical staining approach found a large single peroxisome in filamentous algae (Stewart *et al*., 1972), demonstrating conservation of peroxisome function, if not morphology, in aquatic eukaryotes. In summary, a combination of classical techniques determined peroxisomes were a ubiquitous, single membrane-bound organelle containing tissue-specific enzymes related to a core function of non-energetic peroxide metabolism.

1.1.2 Organelle functions

a. Metabolism of reactive oxygen and nitrogen species

Baudhuin *et al.* (1965a) postulated that "microbodies carry out non-phosphorylative (non-energetic) oxidations". These hypotheses formed the central argument for de Duve's definition of the peroxisome as the site of non-energetic hydrogen peroxide production and disposal (Baudhuin and de Duve, 1966). A current hypothesis proposes low levels of reactive oxygen species (ROS), such as hydrogen peroxide, and reactive nitrogen species (RNS) are signaling molecules for an array of cellular processes including proliferation, gene expression, differentiation, immunity, senescence, autophagy and apoptosis (reviewed by Fransen *et al*., 2011). This suggests the production, management and disposal of ROS/RNS are essential functions. The principal ROS/RNS produced endogenously are superoxide radicals, hydrogen peroxide and nitric oxide (Nathan and Ding, 2010). Many cellular processes contribute to accidental or deliberate ROS/RNS production including oxidative phosphorylation, protein folding, steroidogenesis, amino acid metabolism and lipid metabolism. The organelles with the highest ROS/RNS production are the ER, mitochondria and peroxisomes (Li X *et al*., 2013; Santos *et al*., 2009; Hanukoglu *et al*., 1993; reviewed by Fransen *et al*., 2011). Although short-lived, ROS/RNS are highly reactive and will interact with nearby molecules or macromolecules, including themselves; the latter results in production of other ROS/RNS like hydroxyl radicals and peroxynitrite (Powers and Jackson, 2008). Acute exposure to ROS/RNS results in oxidative

damage to cellular macromolecules and negatively impacts the cellular redox state. These effects are collectively termed oxidative stress (reviewed by Fransen *et al*., 2011).

Several enzymes that both produce and mitigate various endogenous ROS/RNS are found in peroxisomes. Human peroxisomal enzymes that create ROS/RNS include: lipid oxidases (acyl-CoA oxidase 1-3, L-pipecolic acid oxidase, L-α-hydroxyacid oxidase 1/2) and amino acid oxidases (D-amino acid oxidase, D-aspartate oxidase, polyamine oxidase), all of which produce hydrogen peroxide; xanthine oxidase, which produces hydrogen peroxide, superoxide and nitric oxide; and nitric oxide synthase, which produces superoxide and nitric oxide (reviewed by Fransen *et al*., 2011). Peroxisomal anti-oxidant enzyme content is complementary: catalase, which targets hydrogen peroxide; superoxide dismutase 1; peroxiredoxin 5, which targets peroxynitrite and hydrogen peroxide; and epoxide hydrolase 2, which targets epoxides derived from fatty acids (Summerer *et al*., 2002; reviewed by Fransen *et al*., 2011). A meta-analysis strongly suggested the localization of ROS/RNS metabolism was peroxisomal across *Eukaryota*, provided the organelle is conserved, validating de Duve's hypothesis (reviewed by Gabaldón, 2010).

b. β-oxidation of long-chain fatty acids

The core function of peroxisomes, ROS/RNS metabolism, is clearly tied by complementary enzyme activity to another of its core functions, fatty acid oxidation (FAO). Early work on the conversion of stored lipids into sucrose during castor seed germination, a form of gluconeogenesis, determined the enzymes involved, including malate synthase and isocitrate lyase, were located in a homogenate fraction that correlated with peroxisomes (Breidenbach and Beevers, 1967). Gluconeogenesis via FAO begins with the generation of free fatty acids (FFAs) from storage lipids like triacylglycerols (TAGs). FFAs are transported to the mitochondria and oxidized at their β-carbon by trifunctional enzyme to produce acetyl coenzyme A (acetyl-CoA), which then enters either the citric acid or glyoxylate cycles (reviewed by Houten and Wanders, 2010). The discovery of glyoxylate cycle β-oxidation enzymes in peroxisomes challenged the established dogma that mitochondria were solely responsible for lipid oxidation. Again using castor beans, Hutton and Stumpf (1968) reported the highest specific β-oxidation activity occurred in the fraction of homogenates that correlated with peroxisome density and enriched

specific activity of catalase found in particles, or "particulate catalase". This fraction contained all the component enzymes of the β-oxidation pathway (Hutton and Stumpf, 1968). Cytoplasmic granules morphologically resembling microbodies were found in *S. cerevisiae* that had catalase activity and were significantly reduced in respiration-deficient mutants (Avers and Federman, 1968). The enzymatic complement of rat liver peroxisomes was expanded to include several oxidases, particulate catalase and an isomer of isocitrate dehydrogenase, but not all the FAO enzymes found in castor bean peroxisomes (Leighton *et al*., 1969). The role of peroxisomes in gluconeogenesis was resolved using the ciliate protozoan *T. pyriformis*, which uses both the citric acid and glyoxylate cycles. Several integral glyoxylate cycle enzymes and cognates of mammalian oxidases co-sedimented with particulate catalase, strongly suggesting the non-energetic β-oxidation of lipids was a conserved peroxisome function (Müller *et al*., 1968).

The mammalian peroxisome-FAO connection was confirmed by the discovery of an aerobic acyl-CoA oxidizing system in purified peroxisomes isolated from livers of rats fed clofibrate, a drug prescribed to lower serum lipid levels. The long-chain fatty acid (LCFA) derivative palmitoyl-CoA was found to reduce NAD when incubated with purified rat liver peroxisomes in a CoA-dependent manner. The activity was significantly increased in the presence of air and clofibrate treatment (Lazarow and de Duve, 1976). Rat liver peroxisomes were later found to contain all the enzymes required to convert palmitoyl-CoA to acetyl-CoA via β-oxidation (Lazarow, 1978). However, free fatty acid (FFA) side chain length affected pathway efficiency, suggesting peroxisomes oxidized LCFAs while other fatty acids were metabolized by mitochondria (Lazarow, 1978). Differential centrifugation of rat liver found the very long-chain fatty acid (VLCFA) lignoceric acid in fractions enriched for catalase and urate oxidase. The same fractions had the highest rate of KCN-resistant acetate formation, an acetyl-CoA marker, from radio-labeled lignoceric acid without evolving CO_2, indicating peroxisomes were oxidizing VLFCAs independent of energy production (Singh *et al*., 1984).

The cellular source of peroxisomal constituents was determined using clofibrate treatment to induce excess production of β-oxidation enzymes. Cell-free reticulocyte lysate extracted from rat liver was used to translate RNA *in vitro* from free or bound polysomes. Peroxisomal β-oxidation enzymes acyl-CoA oxidase (AOx) and bifunctional enoyl-CoA hydratase-β-hydroxy

acyl-CoA dehydrogenase (HD) were found in the translation products of the free polysome fraction (Rachubinski *et al*., 1984). Thus, peroxisomal enzymes originated in the cytosol and required import into the peroxisomal matrix. Finally, fibroblasts from patients with Zellweger spectrum disorder, which did not have detectable peroxisomes, were unable to metabolize radiolabeled derivatives of the VLFCA arachidonic acid (Gordon *et al*., 1990). As with ROS/RNS metabolism, a meta-analysis determined non-energetic β-oxidation of (V)LCFAs was conserved across eukaryotes that also conserved peroxisomes (reviewed by Gabaldón, 2010).

c. Synthesis of bile acids and ether lipids

The production of bile acids and ether lipids involves multi-organelle processes and is tied to the β-oxidation of fatty acids, as their precursors are generated by the oxidation of FFAs (reviewed by Chiang, 2009; Dean and Lodhi, 2017). Bile acid and ether lipid synthesis are therefore tied directly to the other two core peroxisome functions. Bile acids, derived from cholesterol, are essential for the intestinal uptake of dietary fatty acids and vitamins, regulate metabolism of glucose and lipids, and act as signaling molecules for several cellular processes (reviewed by Chiang, 2009). Bile acids are produced exclusively in the liver or equivalent organ. Their synthesis begins in the mitochondria and peroxisomes and concludes in the ER (reviewed by Chiang, 2009). Ether lipids are a category of phospholipid and make up about a fifth of the total phospholipid content in mammals, with the highest concentrations found in the brain, heart, leukocytes and spleen (reviewed by Dean and Lodhi, 2017).

Elucidation of the bile acid and ether lipid synthesis pathways grew out of research into peroxisomal β-oxidation. Early work on bile acid biosynthesis identified the side-chain oxidation of 26-hydroxycholesterol, a metabolized form of dietary cholesterol, into 3β-hydroxy-5-cholenic acid by rat liver peroxisomes (Krisans *et al*., 1985). This challenged the prevailing hypothesis that the ER and mitochondria were responsible for bile acid synthesis. Presently two bile acid synthesis pathways are known, and both route to the peroxisome prior to secretion (reviewed by Ferdinandusse *et al*., 2009). Peroxisomes take in the cholesterol derivative 3α,7α,12α-trihydroxycholestanoic acid-Coenzyme A (THCA-CoA) and export the conjugated bile salts tauro-CA and glycol-CA (reviewed by Ferdinandusse *et al*., 2009). The peroxisomal enzymes involved, in sequential order, are α-methylacyl-CoA racemase (AMACR; Ferdinandusse *et al*.,

2000), Acyl-CoA oxidase 2 (ACOX2, aka BCOX; van Veldhoven *et al*., 1996), D-bifunctional protein (DBP, aka HSD17B4; Jiang *et al*., 1996; Novikov *et al*., 1997), Sterol carrier protein X (SCPx), a class of thiolase (Antonenkov *et al*., 1997), and Bile acid-CoA:amino acid *N*-acyltransferase (BAAT; Falany *et al*., 1994; Pellicoro *et al*., 2007). Zellweger spectrum disorders (ZSDs) are commonly diagnosed by assessment of serum bile acid levels (reviewed by Ferdinandusse *et* al., 2009).

A required precursor molecule for ether lipids is dihydroxyacetone phosphate (DHAP), a glycolysis intermediate, hence the peroxisomal portion of ether lipid synthesis is also called the DHAP pathway (reviewed by Dean and Lodhi, 2017). The other required precursor molecules are fatty acids produced by a peroxisome-associated fatty acid synthase (FAS), which interacts with the peroxisomal membrane protein PMP70 (Hillebrand *et al*., 2012). The subsequent biosynthesis steps, performed either on the cytosolic side of the peroxisome membrane or within the organelle matrix, are performed by: Fatty acid-CoA ligase 4 (FACL4), encoded by the gene *Acyl-CoA Synthetase Long Chain Family Member 4* (*ACSL4*; Lewin *et al*., 2002); Glyceronephosphate O-acyltransferase (GNPAT; Ofman *et al*., 1998); Alkylglycerone phosphate synthase, (AGPS; de Vet *et al*., 1998), Fatty acyl-CoA reductase 1/2 (FAR1/2; Honsho *et al*., 2013; reviewed by Dean and Lodhi, 2017); and cytosolic Glycerol-3-phosphate dehydrogenase 1 (GPD1, previously DHAP reductase; Burdett *et al*., 1991). Given the importance of this pathway, owing to the general and organ-specific requirements for ether lipids, it is understandable that genetic perturbance of this pathway in humans has pathological outcomes (Hillebrand *et al*., 2012; Ofman *et al*., 1998; de Vet *et al*., 1998; reviewed by Dean and Lodhi, 2017).

1.1.3 Peroxisome biogenesis

It is clear from their enzymatic contents that peroxisomes perform varied and complex cellular functions relating to the metabolism of lipids and disposal of harmful by-products. Many questions were raised as peroxisomes were explored, such as how they came into being, how they were regulated in response to cellular needs and how enzymes reached the peroxisomal matrix. Before the development of modern molecular techniques, investigation relied on the chemical induction of peroxisome proliferation to provide the enzymatic abundance necessary

for specific activity assays. Clofibrate and similar serum lipid reduction drugs were used widely by the research community as peroxisome proliferation agents, despite being potential chemical carcinogens. This hypothesis was based on the ultrastructural similarity of livers from clofibrate-treated rats and tumors caused by hepatotoxic carcinogens (Reddy *et al*., 1980). However, the enlarged livers and increased catalase activity of mice fed these agents were widely considered due to peroxisome proliferation and a resultant increase in β-oxidation, not to carcinogenicity, because high-fat diet had a similar effect on male rats (Ishii *et al*., 1980). A novel 80 kDa protein was found to associate with peroxisomes from studies into clofibrate toxicity, and the protein's abundance correlated with clofibrate-mediated peroxisome proliferation (Ishii *et al*., 1980). This suggested a signal transduction pathway was activated by clofibrate ingestion that prompted peroxisome proliferation. The mystery protein was later identified as a member of the peroxisome proliferator–activated receptor (PPAR) family of hormone-regulated transcription factors, a group that regulates several cell functions in mammals including peroxisome abundance (Dreyer *et al*., 1992).

a. Peroxisome biogenesis factors

Ethyl methanesulfonate (EMS) mutagenesis screens using Chinese hamster ovary (CHO) cells provided the first clues that the control of peroxisome biogenesis was genetic. Zoeller and Raetz (1986) identified EMS-treated CHO cells unable to biosynthesize plasmalogens, a class of ether lipid, had no detectable peroxisomes and lacked detectable AGPS and particulate catalase activities. This suggested the mutants lacked some common factor that was necessary for both the absent enzymatic activity and the missing peroxisomes (Zoeller and Raetz, 1986). Soon afterward, the cDNA sequence for rat liver uricase was identified from a λ phage library (Motojima *et al*., 1988). Placed in the context of the discovery that peroxisomal β-oxidation enzymes were translated in the cytosol (Rachubinski *et al*., 1984), suggesting peroxisomes were assembled in a step-wise manner, it became apparent that both peroxisomes and their constituents were regulated by factors with genetic origins.

Three peroxisome-deficient mutants, named *PAS* (*Peroxisome Assembly*) *1-3*, were identified in *S. cerevisiae* (Erdmann *et al*., 1989). These mutants regained their peroxisomes following mating to wild-type cells, confirming the mutations produced recessive alleles. cDNA

sequence analysis determined *PAS1* was an ATPase and *PAS3* was an integral membrane protein (Erdmann *et al*., 1991; Höhfeld *et al*., 1991). Screens in *H. polymorpha*, *P. pastoris* and *S. cerevisiae* rapidly identified thirteen more *PAS* mutants. Species-specific nomenclature conventions developed. Ongoing research in identifying the genetic causes of peroxisome-related disease used yet another nomenclature style. This prompted adoption of a universal naming convention, and the gene family was renamed "peroxisome biogenesis factors" (reviewed by Distel *et al*., 1996). The common shorthand terms became "Peroxin" and "Pex" but some species-specific nomenclature was retained, for example in humans the written nomenclature uses capital letters. Presently there are fourteen *PEX* genes conserved in mammals and at least another twenty-three in yeasts (Singh *et al*., 2019; reviewed by Fujiki, 2016). Based on their function, *PEX* genes are divided into three categories: organelle membrane assembly, matrix protein import and organelle fission (reviewed by Fujiki, 2016). The mammalian *PEX* genes, their functional category and notable protein characteristics are presented in Table 1 (summarized from Fujiki, 2016). Peroxisome biogenesis requires the *PEX* genes and is hypothesized to proceed by a combination of two mechanisms: *de novo* biogenesis from pre-peroxisomal vesicles derived from the ER (ER-PPVs), and fission of extant, mature peroxisomes.

b. Organelle fission

The fission hypothesis proposes new peroxisomes arise by the growth and division of extant ones via post-translational acquisition of Peroxins, PMPs and matrix proteins from the cytosol until they are competent to divide (Fujiki *et al*., 1984; Rachubinski *et al*., 1984; Lazarow and Fujiki, 1985; reviewed by Heiland and Erdmann, 2005). The model postulates PEX3, PEX16 and PEX19 are responsible for peroxisome membrane protein (PMP) acquisition, matrix import pathways acquire the matrix enzymes, and PEX11 mediates the fission process through interactions with Dynamin-related protein 1 (Drp1) and species-specific kinesin/myosin motor proteins (Motley and Hettema, 2007; reviewed by Lazarow, 2003).

Table 1. Mammalian *PEX* genes, functions and protein characteristics. AAA, ATPases Associated with diverse cellular Activities; CAAX, C-terminal Cysteine-Aliphatic-Aliphatic-Any residue motif; DP, docking protein; PMP, peroxisome membrane protein; PTS1, peroxisome targeting signal 1; PTS2, peroxisome targeting signal 2; RING, Really Interesting New Gene; SH3, SRC Homology 3; TPR, tetratricopeptide repeat; WD40, tandem forty reside domains each ending in tryptophan-aspartic acid (WD).

Gene	**Function**	**Protein characteristics**
PEX1	Matrix protein import	AAA family
PEX2	Matrix protein import	PMP, RING family
PEX3	Membrane assembly	PMP, PMP-DP
PEX5	Matrix protein import	PTS1 receptor, TPR family
PEX6	Matrix protein import	AAA family
PEX7	Matrix protein import	PTS2 receptor, WD40 family
PEX10	Matrix protein import	PMP, RING family
PEX11	Organelle fission	PMP, three isoforms (α/β/γ)
PEX12	Matrix protein import	PMP, RING family
PEX13	Matrix protein import	PMP, PTS1-DP, SH3 domain
PEX14	Matrix protein import	PMP, PTS1-DP, PTS2-DP
PEX16	Membrane assembly	PMP, PMP-DP
PEX19	Membrane assembly	CAAX motif, PMP receptor
PEX26	Matrix protein import	PMP, PEX1-PEX6 recruiter

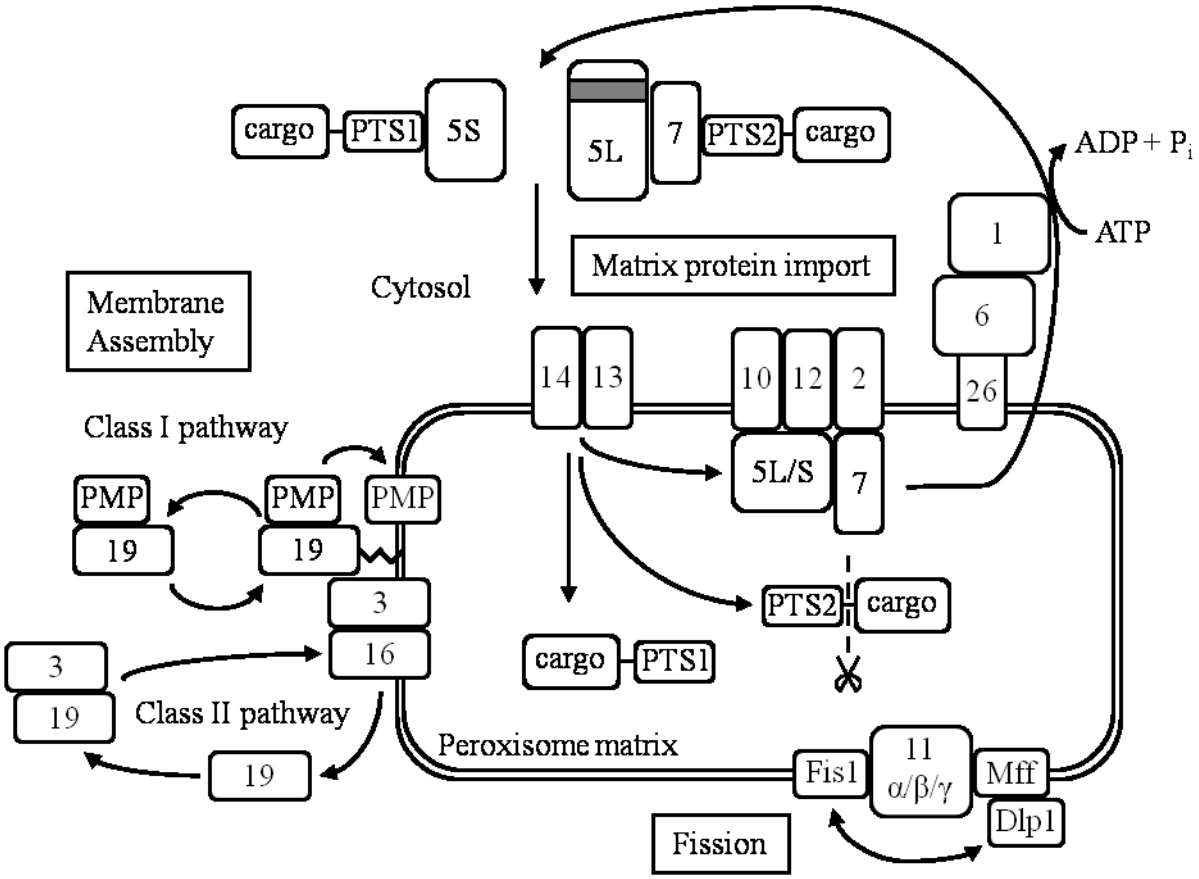
cargo
PTS1
5S
5L
7
PTS2
cargo
ADP + P_i
ATP
1
6
26
Cytosol
Matrix protein import
Membrane Assembly
14
13
10
12
2
Class I pathway
PMP
PMP
PMP
19
19
3
16
5L/S
7
PTS2
cargo
cargo
PTS1
3
19
Class II pathway
19
Peroxisome matrix
Fis1
11 α/β/γ
Mff
Dlp1
Fission

Figure 1. An overview of peroxisome biogenesis in mammals. Numbered rectangles denote peroxisome biogenesis proteins (Peroxins). Peroxins fall into three groups according to function: 1) membrane assembly, comprised of PEX3, PEX16 and PEX19 which assemble the peroxisome membrane by two pathways (Class I and II) and mediate PMP import; 2) fission, which includes three isoforms of PEX11 and accessory proteins of common organelle fission complexes; 3) matrix protein import, which includes the remaining Peroxins. In the cytoplasm, PTS1 cargo is recognized by the short isoform of PEX5 (PEX5S) and PTS2 cargo is recognized by a heterodimer of the long isoform of PEX5 (PEX5L) and PEX7. PEX14 is the convergence point at the peroxisome membrane, forming a translocon with PEX13 to permit receptor-cargo import. The PTS2 motif is cleaved following import, the PTS1 motif is not. PEX5 and PEX7 are retained at the translocon and transferred to the PEX2-PEX10-PEX12 RING complex, which mono-ubiquitinates PEX5. This modification marks PEX5 for export to the cytosol by the PEX1-PEX6-PEX26 AAA-ATPase complex in an ATP-dependent mechanism. Export of PEX5 also removes the ubiquitin modification, restoring PEX5 import competence. PEX7 is recycled in the same manner but there is controversy about whether or not it is mono-ubiquitinated. Modified from Fujiki, 2016, and reprinted with permission from the Proceedings of the Japan Academy, Series B, Editor-in-Chief Masanori Otsuka.

Central to the fission model is the existence of a dynamic peroxisomal reticulum, originally observed in electron micrographs and later supported by live cell imaging, from which peroxisomes bud (Lazarow and Fujiki, 1985; Schrader *et al*., 2000; Motley and Hettema, 2007). Evidence strongly supporting the fission model is the widespread conservation of one or more PEX11 isoforms, the presence of elongated peroxisomes when *PEX11* function is lost, and the interaction of PEX11 with peroxisome proliferator-activated receptor alpha (PPARα; Koch *et al*., 2010). This model is challenged by findings regarding the trafficking, localization and function of PEX3, PEX16 and PEX19, which is discussed in the next section (Karnik and Trelease, 2005; Hoepfner *et al*., 2005). Evidence suggests fission is the preferred biogenesis mechanism in cells which do not rely on peroxisomes for survival, such as yeast (Motley and Hettema, 2007).

c. De novo *biogenesis*

This was the first peroxisome biogenesis model and was proposed after classical electron micrographs of cellular ultrastructure revealed peroxisomes were occasionally found adjacent to, and continuous with, the ER in some mammalian cell types (Novikoff and Shin, 1964; Novikoff and Novikoff, 1972). The two biogenesis models competed for acceptance until Fujiki *et al.* (1984) and Rachubinski *et al*. (1984) identified peroxisome constituents were synthesized in the cytosol and not in the ER, suggesting the rough ER was not necessary for peroxisome protein synthesis and effectively shelving the *de novo* model. Contrariwise, using *Y. lipolytica*, Titorenko and Rachubinski (1998) revealed radio-labeled Pex2 and Pex16 localized to both the rough ER and peroxisomes, and that mutants defective in ER protein secretion also lacked peroxisomes. Similarly, two isoforms of Pex16 were found to localize to both the rough ER and peroxisomes in *A. thaliana* (Karnik and Trelease, 2005). A study of suspension-grown tobacco SV-2 cells reported the peroxisomal isoform of ascorbate peroxidase was found in a peri-nuclear, reticular structure. The enzyme was synthesized in the cytosol on free ribosomes prior to its compartmentalization and was localized by Hsp70 and an unidentified AAA ATPase. The reticular structure lacked the ER-resident proteins calreticulin, calnexin and ER luminal binding protein, suggesting peroxisome biogenesis involved a specialized reticular structure near the nucleus – perhaps the same structure essential to the fission model (Mullen *et al*., 1999). Elegant *S. cerevisiae* experiments by Hoepfner *et al*. (2005) determined Pex3p and Pex19p were synthesized in the cytosol, localized to an ER lumen sub-domain and then shuttled to

peroxisomes. Moreover, both proteins were required by extant peroxisomes to make the organelle import competent, and Pex19p remained cytosolic in *pex3Δ* cells (Hoepfner *et al*., 2005). Thus, new peroxisomes arose by the budding of Pex-enriched ER sub-domains lacking canonical ER resident proteins and subsequent recruitment of peroxisome matrix import proteins. Hoepfner *et al*. (2005) also confirmed the roles of Pex3p and Pex19p in recruiting the other Pex proteins to extant peroxisomes, validating the concurrent cellular use of both biogenesis models. Presently, the literature supports employment of a context-dependent combination of biogenesis models, as yeasts prefer the fission mechanism unless peroxisomes are lost (Motley and Hettema, 2007) whereas mammals employ PEX16-dependent *de novo* biogenesis even in the presence of extant peroxisomes (Kim *et al*., 2006).

1.1.4 Import pathways

The essential function of all peroxisome biogenesis factors, and by extension the peroxisome itself, is to generate the compartmentalized environment necessary for certain enzymes to perform their functions. Accordingly, the bulk of *PEX* genes encode proteins involved in acquiring and importing these enzymes (Table 1). To date, two ATP-dependent, variably-conserved matrix import pathways have been characterized that recognize cargo based on the presence of short peptide motifs termed peroxisome targeting signals.

a. Peroxisome Targeting Signal 1

Imanaka *et al*. (1987) demonstrated ATP-dependent, post-translational import of acyl-CoA oxidase (AOx) into peroxisomes through *in vivo* pulse-chase experiments. Similar work using rat liver AOx identified a C-terminal motif necessary for import that was dubbed the peroxisome targeting signal (PTS; Miyazawa *et al*., 1989). The minimum functional PTS was determined to be the tripeptide Ser-Lys-Leu (SKL) at the absolute C-terminus of client proteins. This sequence could also ectopically relocate non-peroxisomal proteins into the peroxisome matrix, proving the SKL motif was sufficient for peroxisome import (Miura *et al*., 1992). SKL-bearing proteins were found to fold in the cytosol and maintained this state following import, implying they were imported in their active conformation (Walton *et al*., 1995). Following the discovery of another PTS at the N-terminus of a rat thiolase isoform that was also sufficient for peroxisome

localization, the C-terminal PTS was renamed PTS1 (Swinkels *et al*., 1991). Several functional PTS1 variants have been identified and the current accepted consensus sequence is (S/A/C)-(K/R/H)-L, though addition of this tripeptide to a cytosolic protein is not a guarantee of peroxisomal localization and there are some client proteins where PTS1 is internal (Walton *et al*., 1995; Gould *et al*., 1988; Gould *et al*., 1990; reviewed by Brocard and Hartig, 2006). The list of PTS1-bearing proteins varies by species in accordance with the presence a second PTS pathway (PTS2) however the majority of peroxisome matrix proteins employ the PTS1 motif (reviewed by Brocard and Hartig, 2006).

The presence of a tripeptide signal on certain cytosolic proteins and their import into peroxisomes strongly suggested the import mechanism required a receptor protein. Molecular genetic approaches confirmed *PEX5* encoded the receptor and that the gene was widely conserved (reviewed by Distel *et al*., 1996). PEX5 localizes to both the cytosol and peroxisomes. In the cytosol, it binds PTS1-bearing cargo at the PTS1 motif. Once at the outer surface of the peroxisome membrane, cargo-loaded PEX5 interacts with PMPs PEX13 and PEX14 (Gould *et al*., 1996; Albertini *et al*., 1997). This forms a transmembrane pore called a translocon that permits cargo-receptor entry (Urquhart *et al*., 2000; reviewed by Fujiki, 2016). Once in the matrix, PEX5 detaches from its cargo and is passed along the interior membrane surface to a PMP/E3 ligase complex comprised of PEX2, PEX10 and PEX12, where PEX5 is mono-ubiquitinated (Chang *et al*., 1999; Okumoto *et al*., 2000; Platta *et al*., 2007; Okumoto *et al*., 2011). This modification marks PEX5 for recycling to the cytosol, in an ATP-dependent manner, by the PMP AAA complex PEX1/PEX6 and species-specific accessory proteins like mammalian PEX26 (Platta *et al*., 2004; Tamura *et al*., 2014). Recycling removes the ubiquitin tag, rendering PEX5 import competent once more. Mammalian *PEX5* encodes two isoforms, short (PEX5S) and long (PEX5L). PEX5S is the PTS1 receptor and PEX5L is a co-receptor for PTS2; the isoforms share the import and recycling pathway (Kunze *et al*., 2015; Braverman *et al*., 1998). Altogether, a minimum of nine Peroxins are required for PTS1 function (Figure 1).

b. Peroxisome Targeting Signal 2

Molecular and genetic studies found two cDNAs for rat liver peroxisome thiolase (SCPx). These cDNAs were determined to be splice isoforms (Bodnar and Rachubinski, 1990). The

second isoform was induced at only a fifth the rate of the first upon clofibrate treatment, suggesting differing mechanisms of peroxisome enzyme regulation existed that may have involved matrix enzyme import (Bodnar and Rachubinski, 1990). Neither SCPx isoform had a C-terminal PTS1 sequence, although both had two sequences internally, and both were also synthesized as larger precursors subject to post-import N-terminal cleavage. However, the novel isoform had an additional ten residues in its N-terminal region (Bodnar and Rachubinski, 1990; Swinkels *et al*., 1991). Nine of the ten residues, a sequence identified as (R/K)-(L/V/I)-X5-(H/Q)-(L/A), were sufficient for peroxisome targeting, were conserved in thiolase sequences across several species, and were wholly inside the cleaved N-terminal portion. The sequence was dubbed peroxisome targeting signal 2 (PTS2; Swinkels *et al*., 1991).

Discovery of a second PTS implied there was another cognate receptor. *S. cerevisiae* mutagenesis screens identified a recessive allele that impaired thiolase import without also impacting that of PTS1 cargo, and determined the gene belonged to a new peroxisome biogenesis complementation group: *PEX7* (reported as *PAS7* by Marzioch *et al*., 1994; reported as *PEB1* by Zhang and Lazarow, 1995). A *PEX7* ortholog was found in various human and mouse tissues but not in *C. elegans* or some diatoms, suggesting it and the PTS2 it recognized were less conserved than *PEX5* and PTS1 (Braverman *et al*., 1997; Motley *et al*., 2000; Gonzalez *et al*., 2011). Complementation studies of deletion mutants in yeast by Ghys *et al.* (2002) determined the Pex7 PTS2 recognition motif lay inside its N-terminal domain, upstream of its first WD40 motif. Yeast Pex7 was observed to cycle between the cytosol and peroxisome matrix, suggesting it functioned like Pex5 (Zhang and Lazarow, 1995; Mukai *et al.*, 2002; Nair *et al.*, 2004; Miyata *et al*., 2009). Unlike Pex5 however, Pex7 was not sufficient for PTS2 cargo import. Species-specific co-receptors PEX5L (human), Pex18/21 (*S. cerevisiae*) and Pex20 (*Y. lipolytica*) were necessary for Pex7 to interact with the PMP Pex14 and permit cargo import (Braverman *et al*., 1998; Titorenko *et al*., 1998; Purdue *et al*., 1998). This supported the hypothesis that PTS1 and PTS2 shared a common import pathway after cytosolic cargo loading. It is unknown if Pex7 is mono-ubiquitinated and subsequently recycled like Pex5, however human PEX7 did acquire protection from protease activity following matrix import, suggesting a post-translational modification, and when PEX5L export was inhibited so was that of PEX7 (Rodrigues *et al*., 2014).

1.1.5 Peroxisome biogenesis disorders

a. Zellweger spectrum disorders

A correlation between peroxisome loss and human disease was discovered by examination of liver samples from cerebro-hepato-renal (Zellweger) syndrome patients. Although total catalase activity was not significantly affected, there were no visible peroxisomes in patient hepatic cells or renal proximal tubules (Goldfischer *et al*., 1973). In affected patient brains the neutral lipid cholesterol ester was increased 28x in white matter, reaching 14 % of total mass (Goldfischer *et al*., 1973). Cultured fibroblasts from Zellweger patients had significantly increased levels of some VLCFA species (Moser *et al.*, 1984). Clofibrate treatment did not affect VLCFA accumulation in patient fibroblasts, although PMP and matrix enzyme transcription were detected in these cells, suggesting the issue lay in some combination of peroxisome assembly and import rather than proliferation (Lazarow *et al*., 1985; Lazarow *et al*., 1986; Suzuki *et al*., 1988). Tracing the release of ^{14}C from radio-labeled fatty acids revealed Zellweger patient fibroblasts released less CO_2 when fed VLFCAs but not long-chain fatty acids (LCFAs), indicating loss of peroxisomes correlated with impaired VLCFA β-oxidation (Moser *et al*., 1984). Similar VLCFA accumulation was noted in patient fibroblasts from neonatal adrenoleukodystrophy (NALD) and infantile Refsum disease (IRD) patients (Singh, *et al*., 1984; Beard *et al*., 1985). Zellweger syndrome, NALD and IRD, which respectively have progressively milder symptoms, were grouped as the "Zellweger spectrum of disorders" (ZSD; Reuber *et al*., 1997). The ZSDs are characterized by kidney abnormalities, facial dysmorphia and progressive liver and neurological disease. Zellweger patients rarely survive beyond their first year, though a few patients with the comparatively mild IRD have survived into their thirties (Reuber *et al*., 1997).

Presently, thirteen *PEX* genes have known ZSD-causing variants, all of which are inherited recessively (Shimozawa *et al*., 1993; reviewed by Fujiki, 2016). Mutation of the fourteenth *PEX* gene, *PEX7*, is associated with another class of peroxisome biogenesis disorder (PBD). Half of all PBDs arise due to mutation in *PEX1*, and another 30 % are due to mutation in *PEX6*, implicating failed receptor recycling as the major cause of PBD symptoms (Reuber *et al*., 1997; Geisbrecht *et al*., 1998). Zellweger syndrome severity correlates with remaining functionality of

a given mutation and may arise due to compound heterozygosity (Warren *et al*., 1998). NALD arises due to mutation in one or more of *PEX1*, *PEX5*, *PEX6*, *PEX10*, *PEX12*, *PEX13* and *PEX26*, suggesting deficiency in the metabolites produced by one or more PTS1 cargo enzymes (reviewed by Fujiki, 2016). IRD occurs resultant of mutation in one or more of *PEX1*, *PEX2*, *PEX12* and *PEX26*, suggesting the mono-ubiquitination and recycling of PEX5/PEX7 are impacted. The continued cytosolic synthesis of new receptors, which is not impacted by mutation in any of these *PEX* genes, may contribute to the comparative mildness of IRD symptoms (Reuber *et al*., 1997; reviewed by Fujiki, 2016). The specific *PEX* gene mutated in a given ZSD patient, and by extension how peroxisome contents are altered, affects peroxisome morphology (Chang *et al*., 1999). Altered peroxisome morphology has yet to be explored for diagnostic use.

b. Rhizomelic chondrodysplasia punctata

Before biochemical, genetic and molecular analyses, diseases were described and grouped by symptoms. A characteristic symptom of Zellweger syndrome, the most severe ZSD, is inappropriate calcification of the cartilage in the long bones of infants, for which the medical term is "chondrodysplasia punctata" (Hoefler *et al*., 1987). The rhizomelic form of this symptom, in which bones of proximal limbs are also affected, was termed rhizomelic chondrodysplasia punctata (RCDP; Spranger *et al*., 1971). Prior to the discovery of *PEX* genes, biochemical examination of RCDP patient plasma and fibroblasts identified a unique set of abnormalities: defective ether lipid synthesis, reduction or loss of phytanic acid oxidation, as with other PBDs, and detection of an unprocessed, inactive form of peroxisomal 3-oxoacyl-CoA thiolase (SCP2), exclusive of its processed form (Hoefler *et al*., 1987). These symptoms correlated with so-called "pseudo-Zellweger syndrome", which was caused by loss of the same thiolase (Goldfischer *et al*., 1986). The presence of both forms of SCP2 in normal cells suggested the enzyme was processed into its active form in peroxisomes, and that RCDP arose because the factor responsible for translocating the enzyme was absent (Singh *et al*., 1991). Concurrent work in rats identified an isoform of the homologous thiolase that employed a novel N-terminal peroxisome targeting signal (PTS2; Bodnar and Rachubinski, 1990; Swinkels *et al*., 1991). The human PTS2 receptor, *PEX7*, was subsequently confirmed to be the aberrant factor in a subset of RCDP patient fibroblasts, and rescued thiolase localization in both yeast and mouse models when expressed transgenically (Braverman *et al*., 1997; Purdue *et al*., 1997). RCDP is presently

a blanket term describing five genetic diseases, inherited recessively, that are related to mutation in a PTS2-related element. RCDP type 1 results from *PEX7* mutation, type 2 from *GNPAT* mutation, type 3 from *AGPS* mutation, type 4 from *FAR1* mutation and type 5 from *PEX5L* mutation (reviewed by Fujiki, 2016). In summary, RCDP1 arises from a general failure in PTS2 function, RCDP2, 3 and 4 result from mutations in genes responsible for ether lipid synthesis and RCDP5 results from the loss of the human-specific PEX7 co-receptor PEX5L.

1.2 *Drosophila melanogaster* as a model system for studying human disease

1.2.1 Historical overview and significant contributions

It is interesting that although peroxisome biogenesis disorders are generally portrayed as metabolic in nature, much of their pathophysiology is actually developmental and resultant of defects in one or more major peroxisome function(s). As demonstrated here, the majority of work done to elucidate peroxisome biogenesis, the genes responsible and the related human disorders used patient fibroblasts and yeast models. Modeling PBD symptoms requires an organism with analogous structures to those affected in order to investigate how tissue-specific phenotypes result from total loss of gene function. The similarities between mice and humans make them an attractive choice. However, cost aside, there are only 13 mutant strains available presently for genes associated with peroxisomes (reviewed by Baes and Van Veldhoven, 2012). *Drosophila* has a long history of laboratory use in discovering the effects of genetics on development, which in combination with the model's genetic tractability, fast generation time and low comparative cost, affords a wealth of tools to investigate any gene of interest.

The use of the fruit fly *Drosophila melanogaster* in the laboratory has its roots at the turn of the twentieth century (reviewed by Tolwinski, 2017). Thomas Hunt Morgan is widely credited with pioneering use of flies in the laboratory. He, along with several of his students, discovered sex-linked inheritance of over a hundred characteristics from 1910-1916 (Morgan and Bridges, 1916). For this work, Morgan was awarded the Nobel Prize in Medicine or Physiology in 1933. Morgan's student Calvin Bridges went on to produce the first hand-drawn images of the banding patterns on polytene chromosomes isolated from *Drosophila* larval salivary glands, creating a

chromosome mapping system that is still used to physically locate genes (Morgan, 1940). Another student of Morgan's, Hermann Muller, established X-rays were a mutagen using flies (Muller, 1928). Muller's discovery led to the creation of balancer chromosomes, used presently in the preservation of alleles by preventing meiotic recombination, and won Muller the Nobel Prize in Medicine or Physiology in 1946. Other notable fly firsts include Seymour Benzer's use of *Drosophila* to link behaviour and genetics, identifying at least twenty-four genes with specific behavioural effects (reviewed by Benzer, 1971). Of particular note is the work of Christiane Nüsslein-Volhard and Eric Wieschaus, whose screen of segment number and polarity mutants in *Drosophila* embryos led to the current model that genes control embryonic development and inherited gene mutations are a major cause of developmental disorders (Nüsslein-Volhard and Wieschaus, 1980). This work earned Nüsslein-Volhard and Wieschaus the Nobel Prize for Medicine or Physiology in 1995. Three more Nobel prizes have since been awarded to *Drosophila* researchers for similar linkage of gene pathways to fundamental cell and developmental biology phenomena: Richard Axel in 2004 "for (his discovery) of odorant receptors and how the olfactory system is organized", Jules A Hoffman in 2011 "for (his discovery) concerning the activation of innate immunity", and the trio of Jeffrey C Hall, Michael Rosbash and Michael W Young in 2017 "for their discoveries of molecular mechanisms controlling the circadian rhythm" (NobelPrize.org). The utility of *Drosophila* in addressing all manner of genetic and physiological questions, combined with the reagents and techniques that stem from this remarkable research history, clearly demonstrate its efficacy as a model system for understanding fundamental biological processes, including those underlying human diseases.

1.2.2 Stages of Drosophila melanogaster *development*

The *Drosophila* life cycle has four main stages: embryo (egg), larva, pupa and adult. Each stage is characterized by specific developmental milestones and morphology. Under controlled laboratory conditions, the time required to generate adult offspring from a mated pair of sexually mature adults is 9-11 days.

a. Fertilization and embryogenesis

Once mated, female *Drosophila* store spermatozoa and use them for up to fourteen days after copulation. In mated females, spermatozoa are stored in two organs, the ventral receptacle and the spermathecae (Lefevre and Jonsson, 1962). As a mature ovum descends through the uterus into the oviduct, one or a few spermatozoa are released from the spermathecae to fertilize it (Lefevre and Jonsson, 1962; reviewed by Hales *et al*., 2015). After gamete fusion, in which a successful sperm sheds its entire cytoplasm and its pronucleus completely enters an ovum, the egg-encased zygote is oviposited near or onto a food source (reviewed by Hales *et al.*, 2015). Under ideal circumstances hatching takes 12-15 h although population density and temperature affect this range (Ashburner *et al*., 2005). Using accepted husbandry techniques and accounting for these variables, hatching required 20-24 h in the present studies. The process of embryogenesis itself is the sum of all developmental processes that occur between fertilization and hatching. A timeline of important developmental milestones and when they occur is summarized in Table 2 (Campos-Ortega and Hartenstein, 1985; Hartenstein, 1993).

b. Hatching and larval stages

Hatching occurs upon completion of embryogenesis. *Drosophila* undergo three larval stages, termed instars, and progress through each is defined by a molt (reviewed by Hales *et al*., 2015). Optimally, the first and second instars (L1 and L2, respectively) last 24 h each and the third instar (L3) lasts 48 h (Ashburner *et al*., 2005). L1 instars burrow into their food source upon hatching and are identified by their posterior spiracles, which they keep above the food surface for respiration. This behaviour persists through the first molt, L2, the second molt and most of L3 (Ashburner *et al*., 2005). L3 instars signal the end of the larval stage with characteristic "wandering" behaviour, in which they move to the surface of the food and find a suitable nearby location away from the food to pupariate (reviewed by Hales *et al*., 2015). The L3 instar then begins its transition to prepupa.

c. Pupariation, pupation and adulthood

Formation of the puparium signals the onset of metamorphosis, which begins about five days after egg laying (at 25 °C). This event relies critically on sufficient nutrient uptake (Robertson, 1963). Twelve hours after pupariation begins the head everts (draws inward) and

over another 24 h the prepupa metamorphoses into a pharate adult (Poodry and Schneiderman, 1970). Metamorphosis then usually takes another 84 h to complete (Hartenstein, 1993). Metamorphosis from L3 larva to pharate adult optimally takes 98 h for females and 102 h for males (Bainbridge and Bownes, 1981). Once the pharate adult sub-stage begins, the pockets of undifferentiated epithelial tissue which were set aside during embryogenesis, termed imaginal discs, differentiate into various adult structures such as antennae, limbs, eyes, genitals and wings (reviewed by Beira and Paro, 2016). Most adult structures, including musculature and organ systems, develop during the larval stages and achieve their adult form during metamorphosis and eclosure (Hartenstein, 1993). The exception to this transformation is the central nervous system (CNS), which develops during embryogenesis and survives metamorphosis largely unchanged (Hartenstein, 1993; see Table 2). Accordingly, larval and adult phenotypes relating to neural function, such as geotaxis, mating behaviour and eclosure, may be traceable to an embryonic developmental defect. When adults eclose from the pupa case they relocate to permit wing expansion and cuticle darkening, which takes about 70 minutes (Johnson and Milner, 1987). Females are averse to mating for 12 h following eclosure and this is when researchers can collect virgins for planned crosses (Manning, 1962). In the wild, mean adult lifespan is 45-60 days although population density and food availability may reduce that (Sang, 1949).

Table 2. Developmental milestones during *Drosophila* embryogenesis. Summarized from Campos-Ortega and Hartenstein, 1985.

Stage number	Minutes after fertilization	Developmental activity
1	0-15	Pro-nuclear fusion
2	15-70	Early cell division, start of cleavage
3	70-90	Pole bud formation
4	90-130	Syncytial blastoderm, end of cleavage divisions
5	130-180	Cellularization of blastoderm
6	180-195	Gastrulation to form mesoderm and endoderm
7	195-200	Germ band elongation
8	200-230	Rapid germ band elongation, mesodermal parasegmentation
9	230-260	Slow germ band elongation, segmentation of neuroblasts, cephalic furrow formation
10	260-320	Formation of head features, stomodeal invagination
11	320-440	Epidermal para-segmentation, tracheal pits invaginate, end of neuroblast formation
12	440-580	Germ band retraction, optic lobe invagination, segment formation, midgut fusion
13	560-620	Germ band retraction ends, CNS/PNS differentiation
14	620-680	Dorsal closure of midgut and epidermis - head involution begins
15	680-800	End of dorsal closure, head involution, discs invaginate, cuticle deposition begins
16	800-900	Advanced denticles visible, ventral nerve cord shortens
17	Until hatching	Tracheal tree fills with air, continued retraction of the ventral cord

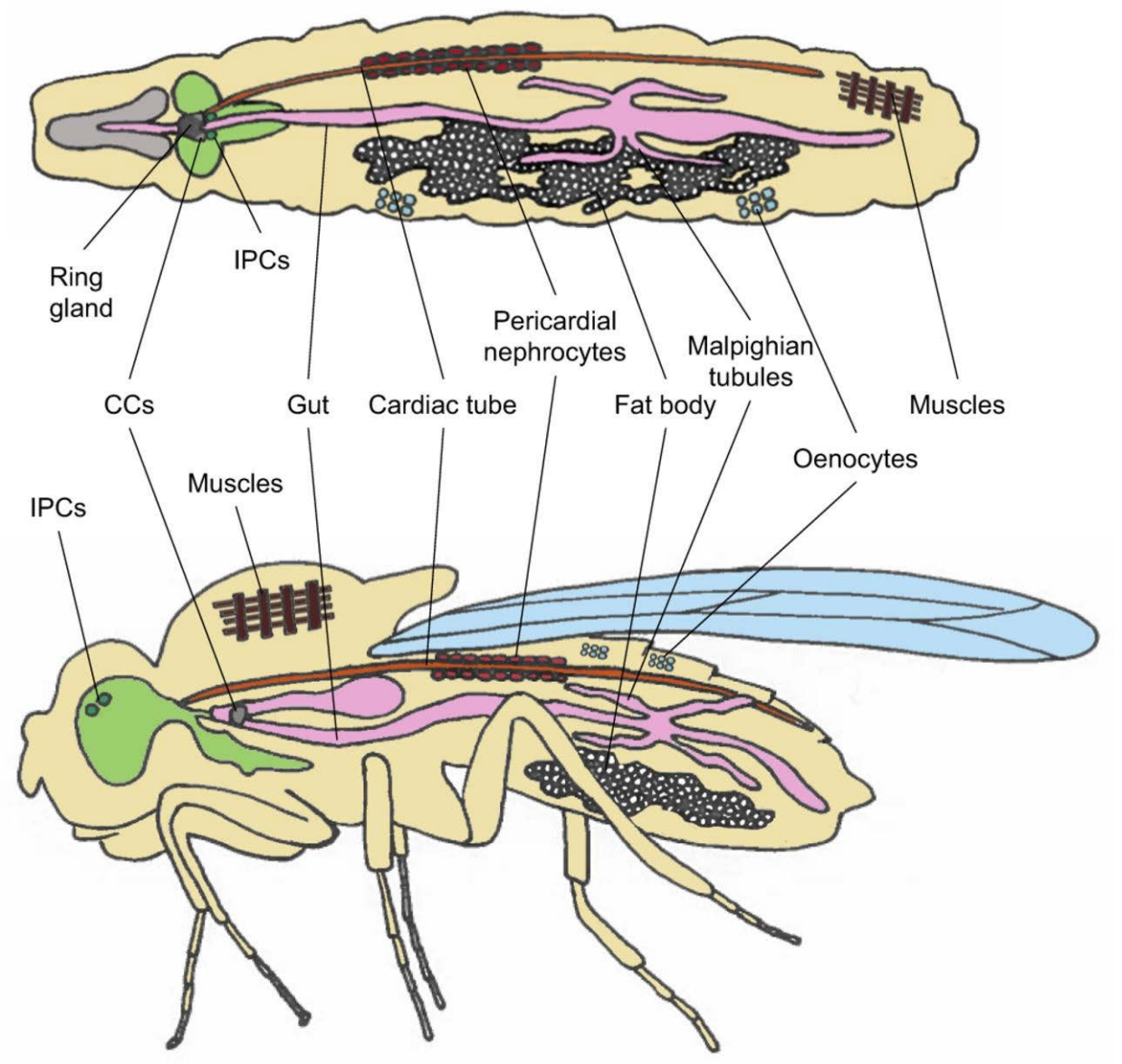
Ring gland
IPCs
CCs
Gut
Cardiac tube
Pericardial nephrocytes
Fat body
Malpighian tubules
Muscles
Oenocytes
IPCs
Muscles

Figure 2. Schematic of *Drosophila* tissues that contribute to metabolic homeostasis. Schematic lateral views of (top) a third instar larva and (bottom) an adult *Drosophila*, showing the cells, tissues and organs involved in metabolism. Larval and adult forms are not drawn to scale. Comparisons between *Drosophila* and human organs are made to aid understanding. Insulin-producing cells (IPCs) regulate carbohydrate homeostasis, similar to mammalian pancreatic β cells. Corpora cardiaca cells (CCs), in the ring gland of the larvae and at the junction between the crop and the gut in adults, regulate carbohydrate and lipid homeostasis. The gut regulates nutrient digestion and absorption. The fat body serves as a primary glycogen and lipid storage organ, similar to adipose tissue in mammals. Oenocytes accumulate mobilized lipids from the fat body upon starvation and have a similar function in this regard to the mammalian liver. The cardiac tube promotes nutrient and hormone circulation and is equivalent to the mammalian heart. Pericardial nephrocytes regulate waste filtration, similar to mammalian kidney podocytes. Malpighian tubules regulate waste excretion and osmoregulation, similar to mammalian renal tubules. Figure image and text reprinted from Hirabayashi (2016) under an International Creative Commons 4.0 license. Figure text edited for accuracy and clarity.

1.2.3 Use in molecular genetics

Drosophila is a diploid organism with two sexes and four chromosomes, so mapping genes and tracking genetic alterations is relatively easy (Morgan and Bridges, 1916; Morgan, 1940). Male gametes do not undergo intra-chromosomal recombination during meiosis, meaning males pass on traits as they inherit them, so keeping interesting alleles across generations is possible by tracking paternity (Morgan and Bridges, 1916). Inversion-replete balancer chromosomes containing easy-to-score marker mutations were created using X-rays to prevent intra-chromosomal recombination on all chromosomes (Muller, 1928; reviewed by St Johnston, 2002 and Hales *et al*., 2015). Balancer chromosomes also carry recessive lethal alleles to aid in the preservation of desired alleles. There are many mutagenesis tools available to generate mutant alleles. Large-scale efforts have produced libraries of uncharacterized mutant strains. One example are "insertion lines" containing engineered P-element or Minos transposons in one or more of thousands of genes (Bellen *et al* 2004; Venken *et al*, 2011; reviewed by Hales *et al*., 2015). Systematic screening of engineered insertions containing the exogenous Gal4 gene and an upstream activating sequence (UAS), elements native to *S. cerevisiae* with no homolog in *Drosophila*, produced libraries of "enhancer trap" lines with very specific expression patterns (Brand and Perrimon, 1993; Pfeiffer *et al*., 2008).

The randomness of P-element insertion and labour-intensive follow-up screening to identify useful mutants was overcome using bacteriophage φC31 integrase, which uses specific gDNA sequences called "landing sites" as integration targets. This was exploited by generating fly strains containing engineered "landing sites" at specific chromosomal locations for insertion of custom DNA fragments, also overcoming positional effects on insert expression (Groth *et al*., 2004; Venken *et al*., 2006). The φC31 system can be combined with the Gal4-UAS system to produce strains capable of conditional, targetable over-expression. I make use of the φC31 and Gal4-UAS systems to generate conditional over-expression strains in Chapter Three.

The use of directed mutagenesis via CRISPR-Cas9 permits the practical generation of targeted deletion mutations and targeted genomic insertion of engineered DNA (Gratz *et al*, 2015). A library of strains employing this technique, called the TRiP Toolbox, is presently being

generated by the Harvard Medical School DRSC/TRiP Functional Genomics Resources group. The TRiP Toolbox combines the specificity of Gal4-UAS and the site-specific mutagenesis ability of CRISPR-Cas9 to induce insertion or deletion mutations in a specific gene at a specific place and time *in vivo* (Lin *et al*., 2015). This technique can be used to produce knockout mutants (TRiP-KO) and over-expression strains (TRiP-OE). I make use of TRiP-KO strains to explore the effects of *Pex7* mutation in Chapter Three.

1.2.4 Use in cell biology

The utility of *Drosophila* extends beyond whole animal studies. Presently there are 159 *Drosophila* cell lines available from the *Drosophila* Genomics Resource Center (DGRC; dgrc.bio.indiana.edu). Most cell lines were isolated by bulk protease digestion or mechanical separation of undifferentiated tissues, such as embryos or larval imaginal discs, and screened for spontaneous immortalization from primary cultures (Echalier and Ohanessian, 1969; Schneider 1972; Ui K *et al*., 1987). The *Drosophila* cell lines used most widely are Schneider 2 (S2) and Kc167; these are male and female versions, respectively, of presumptive hematopoietic stem cells isolated from late-stage embryos (Echalier and Ohanessian, 1969; Schneider 1972). S2 cells have high transfection efficiency for both dsRNA and plasmids, and are used routinely in genetic screens to produce recombinant proteins or to express fluorescent markers for imaging *in vivo* (reviewed by Hales *et al*., 2015; reviewed by Cherbas and Gong, 2014).

1.3 Peroxisomes in *Drosophila*

1.3.1 Overview

Beard and Holtzman (1987) observed peroxisomes were abundant in wild-type *Drosophila* Malpighian tubules and gut, and found detectable xanthine dehydrogenase (XDH) activity in the eye (Figure 2). Contrariwise, *rosy* mutants lacked detectable XDH activity and had reduced peroxisomal catalase activity (Beard and Holtzman, 1987). Reaume *et al*. (1989) discovered *rosy* mRNA was present in the Malpighian tubules, fat body, and retinal basement layer, and used mosaic analysis to determine the gene product, XDH, was transported to the eye from the retina

(Reaume *et al*., 1989). The Malpighian tubule is an excretory/osmoregulatory system akin to the nephron of the vertebrate kidney (Figure 2; reviewed by Gautama *et al*., 2017). The fat body is an insulin-regulated layer of cells, adjacent to the inner surface of the cuticle, which is equivalent to adipocytes (Figure 2; DiAngelo and Birnbaum, 2009). The retinal basement layer is the basement membrane of the *Drosophila* eye that maintains the organ's overall shape and affects neural differentiation (reviewed by Ramos-Lewis and Page-McCaw, 2019). XDH relocation established a precedent in *Drosophila* for potential differences in transcript and polypeptide localization for genes related to peroxisome function. A comprehensive examination of the peroxisomes in adult *Drosophila* heads determined peroxisome abundance varied with tissue type, suggesting the factors that govern peroxisome biogenesis and function might be tissue-specific (St. Jules *et al*., 1990).

1.3.2 Conservation of peroxisome functions in Drosophila

a. Detoxification of reactive oxygen species

Catalase and XDH were found in structures characteristic of peroxisomes in several adult *Drosophila* tissues (Beard and Holtzman, 1987). Catalase manages the reactive oxygen species (ROS) hydrogen peroxide by catalyzing its conversion into water. The conservation of other ROS-managing enzymes was incidentally explored in the course of studying the effects of ROS on aging. The activities of the antioxidant enzymes Superoxide dismutase (SOD), Catalase and Glutathione reductase (GR) were examined across the lifespan of adult male *Drosophila*, and found to exhibit individual patterns of change with age (Sohal *et al*., 1990). Measures of oxidative stress like $NADPH/NADP^+$ and $NADH/NAD^+$ ratios increased with age, indicating oxidative stress increased as flies got older. Total SOD activity also increased, though catalase activity decreased sharply within ten days prior to death, suggesting changes in ROS scavenger enzyme activity resulted in age-related changes to redox state (Sohal *et al*., 1990). Over-expressing catalase and SOD decreased overall oxidative stress by staving off these end-of-life changes, improved old-age fly activity and oxygen consumption rates, and enhanced longevity (Orr and Sohal, 1994). Over-expressing human *SOD1* in *Drosophila* motor neurons had a similar effect, suggesting age-related increases in oxidative stress impacted nervous system function (Parkes *et al*., 1998). Ectopic catalase expression in mitochondria was found to increase adult

oxidative stress resistance but not enhance longevity, supporting the hypothesis that only peroxisomal ROS management correlated with longevity (Mockett *et al*., 2003). Caloric restriction was found to reduce peroxisome proliferation and improve longevity whereas mitochondrial gene expression had the opposite relationship, suggesting peroxisomal enzymatic activity was shifted to supporting the overall cellular redox state when organelle-specific metabolic functions like lipid β-oxidation were reduced by limited substrate availability (Zhou *et al*., 2012). Together, these data revealed the ROS management activities of peroxisomes were functionally conserved, *Drosophila* peroxisomes mediated a diet-responsive oxidative state, and there were tissue- and age-specific sensitivities to oxidative stress and overall redox state that were impacted by the complementary ROS management activities of mitochondria and peroxisomes. Accordingly, it could be inferred that lipid metabolism, a major source of ROS/RNS and produced by these organelles in other species, occurred in *Drosophila* peroxisomes.

b. Fatty acid metabolism

The characterization of *Drosphila* fatty acid metabolism enzymes was aided by advancements in bioinformatic analysis of large data sets and indirect immunofluorescence. For example, analysis of the *Drosophila* proteome for orthologs of the five human peroxisomal β-oxidation enzymes revealed at least two uncharacterized candidates for each, totaling ten candidate orthologs (Faust *et al*., 2012). Reporter fusions of the five *Drosophila* candidate orthologs best supported by bioinformatic analysis all co-localized at least 75 % with GFP-PTS1, suggesting their function involved peroxisomes (Baron *et al*., 2016). The remaining signal was presumed to be cytosolic, suggesting *Drosophila* conserved the synthesis of peroxisomal matrix enzymes on free polysomes and, by extension, the mammalian model of peroxisome biogenesis (Baron *et al*., 2016; Figure 1).

One predicted *Drosophila* FAO enzyme otholog, CG3415, had its quaternary structure resolved by x-ray scattering and was found to be very similar to that of human Multifunctional enzyme type 2, a member of the peroxisomal FAO pathway (Mehtälä *et al*., 2013). Another of the predicted genes, *Acsl* (CG8732), regulated the conversion of VLCFA C16:1 to C16:1-CoA (Huang *et al*., 2016). *Acsl* loss resulted in overgrowth of neuromuscular junctions and increased

phosphoethanolamine ceramide (CerPE) levels, the *Drosophila* equivalent of sphingomyelin, in motor neurons. These phenotypes were rescued by expression of human *ACSL4*, which encodes the peroxisomal enzyme Fatty acid-CoA ligase 4, establishing *Acs1-ACSL4* homology and the conservation of peroxisomal FAO in *Drosophila* (Huang *et al*., 2016). Similarly, loss of the predicted homolog *Drosophila ACOX1* (*dACOX1*) resulted in glial/axonal loss, reduced lifespan, impaired synaptic transmission and pupal death (Chung *et al*., 2020). These phenotypes were rescued by expression of human *ACOX1* (*hACOX1*), which encodes the first enzyme of the peroxisomal β-oxidation pathway. Surprisingly, dACOX1 localized to pupal/adult glia and, when a constitutively-active form was over-expressed, induced neurodegeneration that was rescued by either over-expression of catalase or use of a food-supplemented chemical anti-oxidant (Chung *et al*., 2020). This suggested *dACOX1* conserved the rate-limiting, peroxide-producing, peroxisomally-localized first step of VLCFA β-oxidation. A screen for factors in *Drosophila* that affected the response to viral infection identified a novel peroxisome-localized factor named Sgroppino. Loss of *Sgroppino* increased adult triglyceride levels, the *Drosophila* lipid storage molecule, increasing body mass and thickening abdominal fat tissue (Merkling *et al*., 2019). Together, these data linked *Drosophila* peroxisomes to lipid storage and the non-energetic oxidation of VLCFAs.

c. Ether lipid synthesis

It is unknown if ether lipid synthesis occurs in peroxisomes in *Drosophila*. The conservation of ether lipid synthesis enzymes in *Drosophila* is presently based on prediction of homology using cDNA sequence identity. The exception is the cytosolic DHAP reductase/GPD1 homolog *Gpdh1*, whose oxidase (dehydrogenase) function was characterized without observation of its sub-cellular localization (Niesel *et al*, 1980; O'Brien and Macintyre, 1972). The DHAP reductase function of Gpdh1, as required by the ether lipid synthesis pathway, has not been explicitly observed in *Drosophila*. However, Gpdh1 is considered orthologous to human GPD1, a bi-functional enzyme with oxidase and reductase capability, and a variant PTS1 motif has been observed at the Gpdh1 C-terminus (Reyes *et al*., 2015; Wojitas *et al*., 1997; ncbi.nlm.nih.gov/gene). Several homologs were predicted for the remaining three enzymes in the ether lipid pathway by Faust *et al*. (2012), though they reported their proteome analysis could find no GPD1 homolog and they did not discuss *Gpdh1*. A reporter fusion of the predicted AGPS homolog

CG10253 co-localized with the peroxisome marker PMP34-Cerulean, but only when tagged at the N-terminus (Faust *et al*., 2012). This suggested CG10253 used PTS1 to achieve peroxisomal localization, whereas in mammals AGPS contains PTS2. The cellular localization of reporter fusions of the predicted homologs CG4625 (GNPAT), CG5065 (FAR1) and CG10253 (AGPS) were observed to co-localize 75-90 % with GFP-PTS1 (Baron *et al*., 2016). Again, *Gpdh1* was not examined.

1.3.3 Conservation of mammalian PEROXIN *function in* Drosophila

Mast *et al*. (2011) used amino acid sequences to identify fifteen potential *Drosophila Peroxins*. To begin confirming conservation, knockdown of the predicted genes in S2 cells stably expressing the peroxisome marker GFP-PTS1 was performed via RNA interference (RNAi). GFP-PTS1 marks import-competent peroxisomes. The marker's localization was affected by knockdown of eleven predicted *Peroxins*. The phenotypes fell broadly into two categories, the cytosolic mislocalization of and/or reduction in GFP puncta (*Pex1, Pex2, Pex5, Pex6, Pex12, Pex13, Pex14, Pex16, Pex19*), and aberrant peroxisome morphology/number (*Pex3, Pex11*). No effect was observed for knockdown of the potential homologs of *Pex7, Pex20* or *Pex23*, although the weak identity scores of *Pex20* and *Pex23* may have contributed to their lack of effect (Mast *et al*., 2011). The cellular localization of reporter fusions containing fourteen putative *Peroxins* was observed by Baron *et al*. (2016) in S2 cells. They observed twelve Pex reporters co-localized ≥ 50 % with GFP-PTS1, including a Pex7 reporter, a Pex3 reporter overlapped 25 ± 5 % and a Pex19 reporter overlapped 35 ± 5 % (Baron *et al*., 2016). The Pex7 observation was notable because the PTS2 tag was not found in the *Drosophila* proteome and a PTS2-mCherry reporter fusion did not traffic to peroxisomes in S2 cells (Faust *et al*., 2012). Contrariwise, the ER-targeting signals within an N-terminal transmembrane domain of the yeast, human and *Drosophila* versions of *Pex3* were found to function in both yeast and S2 cells, suggesting they were orthologous and that *Drosophila* conserved the Pex3-based sorting mechanism to route Peroxins to PPVs that was first observed in yeast (Fakieh *et al*., 2013).

Molecular genetic studies have determined that the predicted *Drosophila* genes *Pex1*, *Pex2*, *Pex3*, *Pex10*, *Pex16* and *Pex19* regulate canonical peroxisome functions (Table 1, Figure

3). Two homozygous *Pex1* mutant strains, each generated by different means, were observed to have defective larval growth, severely reduced lifespan, malformed/disorganized embryonic CNS/PNS and glia, and a lack of co-ordinated movement despite unaffected muscular development (Mast *et al*., 2011). These phenotypes generally matched the symptoms of human Zellweger syndrome patients, over half of whom have function-impairing *PEX1* variation. These data suggested *Drosophila Pex1* was homologous to human *PEX1* and established a fly PBD model.

Pex2 and *Pex10* mutants displayed recessive inheritance of some PBD symptoms: impaired peroxisomal matrix protein import, elevated VLCFA levels and slowed growth (Chen *et al*., 2009). The elevated VLCFA levels resulted in spermatogenesis defects traced to a failure in meiotic cytokinesis. Reducing VLCFA levels rescued the defect, though *Pex2* over-expression could not rescue *Pex10* loss even though their mutant phenotypes were similar (Chen *et al*., 2009). Null *Pex16* mutants had reduced body weight, the *rosy* eye phenotype, elevated VLCFA levels, locomotor problems and defects in the dendritic trees of pupal/adult optic lobes (Nakayama *et al*., 2011). Adult *Pex16* males shared the *Pex2/Pex10* sterility phenotype, though the defect was traced to arrested spermatocyte development rather than failure in meiotic cytokinesis (Nakayama *et al*., 2011). Further study of *Pex2* and *Pex16* found their loss induced sensitivity to glucose starvation, suggesting an inability to metabolize lipids for energy, and had altered VLCFA levels, reduced lifespan and adult locomotion problems (Wangler *et al*., 2017). Metabolite analysis revealed *Pex2* or *Pex16* adult mutants accumulated ether lipid precursor molecules and had reduced abundance of ether lipid catabolism products, linking the genes biochemically to a canonical peroxisome function (Wangler *et al*., 2017).

Loss of *Pex3*, either by knockout or knockdown, caused global loss of peroxisomes in *Drosophila* larvae. Null *Pex3* larvae displayed growth retardation and altered lipid metabolism, and died at or before pupariation (Nakayama *et al*., 2011; Faust *et al*., 2014). Strong muscle-specific *Pex3* knockdown was semi-pharate lethal, meaning they died during eclosure, and weaker *Pex3* knockdown produced adults incapable of wing extension after they eclosed (Faust *et al*., 2014). A novel role for peroxisomes in adult muscle development was uncovered, however

the apparent pleiotropy of fly *Pex3* and its differing knockout/knockdown phenotypes prevented establishment of a PBD model (Faust *et al*., 2014).

In mammals, PEX19 works with PEX3 and PEX16 to recruit PMPs and mediate *do novo* peroxisome biogenesis (Table 1). Loss of both maternal and zygotic *Pex19* in *Drosophila* caused embryonic peroxisome loss and failure to hatch (Bülow *et al*., 2017). Zygotic *Pex19* null mutants had a strong reduction in the number of peroxisomes in larval tissues and only 20 % successfully pupated into adults, which then died within 24 h (Bülow *et al*., 2017). Adult escapers had elevated apoptotic activity in their optic lobes, suggesting loss of peroxisomes caused neurodegeneration analogous to classic PBD symptoms. These *Pex19* mutants also had poor negative geotaxis and an inability to fly or inflate wings (Bülow *et al*., 2017). In zygotic *Pex19* null mutant larvae, VLCFAs were increased and LCFAs were decreased, gut fat stores were depleted while oenocytes were filled with lipids, and mitochondrial ROS production was elevated (Bülow *et al*., 2017). Oenocytes are a class of *Drosophila* secretory cell that form tissues analogous to the liver (Figure 2; reviewed by Makki *et al*., 2014). Altered lipid metabolism was traced to hyperactivation of the transcription factor Hnf4 in the absence of *Pex19*, leading to upregulation of *lipase 3* (*lip3*) and increased mitochondrial β-oxidation that resulted in elevated mitochondrial ROS production. Loss of *Hnf4* expression in *Pex19* null mutant larvae rescued the lethal phenotype (Bülow *et al*., 2017). Dietary supplementation of medium-chain fatty acids (MCFAs) with coconut oil restored the regulation of *lip3* via the transcription factor Schlank, ameliorating *Pex19* loss (Sellin *et al*., 2018). Interestingly, this also lessened the phenotype severity of *Pex2* and *Pex3* null mutants, suggesting Schlank responded to peroxisomal MCFA production by regulating mitochondrial β-oxidation (Sellin *et al*., 2018). Figure 3 summarizes what is currently known about the conservation of *Peroxins* in *Drosophila*, based on their function relative to human *PEROXINS*.

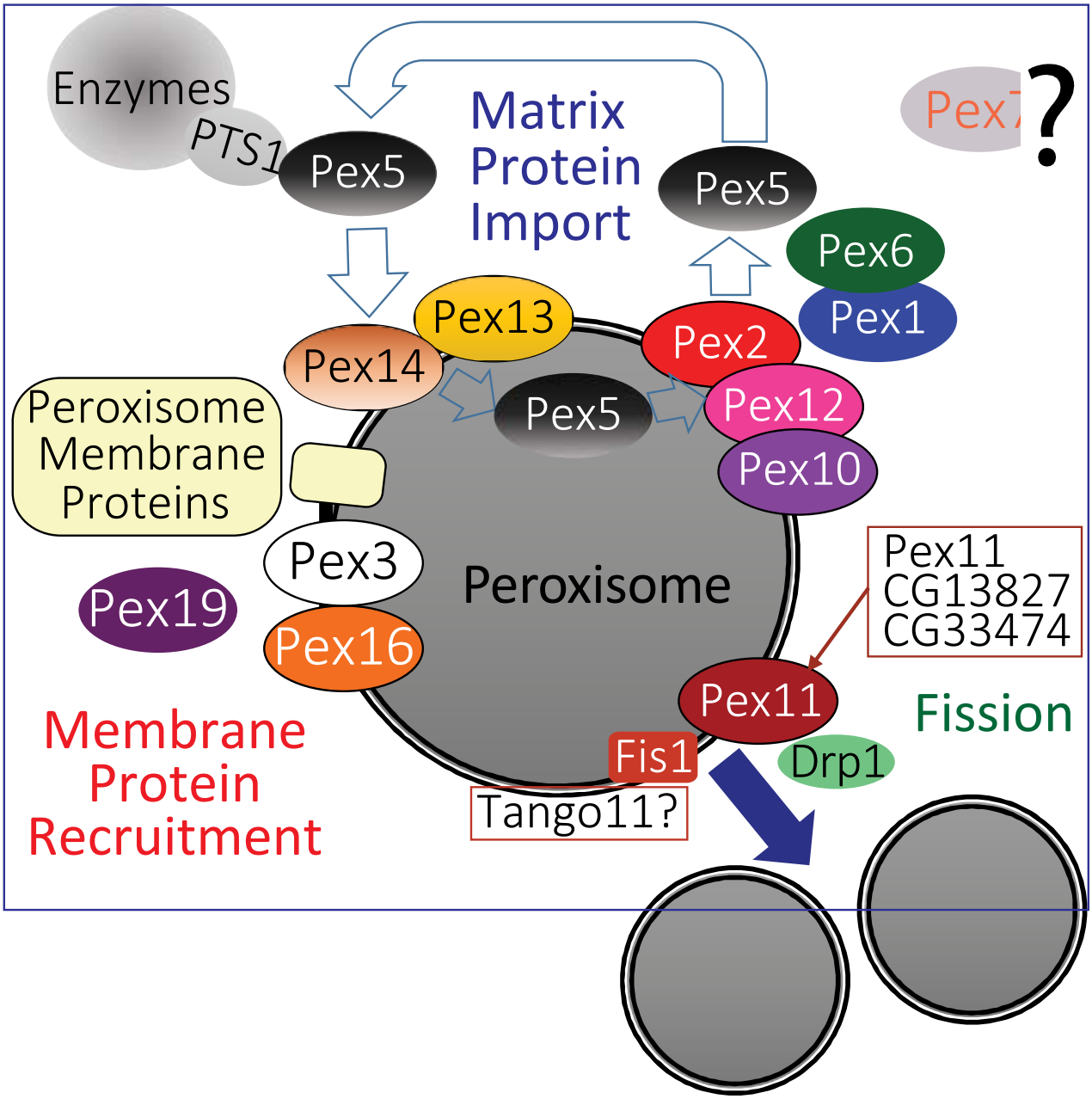
Enzymes
PTS1
Pex5
Matrix
Protein
Import
Pex5
Pex7
?
Pex6
Pex1
Pex13
Pex14
Pex2
Pex5
Pex12
Pex10
Peroxisome
Membrane
Proteins
Pex3
Peroxisome
Pex19
Pex16
Pex11
CG13827
CG33474
Pex11
Fission
Fis1
Drp1
Tango11?
Membrane
Protein
Recruitment

Figure 3. A model for the role of the *Drosophila* homologs of peroxisome biogenesis factors. Model based on one proposed for mammalian peroxisomes by Fujiki (2016). *Pex3*, *Pex16* and *Pex19* are all conserved in *Drosophila*, suggesting the membrane pathway is conserved. The peroxisome fission machinery appears putatively conserved as there are three *Pex11* candidates (*Pex11*, CG13827 and CG3374). *Fis1* is the homolog of *Fission, mitochondrial 1* (*FIS1*), *Tango11* is homologous to *Mitochondrial fission factor* (*MFF*) and *Drp1* is the homolog of *Dynamin 1 like* (*DNM1L*), all of which are required for peroxisome fission in mammals. *Drosophila* peroxisome matrix protein import in flies appears dependant on PTS1, mediated by Pex5 binding to PTS1 (Table 1), although some matrix proteins do not have a PTS1 motif. The docking complex proteins Pex13 and Pex14 are putatively conserved in *Drosophila*. The RING-E3-ligase complex of Pex2, Pex10 and Pex12 is conserved based on mutant phenotypes, as is the AAA-ATPase Pex1. Thus, it is likely that the mammalian import pathway is conserved in Drosophila. A *Pex7* homolog exists in *Drosophila*, but its role in peroxisome function is unclear. Image published originally in Pridie, Ueda and Simmonds (2020).

1.3.4 Novel peroxisome-related functions

a. Loss of Peroxisome Targeting Signal 2

A proteomic analysis by Faust *et al*. (2012) determined the PTS2 motif was missing from predicted *Drosophila* homologs of canonical PTS2-bearing enzymes like thiolase (SCPx), which instead bore variant PTS1 motifs. This suggested *Drosophila*, like *C. elegans*, had lost its PTS2 import system (Motley *et al*., 2000). Fluorescent microscopy data showed a PTS2-mCherry construct was unable to localize to peroxisomes in S2 cells but did so successfully in monkey liver COS7 cells (Faust *et al*., 2012). Contrariwise, although PTS2 was presumed lost, the predicted *Drosophila* gene CG6486 was similar sequentially to human *PEX7* (Mast *et al*., 2011; Faust *et al*., 2012), encoded a protein that localized to both peroxisomes and the cytosol like a cycling receptor would (Baron *et al*., 2016), and was implicated in the ROS burst that preceded the *Drosophila* immune response (Di Cara *et al*., 2017). Further characterization of the developmental roles of *Drosophila Pex7* is the focus of Chapter 3.

b. Use of reactive oxygen species as signaling molecules

The musculature defects observed under *Pex3* knockdown (Faust *et al*., 2014) may be explained in the context of the use of ROS as a paracrine signal by *Drosophila* cardiac tissue. The adult *Drosophila* heart is a tube made of two columns of cardiomyocytes (CMs) encased in a layer of non-muscle pericardial cells (PCs) termed a pericardium (Figure 2). In mammals there is cross-talk between the various PC and CM subtypes that is essential for the heart to respond to physiological and pathological cues (Tian and Morissey, 2012). Elements of that relationship are preserved in *Drosophila*, as PCs influence both myocardial development and heart function (Lim *et al*., 2014). Larval and adult PCs have higher ROS abundance than CMs *in vivo*, establishing a differential in redox state between adjacent cell types of the same organ (Lim *et al*., 2014). ROS reduction in PCs by tissue-specific catalase over-expression (*Dot-Gal4>catalase*) resulted in adult hearts with increased frequency of irregular beats, broader distribution of heart periods and increased beat-to-beat variation, collectively indicative of a significant increase in arrhythmia (Lim *et al*., 2014). The heart tubes of *Dot-Gal4>catalase* adults were narrowed at one week post-eclosure, and by four weeks post-eclosure the diastolic diameter had become so great that the heart tubes had become enlarged (Lim *et al*., 2014). Similar phenotypes were observed following

Dot-Gal4>SOD1 and *Dot-Gal4>SOD2* over-expression, implicating overall PC redox state as the responsible factor. The progressive phenotype was not observed when ROS were altered in CMs, nor did altering PC ROS levels affect CM ROS levels, indicating the phenotype was not due to direct PC → CM ROS diffusion (Lim *et al*., 2014). Lost function of two of the three *Drosophila p38* genes phenocopied the progressive heart phenotypes, implicating the MAPK signal transduction pathway was the mechanism responsible for communicating the PC redox state to CMs (Lim *et al*., 2014). In mammals, this pathway mediates the response to oxygen levels and oxidative stress in cardiac tissue, establishing a precedent for ROS sensitivity in the absence of direct evidence of a conserved mechanism (reviewed by Giordiano, 2015). The Lim study suggested 1) peroxisomes, via maintenance of redox state, regulated muscle development, 2) an indirect relationship existed between peroxisomes and MAPK signal transduction and 3) tissue-specific ROS management was a cue for paracrine signaling. To contrast, there is only indirect evidence that *Drosophila* somatic musculature conserves a ROS-based developmental mechanism, and that is the muscle-specific *Pex3* knockdown effect reported by Faust *et al*. (2014).

c. Role for peroxisomes in innate immune response

The principal line of defense against pathogen infection is the innate immune response. Innate immunity has three mechanisms: phagocytosis, the complement system and defensins. Phagocytosis is performed by specialized immune cells called macrophages. Macrophages circulate through blood and tissues, and are found in vertebrates and invertebrates. In *Drosophila*, macrophages called haemocytes are found circulating in the hemolymph (Rizki and Rizki, 1980). S2 cells are believed to have originated from a haemocyte precursor, although their specific lineage is unknown (Schneider, 1972; reviewed by Cherbas and Gong, 2014). In mammals, macrophages activate other immune responses at the site of infection by inducing inflammation of local tissue via “respiratory burst”, the rapid production of superoxide from oxygen by NADPH oxidase (NOX2) tethered to the exterior surface of their plasma membrane (reviewed by Weigert *et al*., 2018). Macrophage-generated superoxide diffuses into nearby cells through anion channels and alters their redox state, initiating the inflammatory response. If the macrophage is performing phagocytosis, the respiratory burst also damages the pathogen being engulfed. Mitigation of the respiratory burst is achieved by direct inhibition of the NOX2

phosphorylator PKC by PPARγ, a nuclear hormone receptor also responsible for peroxisome proliferation (reviewed by Weigert *et al*., 2018). The conservation of this pathway has yet to be examined in *Drosophila*, though Di Cara *et al*. (2017) did assay it indirectly by performing RNAi of putative *Peroxins Pex5* and *Pex7* in S2 cells then challenging the innate immune response with microbial infection. Knockdown of *Pex5* (*Pex5*-i) or *Pex7* (*Pex7*-i) resulted in compromised phagocytosis, reduced uptake of *E. coli* and *C. albicans* due to defects in actin organization, and defects in hydrogen peroxide (H_2O_2) management (Di Cara *et al*., 2017). *Pex5*-i and *Pex7*-i cells had higher basal H_2O_2 levels, a lower fold-change in H_2O_2 abundance in response to infection, and a longer post-infection H_2O_2 clearance time (Di Cara *et al*., 2017). Nitric oxide (NO), a by-product of superoxide production and indicative of NOX2 activation by macrophages, was not observed to increase under either knockdown condition (Di Cara *et al*., 2017). Strong over-expression of catalase rescued phagocytosis in *Pex7*-i cells but not *Pex5*-i cells. At the organism level, bacterial infection killed all *Pex5*-i and *Pex7*-i adult flies within seven days, whereas control flies maintained 70-80 % survivorship (Di Cara *et al*., 2017). *Pex5/7*-i flies were also more sensitive to injury by injection. Together, these data strongly suggested the respiratory burst mechanism was conserved in *Drosophila*, apart from NOX2 activation, and that ROS generated by the respiratory burst were managed in a *Pex5/7*-dependent manner. A study of the immune response in the adult *Drosophila* midgut confirmed gut-specific *Pex5*-i resulted in loss of peroxisome function, compromised gut microbial response and increased gut epithelial cell turnover, collectively due to increased oxidative stress (Di Cara *et al*., 2018). *Pex5* is clearly essential to peroxisome function in *Drosophila*. As some *Pex7*-i phenotypes were rescued by ubiquitous catalase over-expression, and redox state was impacted by *Pex7*-i at the cellular and whole-organism levels, Pex7 may be a co-factor for the import of peroxisomal ROS management enzymes that belong to the catalase enzymatic pathway, e.g. superoxide dismutase, by a mechanism yet to be discovered.

d. Dynamics of organelle movement and fission

Peroxisomes are subject to constant relocation involving dynamic elements of the cytoskeleton. This affects processes like cellular localization, proximity to other organelles, inter-organelle cross-talk, cell growth and division, response to infection and cell differentiation. Electron microscopy of CHO cells revealed multiple peroxisome-microtubule contact sites (Rapp

et al., 1996). *In vivo* kinetic analysis determined chemical disruption of both microtubule and actin filaments reduced peroxisome movement, as did ATP depletion, implying peroxisomes were moved by ATP-dependent motor proteins (Rapp *et al*., 1996). The innovation of the stably transfected GFP-PTS1 reporter in S2 cells permitted identification of Kinesin-1 and Dynein heavy chain, which associate exclusively with microtubules, as the motors responsible for peroxisome movement in *Drosophila* (Kural *et al*., 2005). Peroxisome-associated microtubules contributed to organelle movement if motor proteins were functional, and opposite-polarity motors interacted to promote bi-directional peroxisome movement (Kulić *et al*., 2008; Ally *et al*., 2009). A human *PEX26*-mCherry fusion reporter transfected into S2 cells anchored Kinesin-1 to peroxisomes and regulated retrograde peroxisome movement (Rossi *et al*., 2017). *Drosophila* do not conserve *PEX26* however the plus-end-directed kinesin ATPase Unc-104 localized in a similar fashion (Rossi *et al*., 2017). The involvement of *Peroxins* in *Drosophila* peroxisome dynamics remains unknown.

Studies of peroxisome dynamics elucidated important roles for genes besides *Peroxins* in peroxisome biogenesis. A siRNA screen for factors regulating mitochondrial fission found *Fis1*, *Drp1* and *Tango11* all localized to both peroxisomes and mitochondria, and that knockdown of any of these genes resulted in aberrant peroxisome morphology (Figure 3; Gandre-Babbe and van der Bliek, 2008). Fis1 and Drp1 are known regulators of mitochondrial fission and operate within the same complex, but the function of the human *Tango11* homolog *Mff* was not affected by *Drp1/Fis1* siRNA, indicating Mff (and by inference Tango11) are not part of the Fis1/Drp1 complex (Gandre-Babbe and van der Bliek, 2008). Pex11 governs mammalian and yeast peroxisome fission, but a Pex11-Mff relationship has yet to be observed (Table 1, Figure 3). *Drosophila Drp1* null mutants have almost no synaptic mitochondria, altered mitochondrial distribution in the nervous system and altered mitochondrial morphology (Chao *et al*., 2016). Wild-type human *DNM1L* expression complements *Drp1* loss however the pathogenic variants $DNM1L^{A395D}$, $DNM1L^{G350R}$ and $DNM1L^{Y691C}$ displayed dominant-negative peroxisome enlargement and peri-nuclear localization of peroxisomes in salivary glands of third instar larvae, suggesting impaired fission (Chao *et al*, 2016; Assia Batzir *et al*., 2019). Over-expression of either wild-type *DNM1L* or $DNM1L^{\Delta GED}$, in which the GTPase-effector domain (GED) domain was deleted, had no effect on peroxisomes in control larvae (Assia Batzir *et al*., 2019). This was

supported by data indicating the GED was responsible for the conformational changes necessary to permit DNM1L to homodimerize and drive fission of mitochondria/peroxisomes (Mears *et al*., 2011; Zhu *et al*., 2004). Other screens have likewise identified genes besides *Peroxins* that regulate peroxisome proliferation, and research is ongoing (Drake, 2012; Lacey, 2015; Graves *et al*., 2020; A Magico, unpublished data).

1.3.5 Summary of present studies

Chapter Three explores the expression and mutagenesis of *Drosophila Pex7* during embryogenesis. First, the embryonic transcription and translation of endogenous *Pex7* are characterized in strain w^{1118} by qualitative and quantitative means. Next, *Pex7* targeted loss-of-function and over-expression mutations are observed to affect survival. These observations are compared to likewise alteration of conserved *Peroxins*. Lastly, neuro-specific rescue of a homozygous *Pex7* loss-of-function strain is attempted using a UAS-controlled *Pex7* transgene. In Chapter Five, these data are contextualized within the current literature to propose why *Pex7* is conserved in an organism that does not also conserve the PTS2 motif.

Chapter Four continues an unpublished screen begun by Dr. Adam Magico, using S2 cells to look for potential regulators of peroxisome biogenesis outside the *Peroxin* family. Prior data for a cohort of genes obtained via high-throughput screen using transient RNAi is validated by a combined methodology of replication using a different dsRNA synthesis method and software-assisted quantitative assessment of changes in peroxisome abundance. This approach is then applied to transient over-expression of reporter fusions from another cohort of genes obtained from the same initial RNAi screen. In Chapter Five, the genes whose altered expression resulted in substantial changes in peroxisome abundance are discussed in the context of their canonical or presumptive functions. Finally, an emergent trend in the cellular processes associated with altered peroxisome abundance is discussed.

Chapter 2 Materials and Methods

2.1 Cell culture and animal husbandry

E. coli strains Top10 (ThermoFisher) and BL21 (New England BioLabs) were grown on standard LB agar with appropriate antibiotic supplement per manufacturer's protocol. S2 cells (DGRC) were grown in either serum-free HyClone SFX-Insect medium or serum-free SFM4-Insect medium plus L-Glutamine, as available (Cytiva Life Sciences), supplemented with 100 units/ml penicillin and 100 µg/ml streptomycin (ThermoFisher).

Fly strains were maintained on standard cornmeal medium at 25 °C and 35-40 % humidity. Lighting was not regulated because the storage facility had large north-facing exterior windows.

2.2 *D. melanogaster* strains, embryo collection and viability assays

w^{1118} embryos were collected on circular 150 mm diameter x 15 mm depth apple juice/agar plates, supplemented with fresh yeast paste, from a 46 cm x 46 cm x 61 cm clear plastic cage filled with adult flies. Collections were performed for 2-4 h, as required. The plates were removed from the cage, stored upside-down, and the embryos aged on the collection plates at 25°C and 35-40 % humidity. Embryos were washed off the plates in flowing tap water through a three-stage, vertically-stacked sieve assembly with 5, 20 and 150 mm mesh, respectively (Dual Manufacturing Co., Chicago IL, USA), de-chorionated by submersion in 1:1 commercial bleach:water (Clorox) for 90 s then rinsed 3-4 min in tepid flowing tap water. Prepared embryos were flash-frozen in liquid nitrogen for storage prior to quantitative assays or preserved via paraformaldehyde (4 %) fixation and heptane/methanol extraction, as described previously (Lécuyer *et al*., 2008; Hughes *et al.*, 1996), for storage prior to qualitative assays. Commercial fly strains used in this study were obtained from the Bloomington *Drosophila* Stock Center (BDSC) and the Kyoto Stock Center, the latter via the Drosophila Genomic Resource Center (DGRC). Table 3 summarizes the commercial fly strains used.

Table 3. Commercial *Drosophila* strains and their features.

Genotype	Source	Features
w^{1118}	BDSC	White eyes; accepted laboratory substitute for wild-type
w^{-}; *CyO*	BDSC	2nd chromosome balancer marked by curly wings
w^{1118}; sna^{Sco}/*CyO*, P{ActGFP.w[-]}CC2	BDSC	2nd chromosome balancer marked by curly wings and GFP
w^{*} y^{1}; Mi{$y^{+mDint2}$=MIC}*Pex7*	BDSC	P-element insertion in *Pex7* marked by wild-type *yellow* gene
w^{*}; P{$w^{+mW.hs}$-$elav^{C155}$}; P{$y^{+t7.7}$ w^{+mC}-UAS-Cas9.P2}attP40/*CyO*	BDSC	Permits *elav*-targeted, UAS-controlled Cas9 expression
w^{*}; P{$y^{+t7.7}$ w^{+mC}-UAS-Cas9.P2}attP40/*CyO*; P{$w^{+mW.hs}$-pnr^{MD237}}/*TM6B*, Tb^{1}	BDSC	Permits *pnr*-targeted, UAS-controlled Cas9 expression
y^{1} sc^{*} v^{1}; P{$y^{+t7.7}$ $v^{+t1.8}$-QUAS sgRNA}attP40/*CyO*	BDSC	Expresses QUAS sgRNA for CRISPR mutagenesis
y^{1} sc^{*} v^{1}; *P{$y^{+t7.7}$ $v^{+t1.8}$-Pex7sgRNA}attP40/CyO*	BDSC	Expresses *Pex7* sgRNA for CRISPR mutagenesis
y^{1} sc^{*} v^{1}; *P{$y^{+t7.7}$ $v^{+t1.8}$-Pex14sgRNA}attP40/CyO*	BDSC	Expresses *Pex14* sgRNA for CRISPR mutagenesis
w^{*} y^{*}; *P{w^{+mC}-UASp-Pex7}attP40*	BDSC	Expresses *Pex7* coding sequence under control of UAS
w^{*} y^{*}; *P{w^{+mC} -UASp-Pex1}; $Pex1^{*}$/TM6, Tb*	BDSC	Expresses *Pex1* coding sequence under control of UAS; contains balanced *Pex1* null mutant
w^{67c23} y^{1}; *P{w^{+mC}=GSV6}GS15386/Sb^{1}, Ser^{1}, TM3*	DGRC	P-element insertion in *Pex14*; used for its 3rd chromosome balancer

For survival assays, five virgin females were mated to three age-matched males, ±24 h, for 4 d after which the adults were discarded. Virgin females contained one or more of *CyO*, *CyO*-GFP and/or Sb^{1} Ser^{1} *TM3* balancer chromosomes, as appropriate. Crosses for survival assays were housed in Fisherbrand Drosophila Vials (ThermoFisher) filled previously 3-4 cm high with standard cornmeal medium. For egg/larva counting assays, ten virgin females were mated to eight age-matched males, ± 24 h, for 4 d after which the adults were discarded. Crosses for egg/larva counts were housed in clear, round embryo collection cages 35 mm in diameter (Genesee Scientific) atop 35 x 10 mm Petri dishes (ThermoFisher) containing apple juice agar medium (CSH Protocols, 2011) supplemented with fresh yeast paste. Dishes were changed after 48 hrs and the number of eggs was counted. The plates were then aged 48 h, upside-down, and hatched larvae were counted.

2.3 Plasmid construction for reporter fusion proteins

Plasmids bearing coding sequences of genes of interest for the screen detailed in Chapter Four were purchased from the FlyBi Drosophila ORFeome, vFB5.52, maintained by the Arizona State University plasmid repository (DNASU.org). These plasmids were used as templates for dsRNA synthesis via intermediate dsDNA synthesis, and as source for LR Clonase-mediated ORF transfer into compatible destination reporter plasmids of the Drosophila Gateway vector collection (DGRC). Destination plasmids used were pARW for live cell imaging, and either pAFW or pAMW for fixed sample imaging. pARW encodes a fusion reporter expressed under an actin promoter with an RFP monomer at the N-terminus followed by the desired coding sequence. pAFW and pAMW encode fusion reporters expressed under actin promoters with a 3x FLAG tag or a Myc tag, respectively, at the N-terminus followed by the desired coding sequence.

2.4 Transfection, transformation, DNA cloning and dsRNA treatment

Confluent cultures of S2 cells were counted via hemocytometer and spun at 1000 rcf (5 min). The supernatant was discarded and the pellet was re-suspended at 5 x 10^{6} cells ml^{-1} in fresh serum-free medium. 100 µl new cell suspension was aliquoted into each well of an 8-well slide

(Nunc Lab-Tek II Chamber Slide System, ThermoFisher) and 2.5 µg dsRNA was added to each aliquot. Cells sat 30 min then 300 µl fresh serum-free medium was added to each well. Samples were incubated 72 h and either imaged directly or fixed and prepared for indirect immuno-fluorescence (IF), depending on the reporter employed.

For transient over-expression, confluent cultures of S2 cells were counted and spun as above, then diluted to 2.5 x 10^6 cells ml^{-1} and aliquoted into an 8-well slide at 500 µl per well. Plasmid transfection was performed with Effectene transfection reagent (Qiagen) per manufacturer's protocol, using the volumes formulated for 24-well plates and adherent cells. Samples were incubated 72 h and either imaged directly or fixed and prepared for IF.

For DNA cloning, transformation of competent *E. coli* with engineered plasmids was performed as described (Inoue *et al*., 1990) using an in-ice incubation time of ten minutes following plasmid addition. Plasmid recovery and purification were performed via QIAGEN plasmid purification following manufacturer's protocol, using mini-prep or maxi-prep volumes as required (Qiagen).

2.5 Cell fixation and immunofluorescence

Phosphate-buffered saline (PBS) was prepared at 1x dilution (CSH protocols, 2006). Following treatment protocol, S2 cells were fixed 10 min in 4 % paraformaldehyde (w/v, PBS), washed 2 min in 0.05 % PBT, permeablized by washing 3 min in 0.1 % PBT then blocked 1 h in 3 % v/v BSA (PBS). The blocking reagent was removed by pipetting, cells were washed 2 x 2 min in 0.05 % PBT, incubated in primary antibody (0.3 % BSA in PBS) for either 1 h at room temperature or overnight at 4 °C, then washed 2 x 2 min in 0.05 % PBT. Cells were incubated in secondary antibody (0.3 % BSA in PBS) for 2 h at room temperature, washed 3 x 2 min in 0.05 % PBT then mounted in 75 µl ProLong Gold anti-fade mountant (ThermoFisher). Primary antibody dilutions were optimized from a baseline of 1:500, with a value from 1:250 to 1:1000 usually sufficient. Secondary antibody dilutions were optimized from a baseline of 1:2000, with a value from 1:1000 to 1:5000 usually sufficient.

2.6 *D. melanogaster* transgenic strain generation and verification

2.6.1 φC31 germline integration

For targeted somatic over-expression, a novel UAS-*Pex7* transgenic strain was established using the plasmid pPMW-attB-*Pex7*. The plasmid was derived from pPMW-attB (Addgene, contributor F Perronet) and pENTR-*Pex7* (gift of M. Anderson-Baron; Baron *et al.*, 2016) using LR Clonase II (ThermoFisher). The derived plasmid was injected into the embryonic pole cells of BDSC strain 24482, whose base genotype is y^1 M{*vas*-int.Dm}ZH-2A w^*; M{3xP3-RFP.attP'}ZH-51C (BDSC), with germline genomic integration accomplished via ΦC31 Integrase (BestGene; Bischof *et al*., 2007; Bateman *et al*., 2006). The derived plasmid bore a mini-*w* gene, permitting transformant selection by eye colour. Somatic over-expression of UAS-*Pex1* was used as a positive control because it is a conserved *Peroxin* that affects Pex5-mediated import of PTS1 client proteins (Mast *et al.*, 2011; Ciniawsky *et al*, 2015; Baron *et al.*, 2016). A strain bearing un-expressed UAS-*Pex7* was used as the negative control.

To confirm the UAS-*Pex7* transgene was expressed in *Pex7* mutant strains, adult flies of the appropriate strain were collected and stored for 1 h in disposable transparent 8 oz. bottles (ThermoFisher) then transferred to a fresh bottle and frozen overnight at -80 °C. Following total gDNA extraction, verification of the UAS-*Pex7* and MiMIC insertions was performed by PCR amplification using Phusion High-Fidelity DNA polymerase (ThermoFisher) in 50 µl volumes per manufacturer's protocol. The targets were a 1.5 kb fragment from the MiMIC transposon eGFP sequence, inserted 35-37 bp from the 3' end of the third *Pex7* exon (Nagarkar-Jaiswal *et al*., 2015) and a 9 kb fragment corresponding to the sequence of the UAS-*Pex7* cassette (Bischof *et al*., 2007). Primer specificity within the fly genome was verified using NCBI BLAST (Geer *et al*., 2010).

Primers used:

MiMIC: 5'-TTGGAATCTGGAGCGTGGTGAG, 5'-ACTTGTACAGCTCGTCCATG
UAS-*Pex7*: 5'-CGGCTCTCGCAAATGCCAGCAG, 5'-CCTTCTAGACGACCAGATCAC

2.6.2 TRiP-CRISPR targeted somatic mutagenesis

Parent strains bearing complementary TRiP-KO constructs were mated to produce progeny in which *Pex7* knockout was directed to neurons (*elav*-Gal4) or the developing PNS (*pnr*-Gal4; Gratz *et al.,* 2015; Lin *et al.,* 2015). Somatic knockout of *Pex14* was used as a positive control as it is a conserved *Peroxin* whose loss prevents import of PTS1 proteins (Mast *et al*., 2011; Baron *et al*., 2016; reviewed by Fujiki, 2016; Table 1). Somatic knockout of the *N. crassa* gene QUAS, which has no known fly homolog, was termed "Scramble" and served as the negative control (Gratz *et al.,* 2015).

2.7 Custom antibody generation and verification

Two adult rabbits were injected with the peptide EQNSNTNSSSTDGQSLGELC, corresponding to predicted *Drosophila* Pex7 residues 46-65. Crude serum was isolated from each final bleed, combined and further purified by affinity chromatography against the original peptide (Pacific Immunology). Purified anti-Pex7 was delivered at a concentration of 0.2 µg/µl (Pacific Immunology). The specificity of the purified antibody was confirmed by western blotting of lysates made from *E. coli* cell strain BL21-DE3 expressing glutathione-s-transferase (GST)-*Pex7*, lysate of S2 cells expressing FLAG-*Pex7*, then lysate of staged w^{1118} embryo collections. GST-*Pex7* was expressed by transformed pDEST15-*Pex7* and FLAG-*Pex7* was expressed by transfected pAFW-*Pex7*. These plasmids were subcloned from pENTR-*Pex7* (Gift of M Anderson-Baron) and either pDEST15 or pAFW (DGRC), respectively, via LR Clonase II (ThermoFisher) following manufacturer's protocol.

2.8 Embryo fluorescent *in situ* hybridization

Digoxigenin-labeled anti-sense RNA probes to each *Pex* mRNA were incubated with staged collections of preserved w^{1118} embryos using fluorescent *in situ* hybridization (FISH). Plasmids containing cDNA clones of *Drosophila Pex* genes (Baron *et al.*, 2016) were used as probe templates. The pattern of *wg* mRNA expression served as control (Baker, 1988). Embryo preparation, probe preparation and FISH were performed as described (Wilk *et al*., 2010;

Lécuyer *et al.*, 2008; Hughes *et al*., 1996). Probe synthesis used the Roche DIG RNA Labeling Kit (Millipore-Sigma) and fluorescent signal was generated via tyramide signal amplification (TSA) using Cyanine-3 Tyramide Reagent (PerkinElmer). For embryos over 16 h old, an additional permeabilization step was added between the first post-fixation step and Proteinase K incubation. An adaptation of a solvent mix published previously (Rand *et al*., 2010), composed of 900 µl (R)-(+)-Limonene (technical grade, Sigma-Aldrich), 50 µl Cocamide DEA (85 % v/v, BiOrigins) and 50 µl Tween-20 (20 % v/v, Sigma-Aldrich), was diluted 1:100 in autoclave-sterilized, 0.22 µm-filtered 1x PBS. Embryos were incubated 10 min in the dilution, washed 3x 5 min in autoclave-sterilized, 0.22 µm-filtered 1x PBS then returned to the FISH protocol.

2.9 Embryo protein analysis

Embryo protein detection by indirect immunofluorescence (IF) was performed as described (Hughes *et al*., 1996). Semi-dry western blotting was performed with a Trans-Blot Turbo transfer system (Bio-Rad) and imaged with an Odyssey infrared imaging scanner (LI-COR Biosciences). Relative, same-lane band intensity was quantified with Odyssey V3.0 software (LI-COR Biosciences). For IF detection of endogenous Pex7 in embryos older than 16 h an additional post-rehydration permeabilization step was performed (see section 2.8). Mouse monoclonal primary antibodies anti-βTub56D (E7, contributor M Klymkowsky), anti-Elav (9F8A9, contributor GM Rubin), anti-Nrg (BP 104, contributor C Goodman), anti-Repo (8D12, contributor C Goodman) and anti-Wg (4D4, contributor SM Cohen) were obtained at supernatant concentration from the Developmental Studies Hybridoma Bank (DSHB). The fluorescent secondary antibodies used were donkey anti-mouse-AlexaFluor488 (ThermoFisher), donkey anti-mouse-AlexaFluor690 (ThermoFisher), donkey anti-rabbit-CF555 (Millipore-Sigma/Merck) and donkey anti-rabbit-AlexaFluor780 (ThermoFisher). For embryo IF, primary antibodies were optimized from a baseline dilution of 1:20, with a value from 1:10 to 1:100 usually sufficient. Secondary antibodies were optimized from a baseline dilution of 1:100 with a value from 1:50 to 1:250 usually sufficient. For western blotting, primary antibodies were optimized from a baseline dilution of 1:1000 with a value from 1:500 to 1:2000 usually sufficient. Secondary antibodies were optimized from a baseline dilution of 1:5000 with a value from 1:2500 to 1:5000 usually sufficient. For relative protein quantification, *P* values for each time point were determined

independently using a paired, two-tailed t-test comparing the pooled replicate change ratios at each time point to a null hypothesis of 0. The *P* value of overall change was calculated using one-way ANOVA, with post-hoc paired t-tests used to calculate the *P* values for differences between time points.

2.10 Microscopy and image processing

2.10.1 Wide field microscopy

Three-dimensional widefield images of whole-mount embryos were captured with an AxioCam HRm camera (Zeiss) using a 20x Apochromatic objective (NA = 0.75) on a Zeiss Observer.Z1 microscope controlled by ZEN 2 Blue software (Zeiss). Post-imaging data deconvolution was performed with Huygens Professional software (Scientific Volume Imaging) using X and Y sampling intervals of 189 nm, and a vertical (Z) sampling recommended by the SVI Microscopy Nyquist rate and PSF calculator (https://svi.nl/NyquistCalculator). Images were rendered into two dimensions as plan images parallel to the Z-plane from de-convolved data using Imaris software (Bitplane/Oxford Instruments) and assembled using Adobe Photoshop CS6 software, 64-bit version (Adobe).

2.10.2 Confocal microscopy

Three-dimensional images of live or fixed cells were captured with a Hamamatsu EM-CCD C9100 digital camera (Hamamatsu Photonics) using a 63x Apochromatic objective lens (NA = 1.4) on a Zeiss Observer.Z1 microscope (Zeiss) coupled to a PerkinElmer UltraView spinning disk confocal scanning unit (PerkinElmer). The apparatus was controlled collectively by Volocity 3D 6.0 software, 64-bit version (PerkinElmer). Post-imaging deconvolution was performed with Huygens Professional software (Scientific Volume Imaging) using X and Y sampling intervals of 42 nm and a vertical (Z) sampling interval of either 100 or 125 nm. Images were rendered into two dimensions as plan images parallel to the Z-plane from de-convolved data using Imaris software (Bitplane/Oxford Instruments) and assembled using Adobe Photoshop CS6 software, 64-bit version (Adobe).

2.11 Semi-quantitative, real-time, reverse transcription polymerase chain reaction

Total RNA was isolated from samples stored ≥ 24 h at -80 °C via chloroform/phenol-guanidinium isothiocyanate extraction (TRIzol, ThermoFisher). Total cDNA was transcribed using the iScript Select cDNA synthesis kit (BioRad). Primers were designed using Fly PrimerBank (Hu Y *et al*., 2013) and verified for target specificity within the fly genome using NCBI Basic Local Alignment Search Tool (BLAST; Geer *et al*., 2010). Primers were synthesized by Integrated DNA Technologies (Iowa, USA). Two primer pairs for each gene passed validation for amplification efficiency by serial primer dilution (Livak and Schmittgen, 2001).

Validated primers:

Pex7-1: 5'-ATGCAGACACAGACACACACC, 5'-CAGCAAGTAGTTAGCCTCGAAAG
Pex7-3: 5'-CCAACACAAATTCCTCATCCACA, 5'-GTCGAACAATCCATCGGACCA
Act5C-2: 5'-AGCGTGAAATCGTCCGTGAC, 5'-GCAAGCCTCCATTCCCAAG
Act5C-3: 5'-AGGCCAACCGTGAGAAGATG, 5'-GGGGAAGGGCATAACCCTC

Individual reactions totaled 20 µl and used 100 ng raw cDNA as template. *Act5C* was the positive control and primer-less reaction was the negative control. PCR reactions were carried out with SYBR Green PCR Master Mix (Applied Biosystems/ThermoFisher) in black, semi-skirted 96-well "twin.tec" real-time PCR plates (Eppendorf) using a Mastercycler Realplex2 EP gradient S thermal cycler (Eppendorf). Experimental and control replicates were carried out on the same plate using aliquots of the same reaction mix. The thermal cycle program used was 2 min at 98 °C, 40x (15 s at 98 °C, 60 s at 61.5 °C), then a melting curve from 55-98 °C. *Pex7* mRNA abundance was measured relative to that of *Act5C* using the $\Delta\Delta C_t$ method (Livak and Schmittgen, 2001) and presented as mean ± standard deviation (SD; Table 1). *P* values for individual time points were determined using a paired, two-tailed t-test by comparing the 2-4 h AEL baseline ΔC_t value to that of each subsequent time point, independently, with a null hypothesis of no change. The *P* value of overall change was calculated using one-way ANOVA, with post-hoc paired t-tests used to calculate the *P* values for differences between time points.

2.12 DNA sequence identity and protein homology prediction

Percent identity matrices (PIMs) were generated by Clustal Omega multiple sequence alignment (Madeira *et al*., 2019) using data acquired from databases curated by the NCBI (Geer *et al*., 2010) and UniProt (The UniProt Consortium, 2018). Protein sequences were aligned using EMBOSS Needle (Rice *et al.*, 2000; Li W *et al*., 2015). Protein domains were predicted using NCBI Conserved Domain Search (Marchler-Bauer *et al*., 2017).

2.13 Generation of dsRNAs

Plasmids containing ORFs of target genes were used as templates for PCR amplification of dsDNA fragments using primer pairs appended at each 5' end with the T7 RNA polymerase promoter sequence TAATACGACTCACTATAG. Two primer pairs (three, in the case of *vvl*) were generated using the Drosophila RNAi Screening Center (DRSC) SnapDragon tool (www.flyrnai.org) and the third (or fourth) was from one of two previous screens (Foley and O'Farrell, 2004; A Magico, unpublished data). In the following list, the primer pairs generated elsewhere are the last pair listed for each gene.

Primers used:

Acam
1: 5'-CAGTTCGACAAGGAGGGAAC-3', 5'-CCTCGTAGTTGATCATGCCA-3'
2: 5'-TGAGTGTTCAGTGACCCCAA-3', 5'-TGATGTGAAGGAAATCGCTG-3'
3: 5'-ATCAAGATGTCCGAACTAACGG-3', 5'-TATCATCCATACGAATTCCTCG-3'

aurB
1: 5'-AACAACAAGCGCAGGACTCT-3', 5'-ACAAATGCGATGGGTAGGAG-3'
2: 5'-TATCTGGTGGCCATGAAGGT-3', 5'-ATTCGCCACTTGGTAGGTGT-3'
3: 5'-AATTTGGACGTGTCTACTTGGC-3', 5'-GATCTTGCTGTAGGTGCTCTCC-3'

borr

1: 5’-TGTGAACATACCCATTCGGA-3’, 5’-GCCGTACACTTGGATATGA-3’

2: 5’-AGCGGACAAACTCGAAAAGA-3’, 5’-CAGCGAATCGATGCTGATAA-3’

3: 5’-CACTCATGGACATCGAGGC-3’, 5’-GATACCAAAGAACTCCAAACGC-3’

Cdk1

1: 5’-AAATACATGGATTCGCTGCC-3’, 5’-GAATAGCGGCTTTCTCGTTG-3’

2: 5’-CCATTCTTTTCTGCCATCGT-3’, 5’-ATGCTCCAAAATGTCCTTGG-3’

3: 5’-GATGTTTTGATGGAGGAGAACC-3’, 5’-CTAAACAACTGGTCAATTTCCG-3’

CG18231

1: 5’-AATCCTTCGATGACAATCGC-3’, 5’-CGTGTCAATTCGTTTATGCG-3’

2: 5’-GGCCTTCTATTCGGGATTGT-3’, 5’-GAGCATTGATTTGGCGTACA-3’

3: 5’-CATGATCAAGTCAAATCCTTCG-3’, 5’-AGTCGTGTCAATTCGTTTATGC-3’

CG7627

1: 5’-TTATGGCCAAATGGGATGTT-3’, 5’-GGCACATTTCTTCACCACCT-3’

2: 5’-TACACCCACAGTCATTCGGA-3’, 5’-CACGAAGAAGGCGAAGAAAC-3’

3: 5’-CCCGTAAGAAGGAGATAAATGC-3’, 5’-ATACGACATGGAGCCATTAACC-3’

feo

1: 5’-ACATCACCAAGAGTACGGGC-3’, 5’-TCGTCATAGCTGACACCCTG-3’

2: 5’-AACATGTCGACCCTTTCCAG-3’, 5’-GCGTTCTGATCGTTGGACTT-3’

3: 5’-CGCGTTAAGCTAGTCAATCTCC-3’, 5’-CAGCAAGATAATGCCACCG-3’

geminin

1: 5’-ATCACGGCAGAGGATCTCAC-3’, 5’-TTAGACCAGCCGTTGTGTTG-3’

2: 5’-ACCCGGCGAGAACTACTACA-3’, 5’-TTAGACCAGCCGTTGTGTTG-3’

3: 5’-ATTGCTGGCGTACAATTAGACC-3’, 5’-CAGAGGATCTCACTAGCACAGC-3’

Incenp

1: 5’-ACTCAAGGAGCCCTCACTCA-3’, 5’-GAGGAGACGGTGGTCACATT-3’

2: 5’-AAGGTCAAGGTTGAGAGCGA-3’, 5’-ACCTTCTTGGAGACCTCCGT-3’

3: 5’-ACCGAGAAATTACTCAAGGAGC-3’, 5’-GTTGTTACAGAGGAGACGGTGG-3’

nmd

1: 5’-CCAATCCAGCACAAGGATCT-3’, 5’-GATTCCCCGTACCACTTGTC-3’

2: 5’-AGCTCACAAATGGCTTCTCG-3’, 5’-TCGTGTGCATCTTTGATTCC-3’

3: 5’-CTAAGAGGGCAAGAGTTTAGCG-3’, 5’-ACATCCTGACTTACTTCCTCCG-3’

pbl

1: 5’-ACGATATCGAAGGATGTCCG-3’, 5’-AGAGCTTCTCCTTATCGCCC-3’

2: 5’-CGTCAACACAATCCGAGATG-3’, 5’-AACATTTGCGAGCCTTCCTA-3’

3: 5’-GAGATCAAGACGATCTTTGGC-3’, 5’-GTGTTGAATCCTTTAGAACGCC-3’

Pex5

1: 5’-AATCCTCTCATGCAACTGGG-3’, 5’-GCGGTTTGCTCTTTTTGTTC-3’

2: 5’-GTCTGATGTGGAGAACCCGT-3’, 5’-ACCAGGTGCTGATACTTGGG-3’

3: 5’-TTAAGGTTCATGCAACATACGC-3’, 5’-TAAGGAGTACCTGTCCAAAGGG-3’

Pex13

1: 5’-ATCAGTGCGAAAAAGCGACT-3’, 5’-AATCCACCCAGTCCACCATA-3’

2: 5’-AGCCACAACCCGAACTAATG-3’, 5’-ATTGGGATCGCTGGCTAATA-3’

3: 5’-GAGTTCCGAGACCATAACAACG-3’, 5’-CATATAAATGAACCGCTGCTCC-3’

sqh

1: 5’-TTCGACGAGGAGAATATGGG-3’, 5’-AGTTTGGACAGGCTGATTGG-3’

2: 5’-ACATGATCGACCAGAACCGT-3’, 5’-CCGATACATCTCGTCCACCT-3’

3: 5’-GTCTGTGAACCGATCACCC-3’, 5’-AGAACCACCAATCCAACAGC-3’

stg

1: 5’-GGAGGAGCTGTCGTTCTACG-3’, 5’-GATCAGCGAGTTTAGGCCAC-3’

2: 5’-CGGCTACAAGGAGTTCTTCG-3’, 5’-CGTCGTGTGCGAGAAACTTA-3’

3: 5’-GAGATCTATCTGCTGCACAACG-3’, 5’-ATGATTAAGGGGTCTGATTTCG-3’

vvl

1: 5’-GTTCTGCGTTCTGACCACTG-3’, 5’-CAATTTGCTTGGGGTTTCAC-3’

2: 5’-CTGCGGTGTTTTGAGGTTTT-3’, 5’-TCATCGACGGACCTCATCTT-3’

3: 5’-CACGTCCATTGACAAGATCG-3’, 5’-CGTACCACCTCCTTCTCCAG-3’

4: 5’- CACGTCCATTGACAAGATCG-3’, 5’-TATTGTTGTTAGCCTGATTGCC-3’

Amplicon size was verified by agarose (0.8 % w/v) gel electrophoresis. Verified dsDNAs were then used as the template for dsRNA production using Ambion T7 RNA Polymerase Plus (ThermoFisher) per manufacturer’s protocol. Template DNA was removed by DNAse I addition (1:50 dilution, 15 min @ 37 °C), dsRNAs were precipitated with ethanol/sodium acetate and re-suspended in RNAse-free water, then [RNA] was determined with a NanoVue Plus spectrophotometer (Cytiva Life Sciences). dsRNA molecule size was verified by gel electrophoresis (0.8 % agarose w/v) and stored at -80 °C prior to use.

2.14 Quantification of peroxisome abundance

Three-dimensional images of fields of S2 cells were acquired and rendered as described (section 2.10.2). Peroxisome abundance was counted using Imaris image rendering software (Oxford Instruments/Bitplane). In the Imaris program, using the “Spots” function under the “3D View” menu generated a “Wizard” tool. The channel reporting GFP puncta was selected as the “spot” source data. The “Segment only a Region of Interest” command was then used to define one to three regions of interest (ROIs) per image. Each ROI corresponded roughly to one cell, subject to the limitation of the square selection shape permitted by the software. An estimated XY diameter of 0.9 nm was selected for the GFP puncta, and due to observed stretching in the Z-channel the estimated Z-diameter was set at 0.36 nm using the “Model PSF-elongation along Z-plane” command. Once the spots were rendered, the left cutoff of the image quality histogram

was set to 1.25 and the right cutoff was set to the right terminus. The number of spots was recorded. To determine the total volume of each ROI, the X, Y and Z voxel counts for each selection were also recorded; Z values were divided by 4 to account for Z-plane stretching. The image metadata, found under the "Volume" tab of the rendered image, reported the total voxels and total volume per image (μm^3). After dividing the total volume by 4, to account for Z-plane stretching, the volume of each image's selection was computed by dividing the selection's voxel total by that of the image, then multiplying the quotient by the total volume. This produced the selection's volume. The number of spots per μm^3 was then calculated by dividing the selection's spot count by its volume. The spots per μm^3 value of each experimental replicate was then compared to that of its cognate negative control to provide a ratio of the difference, with a ratio of 1.00 ± 0.05 indicating no significant change in peroxisome abundance. For RNAi experiments, the mean of these ratios was then calculated and plotted for each dsRNA. For the over-expression experiments, the mean ratio was also calculated for a replicate-specific positive transfection control. To cancel out the effect of transfection alone on peroxisome abundance, the mean replicate:negative ratios were compared to the mean transfection:negative ratios of the same experimental batch to yield normalized mean replicate:negative ratios, which were then plotted. Again, a ratio of 1.00 ± 0.05 indicated no significant change in peroxisome abundance.

Chapter 3 Genetic characterization of *Pex7*

3.1 Hypothesis and rationale

Peroxisomal enzymes are recruited from the cytoplasm and trafficked into peroxisomes. Yeast, plants and mammals employ two cytosolic receptors to mediate protein import, PEX5 and PEX7. PEX5 identifies its cargo via a C-terminal PTS1 motif and PEX7 recognizes its cargo via an N-terminal PTS2 motif. The conserved 1° structure of PEX7 proteins is a series of six or seven WD40 domain repeats, depending on species, which *in vivo* form a series of 2° β-sheets that fold into a 3° β-propeller (Pan *et al.*, 2013; Emmanouilidis *et al.*, 2015). The *D. melanogaster* genome contains a predicted gene sequentially similar to *PEX7*, CG6486, and a fusion reporter of the presumptive protein was observed to overlap about 50 % with peroxisomes in S2 cells (Mast *et al*., 2011; Faust *et al*., 2012; Baron *et al*., 2016). However, no PTS2-bearing proteins are present in the fly proteome, and transgenically-expressed reporter fusions with a canonical PTS2 motif are not trafficked to peroxisomes in S2 cells (Faust *et al*., 2012). Not all eukaryotes conserve *Pex7* or PTS2, for example *C. elegans* and some unicellular diatoms (Motley *et al.*, 2000; Gonzalez *et al*., 2011). To contrast, *Pex7* was found to be required in *Drosophila* larvae and adult tissues, especially by brain and immune cells, suggesting *Pex7* has a function and is not an "evolutionary leftover" (Di Cara *et al*., 2017, Di Cara *et al*., 2019). *Pex7* loss does have an effect on FAO so it may have a role in peroxisome function, though an endogenous gene product has yet to be observed directly (Di Cara *et al*., 2017, Di Cara *et al*., 2019). The role of *Pex7* in *Drosophila* biology and peroxisome biogenesis remain unresolved. In this chapter I observe wildtype Pex7 transcription and translation patterns. I then explore the function of *Pex7* in *Drosophila* embryogenesis.

Hypothesis:

***Drosophila Pex7* is a protein-coding gene whose product is necessary during embryogenesis for normal nervous system development.**

3.2 Introduction

In yeast and mammals, PEX7 is a cytosolic receptor protein that targets enzymes containing the PTS2 motif for import into peroxisomes. The PTS2 motif is not present in the *Drosophila* orthologs of these enzymes yet the fly genome contains the predicted gene *Pex7* (CG6486), which has a similar sequence to yeast and human versions (flybase.org). *Drosophila Pex* transcripts, including that of *Pex7*, were found in most cells during early embryogenesis. *Pex7* mRNA was later restricted to cells similar in pattern to differentiating neurons. Neuro-specific somatic *Pex7* knockout impaired hatching. Total somatic *Pex14* knockout copied the targeted *Pex7* knockout phenotype. *Pex7* over-expression in embryonic neurons was semi-lethal at the larval stage. Ubiquitous *Pex1* over-expression copied the phenotype of neuro-specific *Pex7* over-expression. Targeted over-expression of a *Pex7* transgene in the neurons of *Pex7* homozygous loss-of-function mutants impaired hatching. These data suggest *Pex7* is necessary, but not sufficient, for *Drosophila* neural development during embryogenesis.

3.3 Results

3.3.1 Drosophila Peroxin *transcript localization in embryonic cells*

A spatial assay of the cells expressing *Pex* genes was performed on fixed embryos of strain w^{1118} collected 2-4 and 4-8 h after egg laying (AEL; Figure 4), using FISH to detect endogenous *Pex* mRNAs. Embryos not incubated with a probe served as the negative control (Figure 4A) and a FISH probe for the *wingless* (*wg*) mRNA served as the positive control (Figure 4B). *Drosophila* embryogenesis begins with the fusion of parental pronuclei into one diploid nucleus. The embryo, colloquially “egg”, is deposited on or near a food source as this occurs. The first stage of embryogenesis is the successive division of the nucleus, without cytokinesis, into many nuclei within a common cytoplasm in a layer at the outer layer of the embryo. This developmental stage is called the syncytium or syncytial blastoderm (Hartenstein, 1993). At the core of the syncytial blastoderm is a lipid rich yolk that contains polyploid yolk nuclei, deposited by maternal nurse cells, whose function is to metabolize the yolk into the macromolecules necessary to complete embryo-genesis.

A FISH signal corresponding to *Pex1* mRNA was observed in the yolk in early embryos (Figure 4C, left). The intensity of *Pex1* FISH signal was relatively close to background levels after cellularization (Figure 4C, right). The majority of *Pex3* FISH signal was observed at the cortex as the embryo nuclei began to compartmentalize into cells (Figure 4D, left). The pattern of *Pex3* FISH signal became ubiquitous at the onset of gut formation (Figure 4D, right). The majority of the *Pex5* mRNA FISH signal in the early embryo was observed in the yolk and at the cortex (Figure 4E, left). By 4 h AEL the *Pex5* FISH signal was indistinguishable from the negative control, suggesting it was below the detection threshold (Figure 4E, right). *Pex6* FISH signal was observed in the yolk and at the cortex of the syncytial blastoderm (Figure 4F, left). During gastrulation the *Pex6* FISH signal appeared similar to background (Figure 4F, right). Early during embryo development, the pattern of *Pex7* FISH was similar to that of *Pex6* (Figure 4G, left) however it persisted during gastrulation (Figure 4G, right). The FISH signal corresponding to *Pex10* mRNA was concentrated at the outer (cortical) layer in early embryos (Figure 4H, left); an anterior-ventral pattern of *Pex10* FISH signal was observed following cephalization (Figure 4H, right). The overall pattern of *Pex11* mRNA FISH in early embryos was similar to *Pex10* but with fewer individual foci (Figure 4I, left). Following cephalization, the *Pex11* FISH signal was seen in the developing mesoderm and posterior midgut rudiment (Figure 4I, right). The *Pex13* FISH signal was ubiquitous in the syncytial blastoderm and yolk (Figure 4J, left). During midgut development, *Pex13* FISH signal was concentrated in the head, midgut and within the dorsal germ band (Figure 4J, right). In embryos where blastoderm cellularization was occurring, the *Pex14* FISH signal was observed in the yolk and outer (cortical) layer (Figure 4K, left). Later, during gastrulation, the *Pex14* FISH signal was observed in complementary compartments to that of *Pex13*, localizing to the mesoderm (Figure 4K, right; Hartenstein, 1993). Notably, no *Pex14* FISH signal above that of background was observed in the posterior midgut rudiment or pole cells. The *Pex16* FISH signal was ubiquitous around 2-4 h AEL (Figure 4L, left). During midgut development, *Pex16* FISH signal was restricted primarily to the elongating germ band and head primordium (Figure 4L, right). The *Pex19* FISH signal was observed in the yolk and a para-segmental pattern in the outer (cortical) layer of early embryos (Figure 4M; Nüsslein-Volhard and Wieschaus, 1980). After cephalization the *Pex19* FISH signal was restricted to the posterior midgut rudiment and germ band (Figure 4M, right).

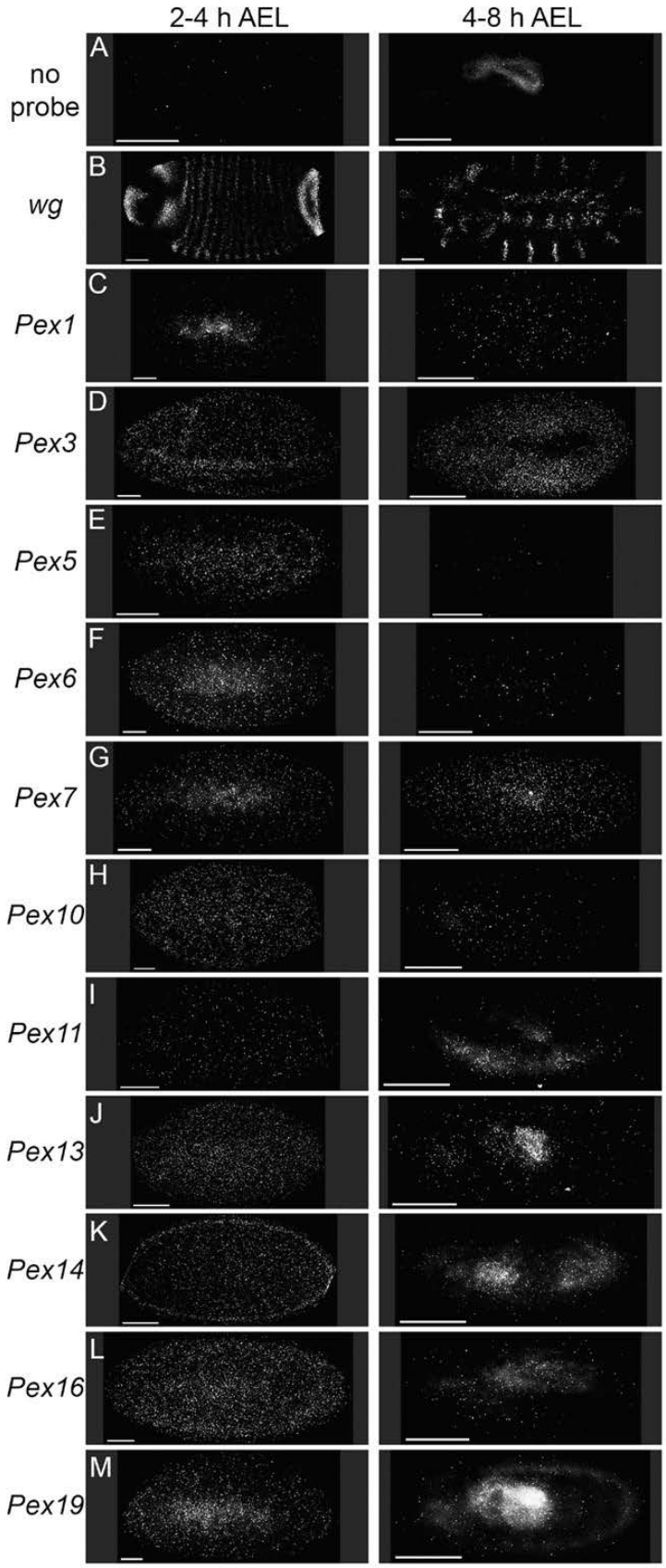
2-4 h AEL
4-8 h AEL
A
no probe
B
wg
C
Pex1
D
Pex3
E
Pex5
F
Pex6
G
Pex7
H
Pex10
I
Pex11
J
Pex13
K
Pex14
L
Pex16
M
Pex19

Figure 4. The location of transcripts encoded by *Drosophila Pex* genes during early embryogenesis. Anterior is left, dorsal is up. (A) Un-probed controls reported non-specific signal and auto-fluorescence. (B) The segmental pattern of *wg* mRNA was the positive control (Baker, 1988). (C) *Pex1* FISH signal was in the yolk in early embryos (left) and was ubiquitous but close to background levels after cellularization (right). (D) Most *Pex3* FISH signal was cortical at cellularization (left) then ubiquitous during gut formation (right). (E) A *Pex5* FISH signal was observed in the embryo yolk and at the cortex in early embryos (left). By 4 h after egg laying (AEL) the *Pex5* FISH signal was below the detection threshold (right). (F) *Pex6* FISH signal was seen in the yolk and at the cortex of the syncytial blastoderm (left) and was close to background during gastrulation (right). (G) *Pex7* FISH signal showed similar patterning to that of *Pex6* in early embryos (left). The pattern was maintained in embryos undergoing gastrulation (right). (H) The *Pex10* FISH signal was concentrated cortically in early embryos (left). An anterior-ventral pattern was observed after cephalization (right). (I) The pattern of *Pex11* FISH was similar to *Pex10* but with fewer foci (left). Following cephalization, FISH signal was seen in the developing mesoderm and posterior midgut rudiment (right). (J) *Pex13* FISH signal was ubiquitous in the syncytial blastoderm and yolk (left). During midgut development (right), *Pex13* FISH signal was seen in the head, midgut and within the dorsal germ band. (K) During blastoderm cellularization, *Pex14* FISH signal was seen in the yolk and outer cortical layer (left). During gastrulation (stages 9-11), the *Pex14* FISH signal pattern was opposite to that of *Pex13*, localizing to the mesoderm (Hartenstein, 1993). No *Pex14* FISH signal was seen in the posterior midgut rudiment or pole cells (right). (L) *Pex16* FISH signal was ubiquitous in early embryos (MZT, left). The signal was restricted to the elongating germ band and head primordium during midgut development (right). (M) At 2-4 h AEL (left), *Pex19* FISH signal was strongest in the yolk and was also seen in para-segmental cortical stripes. After cephalization (right) the *Pex19* FISH signal was restricted to the posterior midgut rudiment and germ band. Scale bars = 50 μm, n = 3. All images are maximum intensity Z-projections.

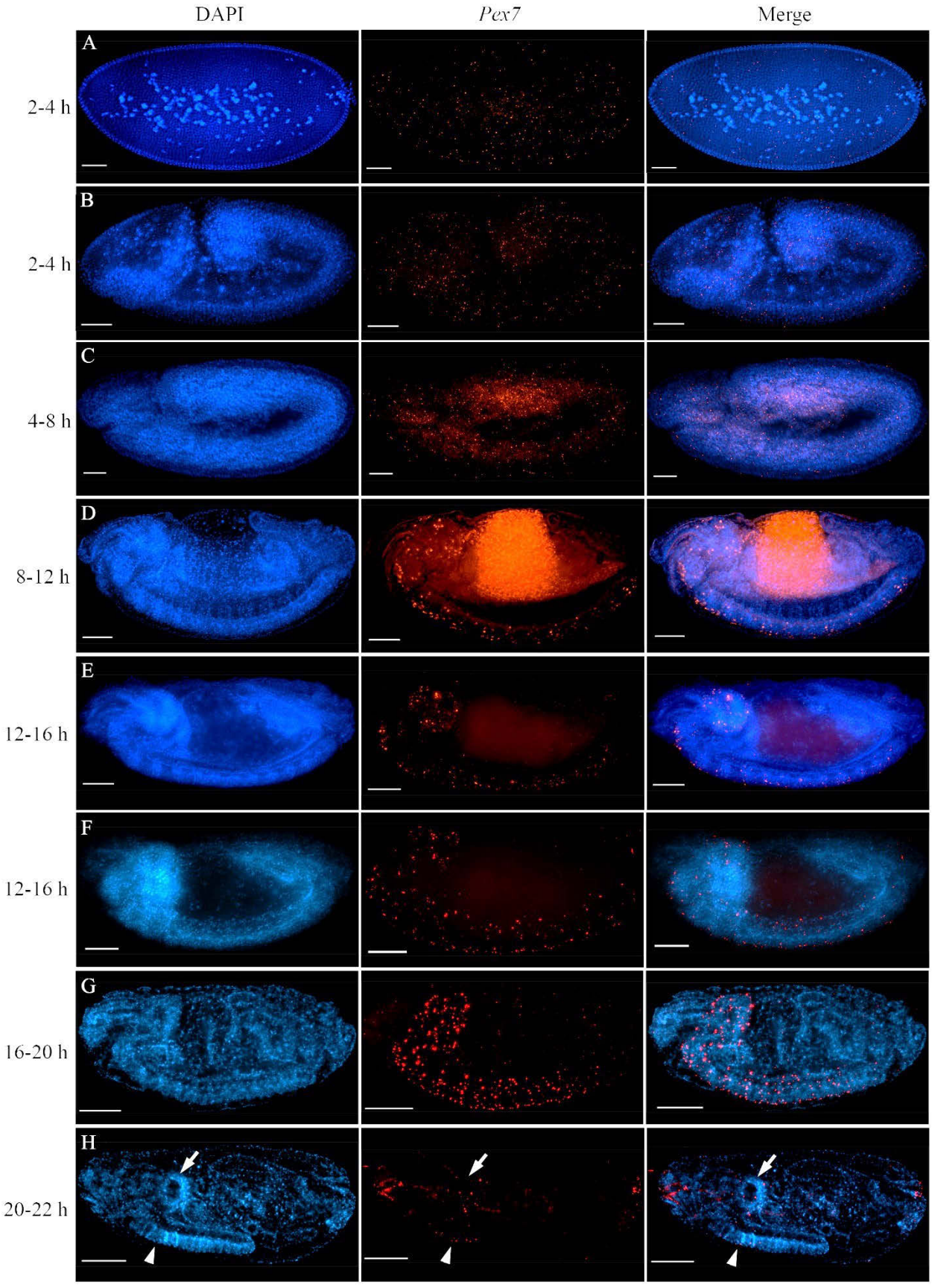
DAPI
Pex7
Merge
A
2-4 h
B
2-4 h
C
4-8 h
D
8-12 h
E
12-16 h
F
12-16 h
G
16-20 h
H
20-22 h

Figure 5. *Pex7* mRNA localization during embryogenesis. Anterior is left, dorsal is up. (A) At 2-4 h after egg laying (AEL) a specific *Pex7* FISH pattern was seen in both the yolk and the syncytium, without overlapping nuclei. (B) Following anterior-posterior axis formation and cephalization, *Pex7* FISH signal was reduced in the yolk. (C) The *Pex7* FISH signal became ubiquitous following formation of the anterior-posterior axis and cephalization. (D) By 8 h AEL, the *Pex7* FISH signal was localized to the supra-oesophageal ganglion and ventral nerve cord of the CNS. (E) The CNS pattern of *Pex7* FISH signal persisted through 16 h AEL. (F) The CNS pattern of *Pex7* FISH signal was unchanged from the previous time point. (G) At 16-20 h AEL, the *Pex7* FISH pattern was most elaborate with many foci in the brain and ventral nerve cord. (H) ~20 h AEL, the *Pex7* FISH signal was restricted to the optic lobes (arrows) and a few foci in the anterior half of the ventral nerve cord (arrowheads). Scale bars = 50 μm, n = 3. All images are maximum intensity Z-projections.

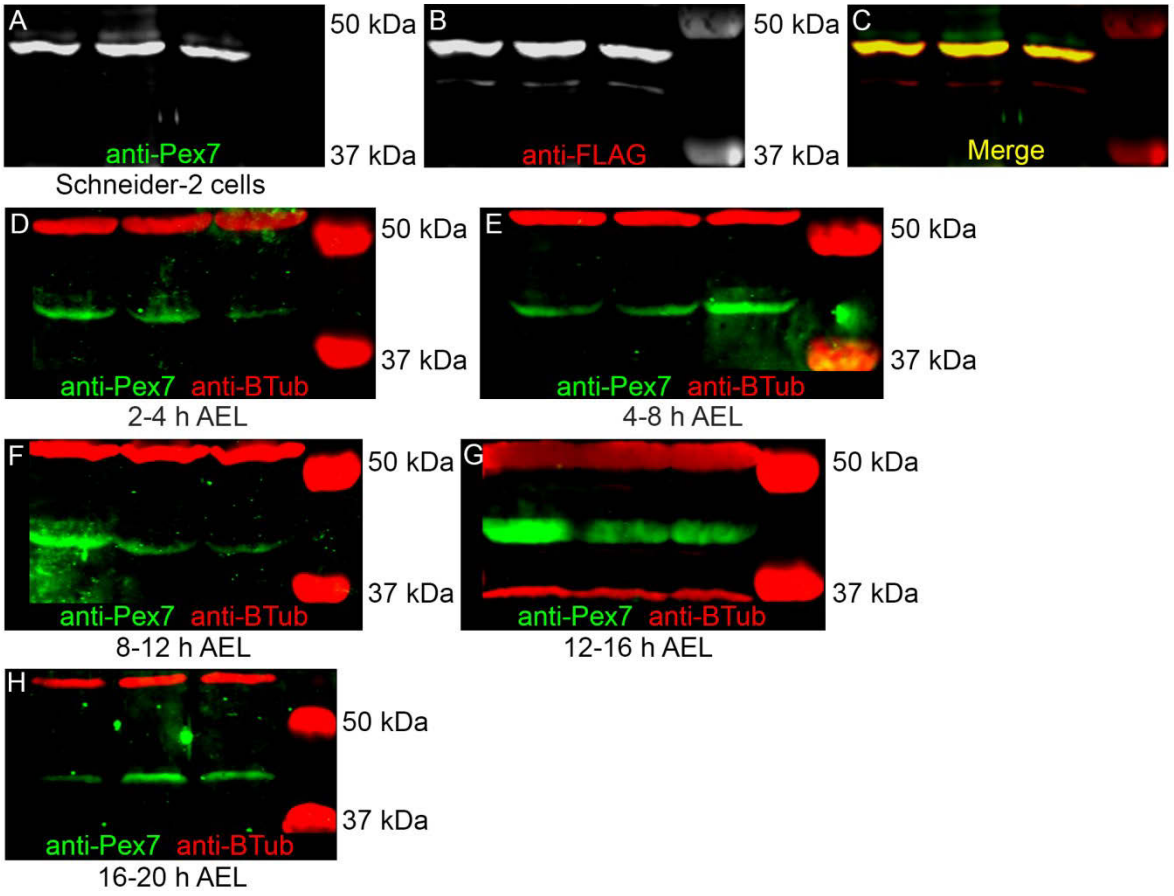

Figure 6. *Pex7* is translated in the developing embryo. (A-C) Specificity of a novel Pex7 antibody was confirmed by western blotting. Bands at far right of each image are ladder bands. Novel anti-Pex7 and anti-FLAG recognized a 3xFLAG-Pex7 fusion protein expressed in *D. melanogaster* Schneider-2 (S2) cells at about 48 kDa. D-H: Blots of lysates from w^{1118} embryos collected at (D) 2-4 h, (E) 4-8 h, (F) 8-12 h, (G) 12-16 h and (H) 16-20 h after egg laying (AEL) were probed with anti-Pex7. A band of about 43 kDa was recognized in all blots (lower green bands). Loading control anti-βTubulin recognized a protein of about 56 kDa (upper red bands). The lower red bands in panels C and G are non-specific. Images D-H are representative images of the western blots used to calculate relative protein abundance in Figure 9B.

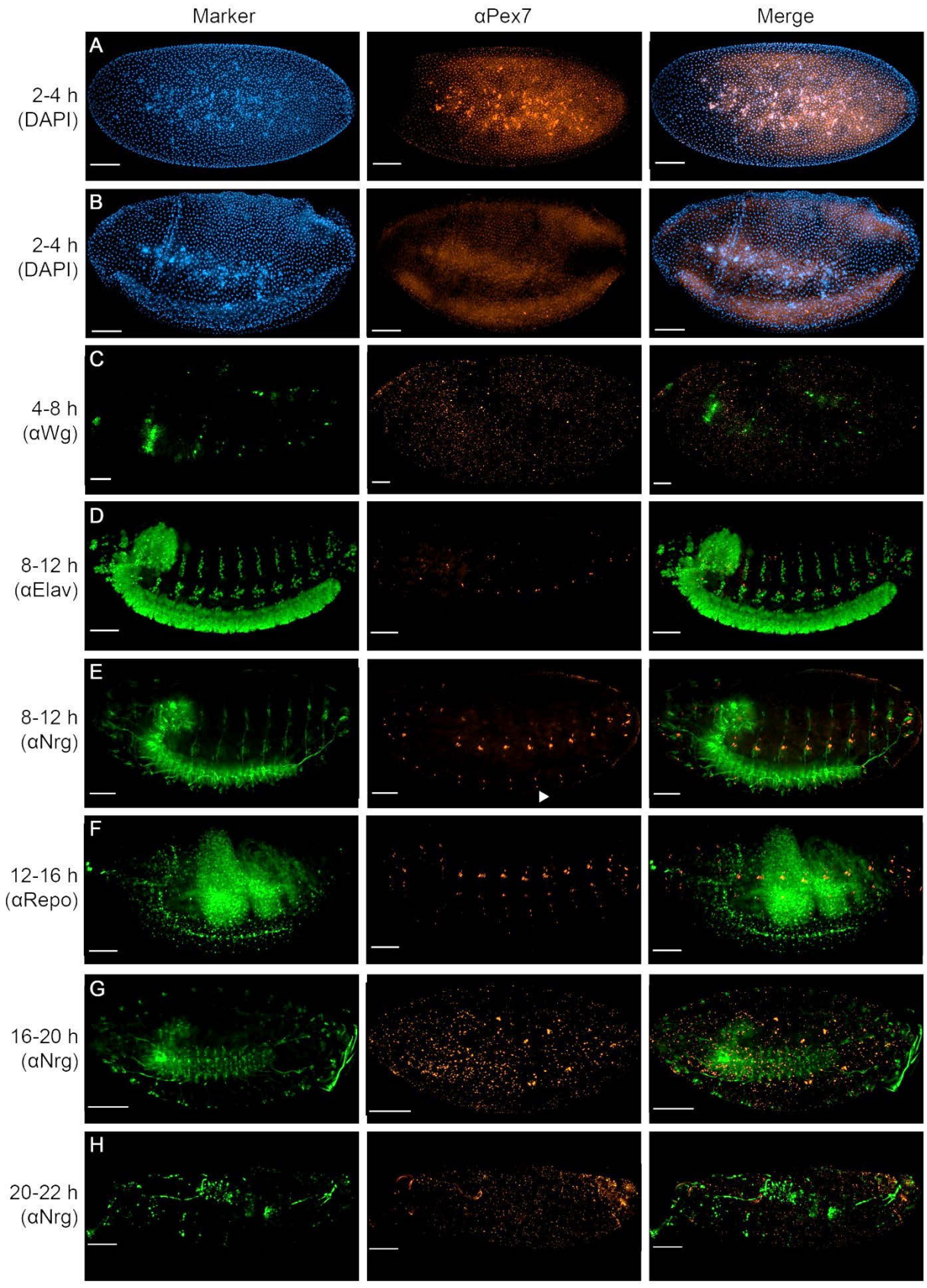
Marker
αPex7
Merge
A
2-4 h
(DAPI)
B
2-4 h
(DAPI)
C
4-8 h
(αWg)
D
8-12 h
(αElav)
E
8-12 h
(αNrg)
F
12-16 h
(αRepo)
G
16-20 h
(αNrg)
H
20-22 h
(αNrg)

Figure 7. The dynamic pattern of cells translating Pex7 during *Drosophila* embryogenesis. Images display anti-Pex7 and various cell marker antibodies detected by indirect immunofluorescence (IF). Anterior is left, dorsal is up. (A) At 2-4 h after egg laying (AEL), the signal from anti-Pex7 was strongest amid polyploid yolk nuclei. (B) Following cephalization the anti-Pex7 signal was at or below background fluorescence. (C) During germ band elongation (4-8 h AEL), the anti-Pex7 signal was ubiquitous and did not overlap that of anti-Wg. (D) At 8 h AEL the anti-Pex7 pattern was para-segmental, adjacent to differentiating neurons marked by anti-Elav without overlapping. (E) By 12 h AEL the anti-Pex7 signal remained para-segental and appeared in the ventral nerve cord (E, arrowhead). The anti-Pex7 signal was adjacent to that of anti-Nrg without overlapping. (F) The cells with the highest levels of anti-Pex7 signal remained within each para-segment through 16 h AEL, adjacent to but not overlapping the glial marker anti-Repo. (G-H) By 22 h AEL the anti-Pex7 signal was restricted to a small group of cells within the CNS, again adjacent to anti-Nrg. All images are maximum intensity Z-projections. Scale bars = 50 μm, n = 3.

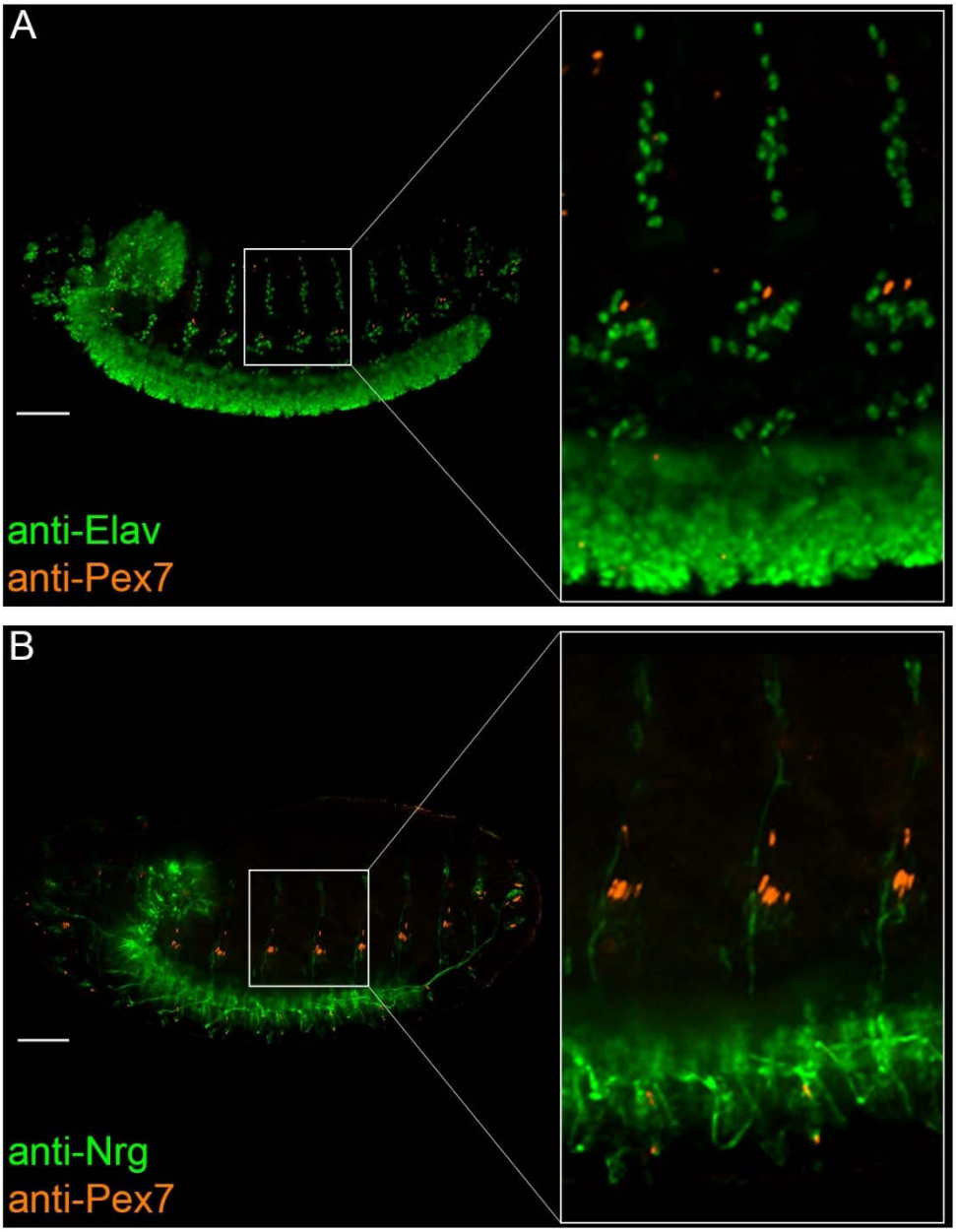

Figure 8. Detail of the adjacency between neural antibody markers and anti-Pex7. Images display anti-Pex7 and various cell marker antibodies detected by indirect immunofluorescence (IF). Embryos are aged 8-12 h after egg laying but are not synchronous. Anterior is left, dorsal is up. (A) Anti-Elav (green) marked neurons. (B) Anti-Nrg (green) marked glia. All images are maximum intensity Z-projections. Scale bars = 50 µm, n = 3.

3.3.2 Pex7 *transcript localization during embryogenesis*

Older embryos found in 4-8 h AEL collections probed via FISH were staged approximately using gross anatomy. In the case of *Pex7*, non-ubiquitous patterns were observed in these later embryos. A time-course study of the pattern of *Pex7* mRNA transcription in w^{1118} embryos was performed from 2-22 h AEL (Figure 5). Roughly 30 min after the maternal-zygotic transition (MZT) of gene transcription, *Pex7* FISH signal was observed as foci in the yolk at the centre of the embryo (Figure 5A). The foci were peri-nuclear just before syncytial cellularization (Figure 5B) then became ubiquitous following formation of the anterior-posterior axis and cephalization (Figure 5C). In embryos 8-12h AEL, *Pex7* FISH signal was restricted to the presumptive supra-oesophageal ganglion and ventral nerve cord (Figure 5D; Hartenstein, 1993). This pattern persisted until 16-20 h AEL when *Pex7* FISH signal was also observed in cells on the cortical (outer) layer of the CNS (Figure 5E-G) in a pattern most similar to neuroblasts (Hartenstein, 1993). Just prior to hatching (20-22 h AEL, Figure 5H) the *Pex7* FISH signal was restricted to the anterior half of the presumptive nerve cord (Figure 5H, arrowheads) and primitive optic lobes (Figure 5H, arrows).

3.3.3 Pex7 polypeptide localization during embryogenesis

An antibody was raised against a peptide sequence specific to *Drosophila* Pex7. A western blot of a 3xFLAG-*Pex7* fusion protein expressed in S2 cells was probed simultaneously with anti-FLAG and anti-Pex7, and showed overlapping bands at about 48 kDa (Figure 6A-C). Pex7 has a predicted mass of 37 kDa (flybase.org). The 3x-FLAG epitope is 23 amino acids and weighs 2.9 kDa (ThermoFisher), making the predicted mass of the fusion protein 40 kDa. Incubating anti-Pex7 on blots of w^{1118} embryo lysates (Figure 6D-H) reported bands at about 43 kDa. Accounting for the roughly 8 kDa of "drag" observed in the 3xFLAG-Pex7 blot, the larvae blots suggested anti-Pex7 was detecting endogenous Pex7 throughout embryogenesis. I acknowledge anti-Pex7 was not tested on *Pex7* null mutants in this study, although no true null mutants were available as of this writing. The Pex7 detected at 2-4 h AEL (Figure 6D) may have been contributed maternally or transcribed from maternally-contributed mRNA, but reported at the same approximate size as Pex7 from later time points.

Novel anti-Pex7 was then used to observe endogenous protein localization patterns during embryogenesis via IF. Beginning at 2 h AEL, Pex7 IF signal was observed in both the yolk and the syncytium (Figure 7A). At the onset of gastrulation about 3.2 h AEL, the signal was below the detection threshold (Figure 7B). At about 3.7 h AEL the signal was ubiquitous and remained so through germ band elongation, gnathal and clypeolabral lobe formation, and germ band retraction at 7.3 h AEL (Figure 7C; Hartenstein, 1993). Beginning at 4 h AEL, the Pex7 IF signal was compared by tandem IF to that of antibodies marking stage- and cell-specific proteins including Wingless (Wg), which contributes to segment polarity junctions and is necessary for morphogenesis of neuromuscular junctions (Nüsslein-Volhard and Wieschaus, 1980; Patel *et al*., 1989; Volk and VijayRaghavan, 1994; Klingensmith and Nusse, 1994), and several neuronal markers. From 7.3-9.7 h AEL the IF signal reported a para-segmental pattern from cells adjacent to those reporting the pan-neural antibody marker 9F8A9, which targets Embryonic Lethal Abnormal Vision (anti-Elav; Figure 7D). The signal did not overlap with Elav. At 12 h AEL the IF pattern appeared as para-segmental repeats of five distinct "branches" near the dorsal-ventral midline along the anterior-posterior axis, with two accompanying para-segmental foci within the ventral nerve cord (Figure 7E, middle panel, arrowhead). Some cells in the extreme anterior/posterior regions also reported IF signal at this time point. The anti-Pex7 pattern (orange) did not overlap with the CNS/PNS marker antibody BP 104, which targets Neuroglian (anti-Nrg, green), or the glial marker antibody 8D12, which targets Reversed Polarity (anti-Repo, green; Figure 7F). In 16 h AEL embryos, the anti-Pex7 pattern was similar to that of Pex7 mRNA FISH, localizing to a subset of cells on the cortical (outer) layer of the CNS (compare Figure 5G to Figure 7G). From 20 h AEL until hatching the anti-Pex7 signal was restricted to cells in the optic lobes and ventral nerve cord (Figure 7H).

3.3.4 Relative quantification of Pex7 *transcript and protein abundance during embryogenesis*

The patterns reported by Pex7 FISH and anti-Pex7 IF suggested that *Pex7* expression was subject to spatio-temporal regulation. The subtle differences in *Pex7* transcript and protein localization patterns may have resulted from post-transcriptional regulation or transport to other cells following synthesis. The latter was observed previously for *rosy* mRNA and its XDH product in flies of strain Oregon-R (Reaume *et al*., 1989). However, it is more likely the disparity

in this case was due either to levels of *Pex7* mRNA undetectable by FISH being translated into levels of Pex7 protein detectable by IF, or to differences in developmental stage not captured by my collection protocol. To resolve this, relative levels of embryonic *Pex7* mRNA and protein were quantified via qRT-PCR and fluorescent western blotting, respectively (Figure 9). The mean ΔC_t between *Pex7* and *Act5C* at 2-4 h AEL was set as the "baseline" ΔC_t and used to compare mean fold-change in transcript abundance (± SD) at subsequent time points using the $\Delta\Delta C_t$ method (Livak and Schmittgen, 2001). Mean fold-change in relative *Pex7* transcript abundance increased by 2.18 ± 0.61 at 4-8 h AEL (P = 0.0186) and 5.99 ± 1.54 by 8-12 h AEL (P = 0.00669), indicating a steady increase in *Pex7* mRNA abundance. This correlated with the increased *Pex7* mRNA FISH signal observed (Figure 5D). In 12-16 h embryos, the mean fold-change increased to 4.36 ± 1.03 (P = 0.0109). The highest relative mean fold-change was 148.21 ± 6.70 at 16-20 h AEL ($P = 2.15 \times 10^{-6}$). Notably, this is when the most elaborate pattern of cells expressing *Pex7* mRNA was observed (Figure 5G). The mean fold-change in *Pex7* mRNA was reduced to 36.59 ± 9.78 in 20-22 h AEL embryos ($P = 7.48 \times 10^{-6}$). One-way ANOVA with post-hoc analysis determined the overall fold-change in *Pex7* mRNA abundance was significant ($P = 4.5 \times 10^{-15}$), as were most differences between time points (Figure 9A). The exception was between 8-12 h AEL and 12-16 h AEL (Figure 9A).

Overall abundance of Pex7 protein in developing embryos was measured relative to γ-Tubulin in western blots via IF (Figure 9B, Table 5). Representative images of the western blots used are shown in Figure 6. In 2-4 h AEL embryos, the mean ratio of Pex7 to γ-Tubulin (±SD) was 0.060 ± 0.017 (P = 0.022). The mean ratio increased to 0.076 ± 0.017 in 4-8 h AEL embryos (P = 0.00084), decreased slightly to 0.057 ± 0.014 in 8-12 h AEL embryos (P = 0.0014), and was about the same in 12-16 h AEL embryos with a mean ratio of 0.054 ± 0.015 (P = 0.00013). The mean ratio peaked in 16-20 h AEL embryos at 0.190 ± 0.010 ($P = 6.6 \times 10^{-5}$) then was reduced in 20-22 h AEL embryos at 0.081 ± 0.008 ($P = 4.4 \times 10^{-4}$). One-way ANOVA with post-hoc analysis determined the overall change in relative Pex7 protein abundance was significant ($P = 2.11 \times 10^{-11}$) but only differed significantly between the last three time points (Figure 9B). Altogether, relative quantitation revealed the transcription and translation trends of *Pex7* were similar, suggesting the transcript-protein localization differences were not due to post-transcriptional regulation. This data also suggested that the diffuse pattern of cells observed

expressing low levels of Pex7 by IF or FISH represented a weak or ubiquitous pattern of cells with Pex7 expression below the detection threshold and not background signal.

3.3.5 The effects of targeted somatic Pex7 *mutagenesis*

The dynamic pattern of embryonic *Pex7* expression suggested it had a tissue-specific function. Homozygous adult $Pex7^{MiMIC}$ mutants had impaired negative geotaxis (climbing) and displayed a sub-lethal, semi-pharate (partially eclosed) phenotype (Di Cara *et al*., 2019; Linderman *et al.,* 2012). To determine if these phenotypes were due to affected nervous system development, as was observed for *Pex1* null mutants (Mast *et al*., 2011), targeted somatic *Pex7* mutagenesis was performed using Gal4-UAS paired with CRISPR-Cas9 (TRiP-KO). The target tissues were either post-mitotic neurons (*elav*) or sensory bristles of the PNS (*pnr*), the two neuro-specific TRiP-KO enhancers available at the time. *Pex14* was the positive control because in yeast and mammals PEX14 forms the translocon through which cargo-loaded PEX5 and PEX7 enter the peroxisome, and the fly ortholog was characterized sufficiently to suggest it conserved that function (Faust *et al*., 2012; Baron *et al.*, 2016; Meinecke *et al*., 2010). Mutant adult scores were reduced for *elav>Pex7* and *elav>Pex14* TRiP-KO crosses, as were total adults (Figure 10A, B). Neither *pnr>Pex7* nor *pnr>Pex14* knockout had an effect on mutant or total adult scores (Figure 10A, B). The negative *pnr* results may be due to inefficient knockout, which was not independently verified. Comparing the adult mutant:total ratios for *elav*-targeted knockout revealed a value approaching statistical significance for *elav>Pex7* KO ($P = 0.055$, Figure 10C). Male:total adult ratios did not vary significantly (Figure 10D), indicating no sex-specific effect was observed. The presence, and reduced score, of mutant adults suggested *elav>Pex7* KO was semi-lethal, as was observed previously for homozygous *Pex7* mutants (Di Cara *et al.*, 2019). To determine if targeted *Pex7* loss affected hatching, and thus demonstrate the phenotype was developmental, the number of hatched larva from TRiP-KO crosses was compared to the number of eggs laid. *elav>Pex7* KO resulted in significantly fewer larva 4 d after egg laying ($P = 0.047$, Figure 10E) and a significantly reduced larva:egg ratio ($P = 0.029$, Figure 10F). Loss of *Pex7* in neurons resulted in a semi-lethal phenotype that manifested at or before hatching. It is possible the phenotype was not entirely lethal because the TRiP-KO system was not 100 % efficient, as this was not verified independently.

The effect of ubiquitous and neuro-specific over-expression (OE) of *Pex7* was then compared to that of *Pex1*. In yeast, *Drosophila* and humans, PEX1 plays a key role in recycling PEX5 and PEX7 back to the cytosol after import (Table 1; Platta *et al*., 2004; Mast *et al*., 2011). A previously characterized *Drosophila* strain carrying UAS-*Pex1* was used as a positive control (Mast *et al*., 2011). The total adult and over-expressing adult scores were reduced for *elav>Pex7* and *Act5C>Pex7* OE (Figure 11A and B, respectively). Neuro-specific *Pex7* OE significantly reduced the over-expressing:total adult ratio ($P = 0.026$; Figure 11C). For *Pex1*, *Act5C*-driven OE had a significant effect ($P = 0.0017$), and it was significantly stronger than that of *Act5C>Pex7* OE ($P = 0.015$; Figure 11C). Male:total adult ratios were not affected, indicating no sex-specific effect occurred (Figure 11D). However, the *elav>Pex7* OE replicates with the lowest adult counts also had over-expressing male progeny outnumbering female progeny by 2:1, although the sex ratios of unaffected progeny from the same crosses were normal (Figure 11D). To determine when the phenotype caused by *Pex7* OE first occurred, egg and larva counts were compared. There was a reduction in the egg and larva counts under both *Pex7* OE conditions with no difference in the larva:egg ratio (Figure 11E-F). Overall, neuro-specific *Pex7* OE resulted in a semi-lethal phenotype that manifested prior to hatching.

To confirm if the neuronal cell lineage-specific phenotypes reported previously in homozygous $Pex7^{MiMIC}$ mutants (Di Cara *et al*., 2019) were due to loss of *Pex7* in nervous tissues, a strain of these mutants was created in which *Pex7* was over-expressed in neurons (*elav>Pex7*; $Pex7^{MiMIC}/Pex7^{MiMIC}$). No significant differences were observed in the total adult scores or sex ratios, but egg and larvae scores were reduced when rescue was attempted (Figure 12A-C). This resulted in a significantly reduced larva:egg ratio ($P = 0.037$, Figure 12D). Fly strain genotypes were confirmed by PCR of adult gDNA (Figure 12E, F). *Pex7* transcript abundance was roughly equal between mutants and control w^{1118} adults, with a mean fold-change difference of 1.16 ± 0.06. These mutants were previously reported to express ≤ 10% the *Pex7* mRNA of w^{1118} flies, using the same technique and equipment that I used, but with different primers (Di Cara *et al*., 2019). In *elav>Pex7*; $Pex7^{MiMIC}/Pex7^{MiMIC}$ mutants the mean fold-change in *Pex7* transcription was 24.66 ± 3.40 from the w^{1118} baseline ($P = 0.024$, Figure 12G, Table 6). The attempted rescue thus increased *Pex7* transcription about 25–fold in neurons and resulted in a semi-lethal developmental phenotype.

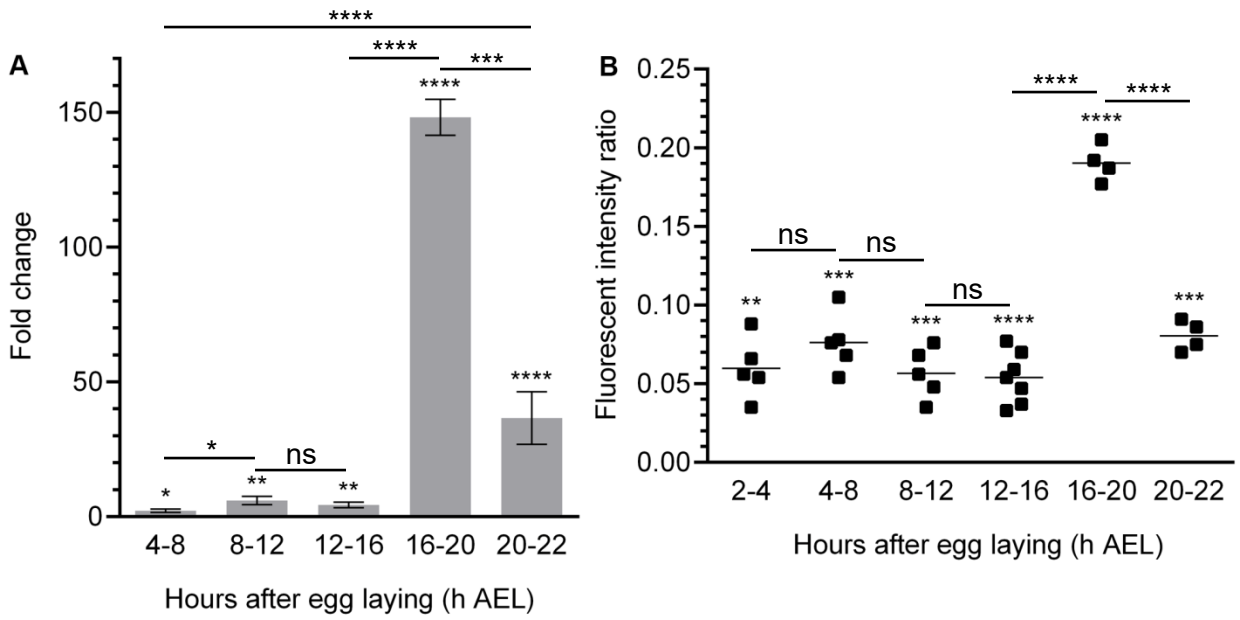

Figure 9. Quantification of embryonic *Pex7* expression. (A) A baseline of mean *Pex7* mRNA abundance relative to that of *Act5C* was determined for w^{1118} embryos collected 2-4 h AEL. This baseline was used to compare *Pex7*:*Act5C* abundance in the same strain at subsequent time points to produce a trend in the relative fold change of *Pex7* mRNA abundance. Data presented are mean fold change ± standard deviation (SD; n = 4 pairwise comparisons). Individual time point *P* values were determined by comparing the 2-4 h AEL baseline mean ΔC_t value to that of each subsequent time point independently with a null hypothesis of no change (Table 4). Whole-set and inter-sample *P* values were determined by one-way ANOVA and post-hoc t-test, respectively. (B) Pex7 abundance in western blots of staged embryo lysates relative to that of γ-Tubulin, expressed as a ratio ($n \geq 4$). Individual time point *P* values were determined by comparing pooled replicate values at each time point to a null hypothesis of 0 (Table 5). Whole-set and inter-sample *P* values were determined by one-way ANOVA and post-hoc t-test, respectively. Representative images of the western blots used are shown in Figure 6. * $P \leq 0.02$, ** $P \leq 0.01$, *** $P \leq 0.001$, **** $P \leq 0.0001$, ns = not significant.

Table 4. Summary of *Pex7* qRT-PCR data.

Mean C_t Scores			Mean ΔC_t: *Pex7* vs *Act5C*				
Name	Mean C_t	St Dev	Pair	ΔC_t	St Dev	$\Delta\Delta C_t$	$2^{-\Delta\Delta Ct}$
2-4 h AEL							
Pex7-1	36.49	0.12	*Pex7-1/Act5C-2*	6.45	0.03	-	-
Pex7-3	35.76	0.19	*Pex7-1/Act5C-3*	5.90	0.16	-	-
Act5C-2	30.04	0.18	*Pex7-3/Act5C-2*	5.72	0.01	-	-
Act5C-3	30.59	0.43	*Pex7-3/Act5C-3*	5.17	0.12	-	-
4-8 h AEL							
Pex7-1	34.02	0.34	*Pex7-1/Act5C-2*	4.87	0.13	-1.58	2.99
Pex7-3	33.54	0.11	*Pex7-1/Act5C-3*	5.10	0.06	-0.80	1.74
Act5C-2	29.15	0.08	*Pex7-3/Act5C-2*	4.39	0.02	-1.33	2.51
Act5C-3	28.92	0.46	*Pex7-3/Act5C-3*	4.62	0.18	-0.55	1.46
8-12 h AEL							
Pex7-1	35.87	0.36	*Pex7-1/Act5C-2*	4.42	0.04	-2.03	4.08
Pex7-3	34.48	0.09	*Pex7-1/Act5C-3*	3.52	0.03	-2.38	5.21
Act5C-2	31.45	0.29	*Pex7-3/Act5C-2*	3.03	0.10	-2.69	6.45
Act5C-3	32.35	0.42	*Pex7-3/Act5C-3*	2.13	0.16	-3.04	8.22
12-16 h AEL							
Pex7-1	36.35	0.22	*Pex7-1/Act5C-2*	4.82	0.09	-1.63	3.10
Pex7-3	35.34	0.21	*Pex7-1/Act5C-3*	3.64	0.12	-2.26	4.79
Act5C-2	31.53	0.05	*Pex7-3/Act5C-2*	3.81	0.08	-1.91	3.76
Act5C-3	32.71	0.46	*Pex7-3/Act5C-3*	2.63	0.13	-2.54	5.82
16-20 h AEL							
Pex7-1	33.08	0.45	*Pex7-1/Act5C-2*	-0.67	0.12	-7.12	139.10
Pex7-3	32.28	0.21	*Pex7-1/Act5C-3*	-1.33	0.13	-7.23	150.12
Act5C-2	33.75	0.68	*Pex7-3/Act5C-2*	-1.47	0.24	-7.19	146.02
Act5C-3	34.41	0.19	*Pex7-3/Act5C-3*	-2.13	0.01	-7.30	157.59
20-22 h AEL							
Pex7-1	32.22	0.54	*Pex7-1/Act5C-2*	0.90	0.06	-5.55	46.85
Pex7-3	31.52	0.18	*Pex7-1/Act5C-3*	1.14	0.13	-4.76	27.10
Act5C-2	31.32	0.65	*Pex7-3/Act5C-2*	0.20	0.24	-5.52	45.89
Act5C-3	31.08	0.29	*Pex7-3/Act5C-3*	0.44	0.06	-4.73	26.54
Summary				Mean $2^{-\Delta\Delta Ct}$	St Dev $2^{-\Delta\Delta Ct}$	P value ΔC_t	
			4-8 h AEL	2.18	0.607	1.855E-02	
			8-12 h AEL	5.99	1.538	6.685E-03	
			12-16 h AEL	4.36	1.033	1.087E-02	
			16-20 h AEL	148.21	6.696	2.147E-06	
			20-22 h AEL	36.59	9.784	7.482E-06	

Table 5. Summary of relative Pex7 protein quantification.

Time point	Replicate	Ratio
2-4 h AEL	1	0.066
	2	0.088
	3	0.035
	4	0.054
	5	0.056
	Mean	0.060
	SD	0.0172
	P value	2.23E-03
4-8 h AEL	1	0.068
	2	0.076
	3	0.078
	4	0.054
	5	0.105
	Mean	0.076
	SD	0.0169
	P value	8.39E-04
8-12 h AEL	1	0.048
	2	0.035
	3	0.056
	4	0.076
	5	0.068
	Mean	0.057
	SD	0.0143
	P value	1.39E-03
12-16 h AEL	1	0.047
	2	0.059
	3	0.070
	4	0.077
	5	0.033
	6	0.037
	7	0.054
	Mean	0.054
	SD	0.0152
	P value	1.30E-04
16-20 h AEL	1	0.192
	2	0.205
	3	0.177
	4	0.187
	Mean	0.190
	SD	0.0103
	P value	6.62E-05
20-22 h AEL	1	0.086
	2	0.091
	3	0.070
	4	0.075
	Mean	0.081
	SD	0.0082
	P value	4.43E-04

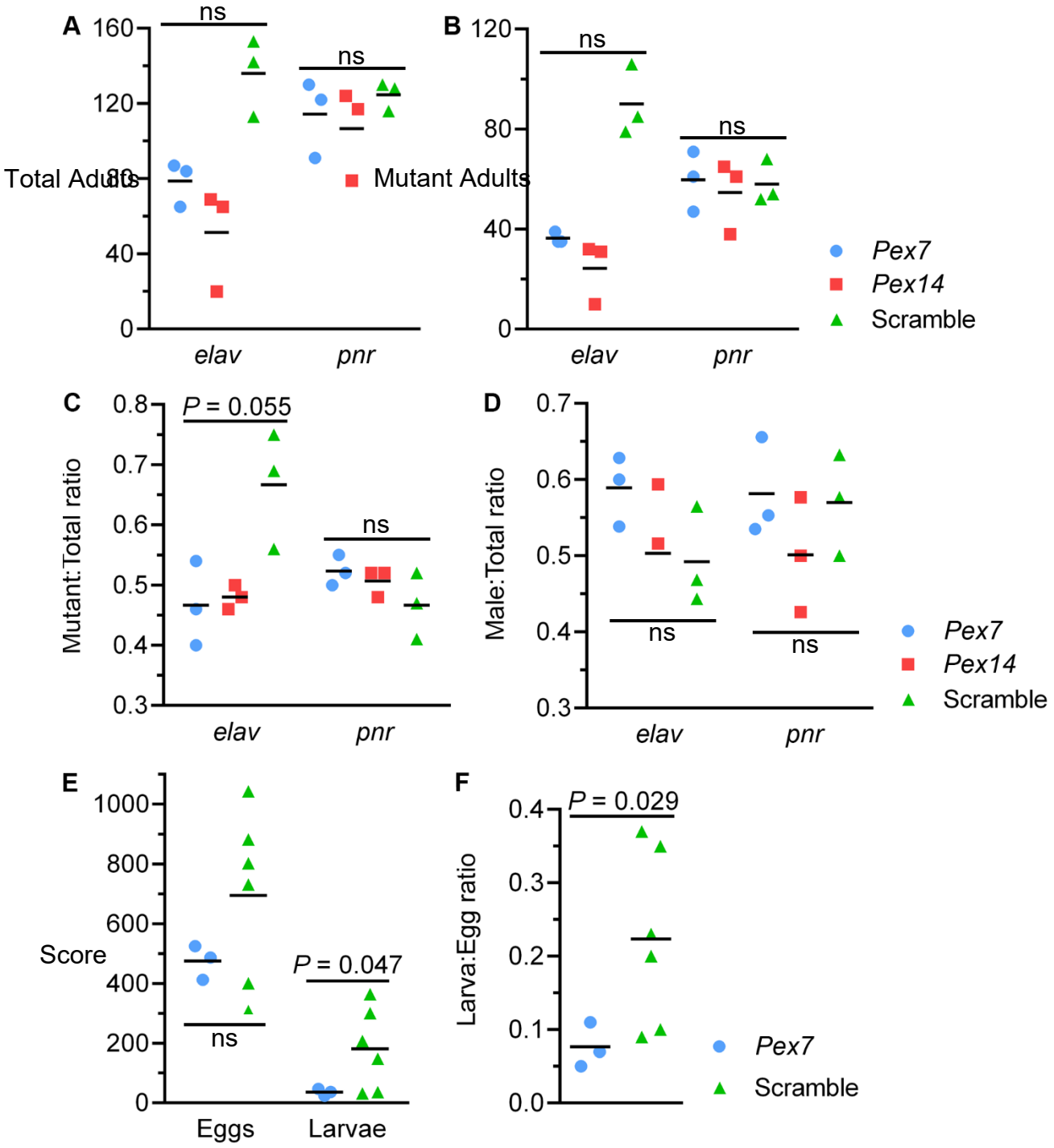
A
B
C
D
E
F
Total Adults
Mutant Adults
ns
P = 0.055
P = 0.047
P = 0.029
elav
pnr
Pex7
Pex14
Scramble
Mutant:Total ratio
Male:Total ratio
Score
Eggs
Larvae
Larva:Egg ratio

Figure 10. Somatic knockout of *Pex7* in differentiating neurons impaired hatching. *elav*- or *pnr*-Gal4 drivers were used to target the somatic knockout of *Pex7* (blue circle), *Pex14* (red square) or QUAS (Scramble; green triangle) in TRiP-KO crosses. (A) Total adults scored from each cross. *elav>Pex7* and *elav>Pex14* TRiP-KO crosses produced fewer adults. (B) Total mutant adults scored independently from each cross. This revealed the reduced progeny scores in (A) were due to reduced mutant counts. (C) Mutant:total adult ratios of the TRiP-KO crosses. (D) Analysis of progeny sex ratios. Adult sex ratios did not significantly differ under any TRiP-KO condition. (E) Total eggs laid and larvae hatched from *elav>Pex7* TRiP-KO crosses. Somatic *elav>Pex7* knockout significantly reduced larvae counts ($P = 0.047$) without affecting egg counts. (F) Larva:egg ratio of *elav>Pex7* TRiP-KO mutants. Somatic *elav>Pex7* knockout significantly reduced the larva:egg ratio ($P = 0.029$). The *elav>Pex7* knockout phenotype resulted from impaired hatching. One data point represents one experimental replicate. ns = not significant.

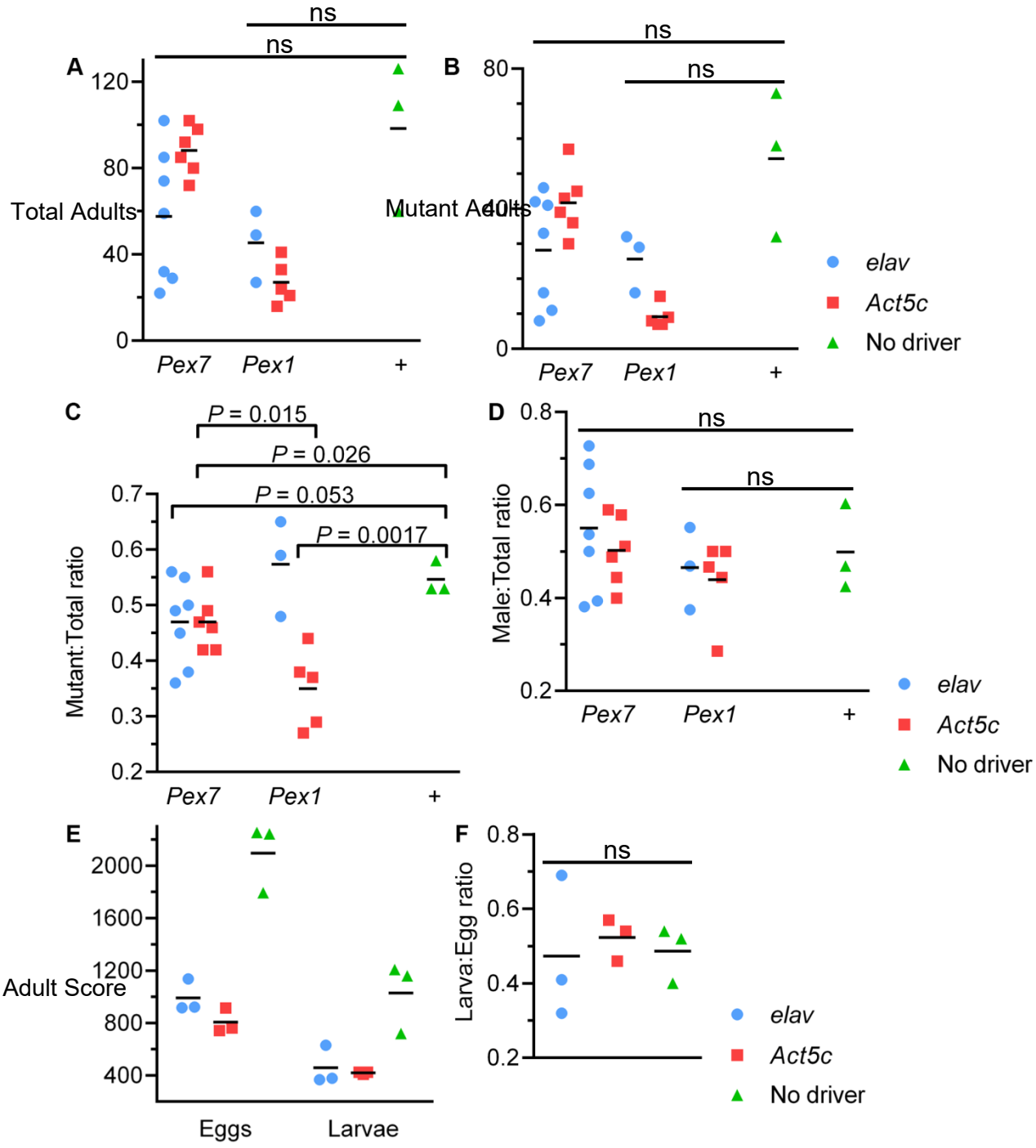
A
B
C
D
E
F
ns
Total Adults
Mutant Adults
Pex7
Pex1
+
elav
Act5c
No driver
P = 0.015
P = 0.026
P = 0.053
P = 0.0017
Mutant:Total ratio
Male:Total ratio
Adult Score
Eggs
Larvae
Larva:Egg ratio

Figure 11. Somatic *Pex7* over-expression affected survival. The *elav* (blue circle) or *Act5C* (red square) Gal4 promoters were used to direct over-expression (OE) of *Pex7* or *Pex1* via Gal4-UAS and compared to crosses bearing the *UAS-Pex7* transgene but no Gal4 driver (green triangle). (A) Total adults scored from each OE cross. *elav>Pex7*, *elav>Pex1* and *Act5C>Pex1* crosses produced fewer adults. (B) Total over-expressing flies scored independently from each OE cross. This showed that population reduction in (A) was due to reduced counts of over-expressing flies. (C) Over-expressing:total progeny ratios of the OE crosses. *Act5C>Pex7* and *Act5C>Pex1* significantly reduced over-expressing:total adult ratios ($P = 0.026$ and $P = 0.0017$, respectively). The effect of *Act5C>Pex1* OE was significantly stronger than that of *Act5C>Pex7* ($P = 0.015$). (D) Analysis of OE cross sex ratios. No difference was observed. (E) Egg and larvae scores were both reduced under all OE conditions. (F) Larva:egg ratios of the OE crosses were not significantly affected, suggesting the semi-lethal OE phenotype was not due exclusively to impaired hatching. One data point represents one experimental replicate. ns = not significant.

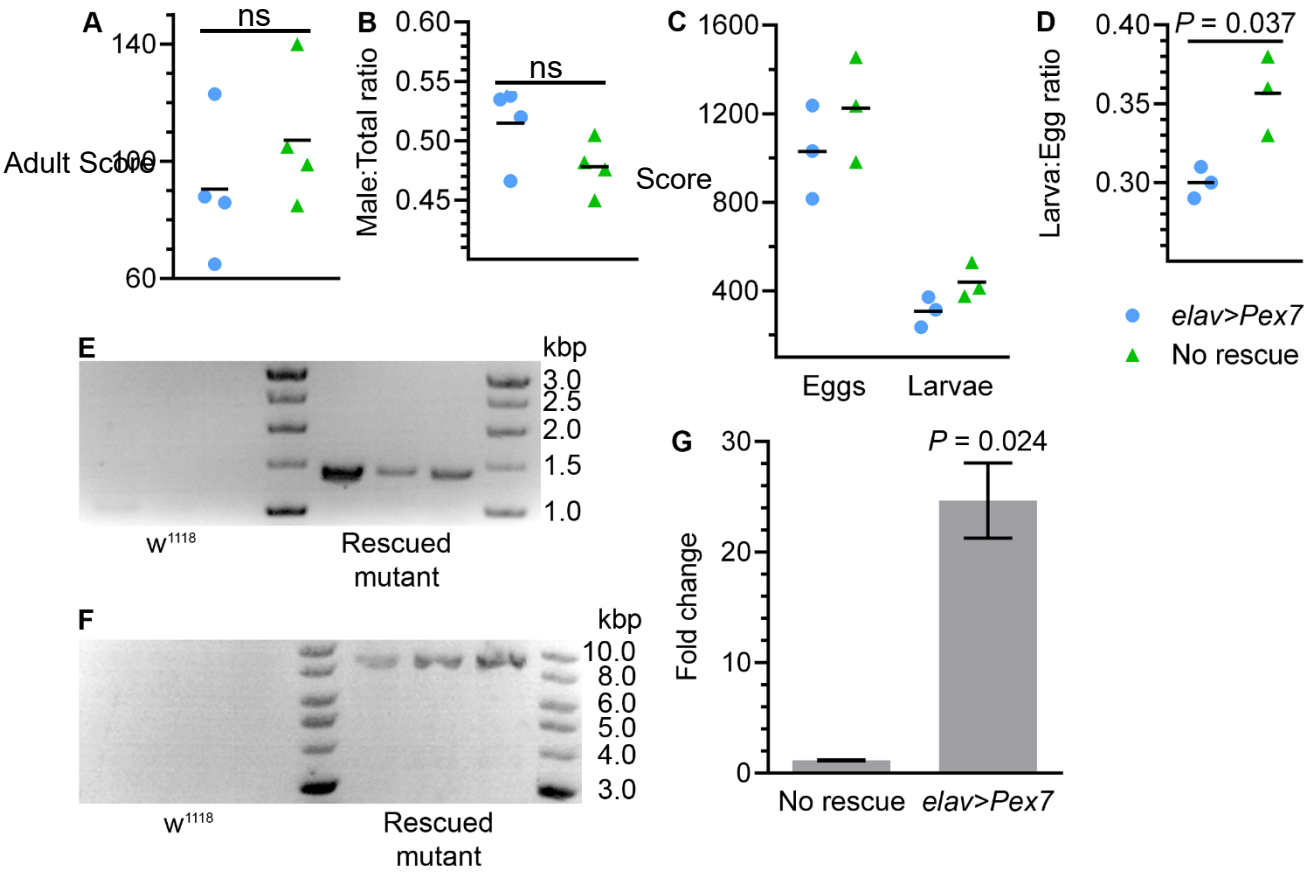
A
ns
140
100
60
Adult Score
B
0.60
0.55
0.50
0.45
Male:Total ratio
ns
C
1600
1200
800
400
Score
Eggs
Larvae
D
0.40
0.35
0.30
Larva:Egg ratio
P = 0.037
elav>Pex7
No rescue
E
kbp
3.0
2.5
2.0
1.5
1.0
w1118
Rescued mutant
F
kbp
10.0
8.0
6.0
5.0
4.0
3.0
w1118
Rescued mutant
G
30
20
10
0
Fold change
P = 0.024
No rescue
elav>Pex7

Figure 12. Targeted *Pex7* over-expression in homozygous *Pex7* mutants impaired hatching. Somatic *elav>Pex7* over-expression (OE) was performed in homozygous *Pex7* mutants (blue circle) via Gal4-UAS and compared to the parent mutant strain (green triangle). (A) Total adult scores from the *elav>Pex7*; *Pex7/Pex7* crosses. No significant difference was observed. (B) Analysis of sex ratios of the *elav>Pex7*; *Pex7/Pex7* progeny. No significant difference was observed. (C) Total egg and larvae scores from the *elav>Pex7*; *Pex7/Pex7* crosses. Fewer mean eggs were laid and fewer mean larvae hatched under *elav>Pex7* OE. (D) Larva:egg ratios of the *elav>Pex7*; *Pex7/Pex7* crosses. The ratio was significantly reduced under *elav>Pex7* OE ($P = 0.037$). One data point represents one experimental replicate. (E) Gel electrophoresis of a PCR reaction targeting a 1.5 kb fragment of the MiMIC insertion inside *Pex7* using gDNA extracted from *elav>Pex7*; *Pex7/Pex7* adults. (F) Gel electrophoresis of a PCR reaction targeting the 9 kb UAS-*Pex7* cassette using gDNA extracted from *elav>Pex7*; *Pex7/Pex7* adults. (G) qRT-PCR of *Pex7* transcript abundance relative to *Act5C* in attempted rescue (*elav>Pex7*; *Pex7/Pex7*) and untreated (*Pex7/Pex7)* mutant adults, reported as fold-change difference from strain w^{1118}. The *elav>Pex7*; *Pex7/Pex7* adults had a significant fold-change in *Pex7* expression ($P = 0.024$, n = 3). The *Pex7/Pex7* mutants used here were previously reported to express ≤ 10% the *Pex7* mRNA of w^{1118} flies (Di Cara *et al*., 2019).

Table 6. Summary of qRT-PCR data for attempted *Pex7* rescue.

Mean C_t Scores			Mean ΔCt: *Pex7* vs *Act5c*				
Name	Ct Mean	Ct Dev	Pair	ΔCt	St Dev	ΔΔCt	$2^{-\Delta\Delta Ct}$
w^{1118}							
Pex7-1	35.49	0.08	Pex7-1/Act5c	3.76	0.000	-	-
Pex7-2	35.82	0.26	Pex7-2/Act5c	4.09	0.090	-	-
Act5c	31.73	0.08					
Mutant							
Pex7-1	35.85	0.23	Pex7-1/Act5c	3.62	0.010	-0.14	1.10
Pex7-2	36.03	0.17	Pex7-2/Act5c	3.80	0.020	-0.29	1.22
Act5c	32.23	0.21					
Mutant + OE							
Pex7-1	33.66	0.54	Pex7-1/Act5c	-1.05	0.110	-4.81	28.05
Pex7-2	34.39	0.68	Pex7-2/Act5c	-0.32	0.040	-4.41	21.26
Act5c	34.71	0.76					
Summary					Mean $2^{-\Delta\Delta Ct}$	St. Dev. $2^{-\Delta\Delta Ct}$	P value ΔCt
			Mutant		1.16	0.060	0.399
			Mutant + OE		24.66	3.396	0.024

3.3.6 Summary

The mRNA distribution of the *Peroxins* I observed was ubiquitous immediately following the MZT and for up to two hours afterward (Figure 4, left column). Beginning at about 4 h AEL, *Peroxin* transcript localization began to shift into distinct patterns that did not necessarily match their predicted functions or putative relationships with other *Peroxins* (Figure 4, right column; Figure 1; Table 1). It is possible that changes in transcript abundance levels, germ layer differentiation and the onset of organogenesis affected *Peroxin* transcription and the apparent signal intensity of the probes (Table 2).

The *Pex7* mRNA probe pattern began as a ubiquitous signal (Figure 5A) that evolved into a pattern similar to the brain and ventral nerve cord (Figure 5D; Hartenstein, 1993). This pattern persisted until the embryo was ready to hatch (Figure 5H). After validating a novel Pex7 antibody (Figure 6), *Pex7* was confirmed to encode a protein detectable in all staged embryo collections (Figure 7). Relative quantification of *Pex7* mRNA by qRT-PCR and protein by relative fluorescent intensity of western blots (Figure 9) confirmed *Pex7* was expressed with variable temporal abundance that supported my FISH and IF observations. The neural marker antibodies anti-Elav and anti-Nrg reported from immediately adjacent to Pex7 (Figure 7D and 6E, respectively), suggesting *Pex7* was expressed in a subset of developing neural cells.

Neuro-specific *Pex7* knockout affected development by impairing hatching, but was not completely lethal (Figure 10). Neuro-specific *Pex7* over-expression affected development by impairing egg and larva scores without affecting hatching (Figure 11). The lack of effect under *pnr* knockout, which targeted dorsal PNS cells fated to become sensory bristles (Figure 10A-D), suggested *Pex7* was necessary for normal CNS development during embryogenesis. Attempted rescue of *Pex7* mutants with neurospecific *Pex7* over-expression instead impaired hatching, similar in effect to targeted *Pex7* knockout (Figure 12A-D). I hypothesize *Pex7* has a peroxisome-associated role and is either required specifically for proper development of the CNS or by all neurons sometime prior to fate acquisition. The presence of viable adults in all mutagenesis experiments indicated *Pex7* was not sufficient for neural development.

Chapter 4 A cell-based screen for genes affecting peroxisomes in *Drosophila*

4.1 Chapter 4 hypothesis and rationale

The relative simplicity of the *Drosophila* genome compared to mammals and plants makes flies an excellent model for screening pathways that regulate cellular processes like organelle biogenesis. This can be done in whole animals or in cultured cells. A small cell-based screen of available mutations on the *Drosophila* X chromosome found eighteen genes outside the *Peroxin* family that affected peroxisome size or number (Graves *et al*., 2020). Notably, these genes encoded proteins known or predicted to be involved in processes besides peroxisome biogenesis or function. Sixteen of the genes had human homologs, nine of which had causative variants for a Mendelian genetic disease (Graves *et al*., 2020).

Conservation of peroxisome regulatory genes besides *Peroxins* has also been reported. RNAi of HSPA9 in human HeLa cells and the orthologous Hsc70-5 in *Drosophila* S2 cells both resulted in loss of peroxisomes by increased pexophagy, and transgenic HSPA9 expression rescued Hsc70-5 knockdown (Jo, Park *et al*., 2019). It is likely that continued screening in *Drosophila* will identify additional conserved genes that regulate peroxisomes. A previous post-doctoral fellow in the Simmonds laboratory, Dr. Adam Magico, completed an unbiased, qualitative RNAi screen of almost all genes in the *Drosophila* genome. His screen identified many known and potential peroxisome regulators, such as *Pex5*, *Pex6*, *Pex13* and *Pex16* (A Magico, unpublished data). Several genes not previously linked to peroxisomes were also found to affect peroxisome presence, morphology or abundance. This chapter reports the validation of the dsRNA knockdown phenotypes for a cohort of the genes identified in the Magico screen. I then continued the characterization of another cohort of genes from the Magico screen in a cell-based over-expression experiment.

Hypothesis:

There are genes outside the currently described *Peroxin* family that regulate peroxisome biogenesis. These genes contribute to processes that alter cellular peroxisome requirements.

4.2 Introduction

There are factors besides *Peroxins* that regulate peroxisomes (Gandre-Babbe and van der Bliek, 2008; Chao *et al*, 2016; Assia Batzir *et al*., 2019; Graves *et al*., 2020). In mammals, the PPARs are a class of nuclear steroid hormone receptor that regulate peroxisome numbers. *Drosophila* does not have an obvious PPAR homolog (flybase.org). Previous high-throughput RNAi-based examinations of all presumptive and actual *Drosophila* coding genes identified candidate peroxisome regulatory factors (A Magico, unpublished data; Lacey, 2015; Drake, 2012). One such screen also identified several *Peroxins*, validating the use of the approach to uncovering novel peroxisome regulatory pathways (A Magico, unpublished data). This screen identified seventeen genes not previously associated with peroxisomes. I used two approaches to validate that the candidate genes played a role in peroxisome proliferation. First, unique dsRNAs were generated to knock down eight candidates and compared to the dsRNAs used previously. Second, transient over-expression of eleven genes was performed to observe effects on peroxisome abundance. Some genes were tested in both experiments. Knockdown and over-expression of *Pex5* and *Pex13* altered peroxisome abundance in ways consistent with the functions of their mammalian orthologs. Bioinformatic analysis of the other genes suggested functional groupings. Half of the genes were involved in late-stage mitotic processes like cytokinesis and abscission. The remainder were predicted to be involved in DNA replication, regulation of cytoskeletal motor proteins, mitochondrial function or membrane transport, suggesting these pathways and functions influence peroxisome biogenesis in *Drosophila*.

4.3 Results

4.3.1 Validation of RNAi phenotypes for genes with novel effects on peroxisome abundance

Validation of RNAi phenotypes was performed for thirteen of seventeen candidate genes identified previously in S2 cells stably expressing GFP-PTS1 (A Magico, unpublished data). Validation of each gene was performed with at least two new dsRNAs complementing different regions of their target mRNAs to account for potential off-target effects. The new dsRNAs were designed using the Drosophila RNAi Screening Center (DRSC) SnapDragon tool

(www.flyrnai.org). Using this approach, an effect on peroxisome abundance was confirmed for eight genes (Figure 13): *Androcam* (*Acam*), *aurora B* (*aurB*), CG7627, CG18231, *fascetto* (*feo*), *Inner centromere protein* (*Incenp*), *no mitochondrial derivative* (*nmd*), and *pebble* (*pbl*). The data are summarized in Table 7. Representative images of each gene's knockdown effect on GFP-PTS1 in individual cells are presented in Figure 14. Validation of this cohort identified five categories of cellular processes or functions, apart from peroxisome biogenesis, that affected peroxisomes: motor protein regulation (*Acam*), cell division/mitosis (*aurB*, *feo*, *Incenp*, *pbl*), transmembrane transportation (CG7627), mitochondrial function (*nmd*) and collagen synthesis (CG18231).

a. The effect of Peroxin *knockdown*

Several studies confirmed *Pex* genes have roles in peroxisome proliferation in *Drosophila*. *Pex1* RNAi resulted in significant loss of peroxisome abundance in S2 cells, establishing a precedent for the effect of *Peroxin* RNAi on peroxisomes (Mast *et al*., 2011). RNAi of *Pex13* resulted in a mean 8 ± 3 % reduction in peroxisome abundance (Figure 13). Mammalian PEX13 forms part of the translocon that facilitates matrix protein import (Figure 1). The effect of *Pex5* RNAi was variable depending on the dsRNA molecule employed, with a 0 ± 11 % change in abundance observed between two replicates (Figure 13). This was similar to ambiguous qualitative findings reported previously (Mast *et al*., 2011). Mammalian PEX5 is the PTS1 receptor, and is found both in the cytosol and within peroxisomes (Figure 1).

b. Genes with a canonical or predicted role in cell division

aurB knockdown resulted in a 12 ± 4 % increase in peroxisome abundance (Figure 13). AurB is a serine/threonine/tyrosine kinase found in the chromosome passenger complex and has several chromatin-related roles during cytokinesis (Giet and Glover, 2001; Radford *et al*., 2012; Mathieu *et al*., 2013). *Incenp* knockdown resulted in a 28 ± 4 % increase in peroxisome abundance (Figure 13). Incenp is also a member of the chromosome passenger complex, where it acts as a targeting subunit for AurB (Adams *et al*., 2001; Chang *et al*, 2006; Radford *et al*., 2012). In *Drosophila,* both the chromosome passenger complex and peroxisomes rely on microtubules. The chromosome passenger complex coordinates chromosome segregation and cytokinesis using the microtubule-based central spindle (Giet and Glover, 2001), and

peroxisomes are moved around the cell by microtubule-associated dynein and kinesin motor proteins (Kulić *et al*., 2008; Ally *et al*., 2009). Presently there is no evidence of a direct interaction between proteins of the chromosome passenger complex and peroxisomes.

feo knockdown resulted in a 28 ± 6 % increase in peroxisome abundance (Figure 13). Feo is an anti-parallel microtubule binder found in the central spindle that is necessary for cytokinesis and centrosome duplication, and is also required for mitochondrial elongation in *Drosophila* spermatids (Wang *et al*., 2015; Verni *et al*., 2004; reviewed by Fabio and Brill, 2012). This established a precedent for the association of Feo with the process of organelle fission, however there is no evidence that Feo interacts directly with peroxisome fission proteins (reviewed by Fabio and Brill, 2012).

c. Genes encoding canonical or predicted motor protein regulators

Acam knockdown resulted in a 32 ± 6 % increase in peroxisome abundance (Figure 13). Acam, sequentially similar to calmodulin, binds the head and neck of the non-muscle myosin VI heavy chain, a motor protein that interacts with the actin cytoskeleton (Martin *et al*., 1999; Frank *et al*., 2006). Acam was found to interact directly with myosin VI at the minus end of the actin cones that mediate *Drosophila* spermatid individualization. This interaction was only observed in the testis (Frank *et al*., 2006). *Drosophila* spermiogenesis involves extensive organelle remodeling and is sensitive to lipid metabolism, linking spermatid individualization to peroxisome function (Ben-David *et al*., 2015; reviewed by Fabian and Brill, 2012).

pbl knockdown resulted in a 7 ± 1 % loss in peroxisome abundance (Figure 13). *pbl* encodes a RhoGEF involved in cytokinesis, actin cytoskeleton organization, cell shape regulation, cell migration during gastrulation and the epithelial-mesenchymal transition (Prokopenko *et al*., 1999; van Impel *et al*, 2009; Smallhorn *et al*., 2004). Specifically, Pbl is essential for the formation of the actin contractile ring during cytokinesis, and subsequent formation of the cleavage furrow, by promoting Rho1 activation (Prokopenko *et al*., 1999; van Impel *et al*, 2009). *pbl* does not interact directly with cell cycle genes, instead responding to cues from the FGFR signal transduction pathway, and is a negative regulator of canonical Wg signaling (Prokopenko *et al*., 1999; Schumacher *et al*., 2004; Greer *et al*., 2013).

d. Genes encoding canonical or predicted transmembrane transport proteins

CG7627 knockdown resulted in a 16 ± 2 % increase in peroxisome abundance (Figure 13). CG7627 is uncharacterized however its primary sequence contains an ATPase domain and the gene is sequentially similar to human ATP binding cassette subfamily C member 4 (ABCC4), which is involved in ATP-coupled transmembrane transporter activity similar to Pex1 (flybase.org; UniProtKB; Table 1). ABCC4 is a member of the multidrug-resistance protein family of ATPases (ncbi.nlm.nih.gov). In mice, clofibrate treatment induced ABCC4 expression by activating PPARα, establishing a connection between a putative CG7627 homolog and peroxisome proliferation (Moffit *et al*., 2006). However, *Drosophila* does not conserve PPARs.

e. Genes encoding canonical or predicted regulators of mitochondrial function

nmd knockdown resulted in a 12 ± 4 % decrease in peroxisome abundance (Figure 13). Nmd is predicted to have ATP-binding activity, is involved in wing disc dorsal/ventral patterning, and its loss caused spermatids to lose their mitochondria (Bejarano *et al*., 2008; Lindsley and Zimm, 1992). *Drosophila* wing disc patterning is a classic model for neural pathway development (Jan *et al*., 1985), a process which peroxisomes and their enzymes are essential to (Mast *et al*., 2011; Di Cara *et al*., 2019; Chung *et al*., 2020). *Pex2*, *Pex10* and *Pex16* loss of function also result in male sterility, although for reasons other than mitochondrial loss (Chen *et al*., 2009; Nakayama *et al*., 2011).

f. Genes encoding canonical or predicted enzymes

CG18231 knockdown resulted in a 10 ± 2 % increase in peroxisome abundance (Figure 13). CG18231 is an uncharacterized gene. Based on its primary sequence, CG18231 is predicted to encode an α subunit of Prolyl 4-hydroxylase, an oxidoreductase involved in collagen synthesis (flybase.org, UniProtKB). Human P4HA1 has two identical α subunits and two identical β subunits, and the two α subunits form the catalytic site (ncbi.nlm.nih.gov). Use of the hypoxia-mimicking chemical dimethyloxaloylglycine (DMOG) on human hepatoma cell line Huh7 inhibited Prolyl 4-hydroxylase enzymatic function and induced pexophagy by up-regulating the pexophagy-promoting transcription factor Endothelial PAS domain protein 1 (EPAS1), reducing peroxisome abundance (Mu Y *et al*., 2020; Walter *et al*., 2014).

g. Genes with no observed effect in the present study

Knockdown of *Cdk1*, *stg* and *vvl* did not result in mean altered peroxisome abundance. Two of four *vvl* dsRNAs did report reduced peroxisome abundance (Figure 13), suggesting some *vvl* dsRNAs were either subject to off-target effects or were ineffective.

In *S. cerevisiae*, which uses the actin cytoskeleton and the myosin V motor Myo2 to mediate peroxisome movement and inheritance, Cdk1 mediates the process via phosphorylation of specific Myo2 adaptor proteins (Peng and Weisman, 2008). The Myo2 peroxisome adaptor is the PMP Inp2, though a relationship between Inp2 and Cdk1 has yet to be determined (Fagarasanu *et al*., 2006). Moreover, Kinesin-1 and Dynein heavy chain are the motors responsible for peroxisome movement along microtubules in S2 cells, ruling out an analogous actin-associated role for Cdk1 in *Drosophila* peroxisome dynamics (Kural *et al*., 2005). Cdk1 also phosphorylates hundreds of targets and has several isoforms, suggesting it is an essential master regulator of the cell cycle that employs redundancy to ensure its function (flybase.org).

stg, aka *cdc25*, encodes a protein tyrosine phosphatase that regulates centriole replication and cell size, implying it is a master regulator of the mitotic cell cycle (Dunphy and Kumagai, 1991; Edgar and O'Farrel, 1989; Mozer and Easwarachandran, 1999). The human ortholog Cdc25C degrades under peroxide-induced oxidative stress, suggesting cellular redox state regulates mitosis by affecting the stability of certain checkpoint proteins (Savitsky and Finkel, 2002).

vvl, aka *drifter*, is a transcription factor that enhances RNApolII activity. Vvl has many binding partners and participates in several processes including cell fate determination, the immune response and nervous system development (Junell *et al*., 2010; Anderson *et al*., 1995; Inbal *et al*., 2003; Certel *et al*., 1996; de Celis *et al*., 1995). No direct interaction between *vvl* and peroxisome biogenesis has been observed previously however *vvl* does promote non-canonical expression of antimicrobial peptide genes (Junell *et al*., 2010). A relationship may therefore be inferred between *vvl* and peroxisome biogenesis in the context of the immune response (Di Cara *et al*., 2019).

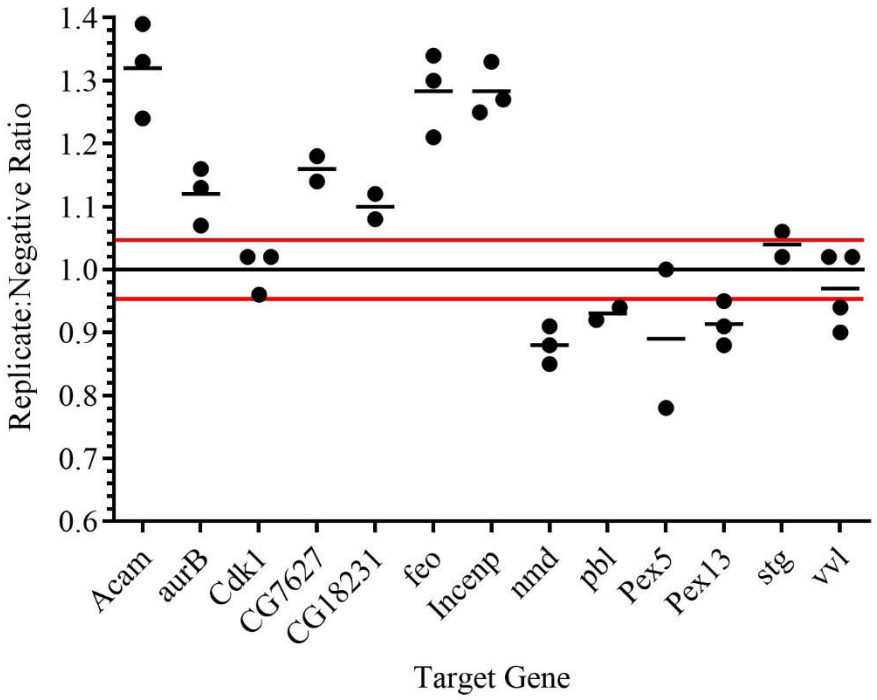

Figure 13. Quantitative effects of transient RNAi on peroxisome abundance. For each gene, each data point represents a ratio of a mean of n = 3 replicates for a unique dsRNA molecule compared to a replicate-specific, untreated control. Short horizontal bars represent each gene's overall mean ratio. The black horizontal line at 1.0 on the Y-axis represents the null hypothesis, i.e. RNAi had no effect, for which the replicate:negative ratio would be 1. The red horizontal lines at 0.95 and 1.05 on the Y-axis represent 0.05 deviation in mean ratio from the null hypothesis and define effect significance.

Table 7. Mean changes in peroxisome abundance resulting from RNAi.

Gene	Mean ratio	Change (%)	SD (%)
Acam	1.32	32	6
aurB	1.12	12	4
Cdk1	1.00	0	3
CG7627	1.16	16	2
CG18231	1.10	10	2
feo	1.28	28	6
Incenp	1.28	28	4
nmd	0.88	-12	2
pbl	0.93	-7	1
Pex5	0.89	0	11
Pex13	0.92	-8	3
stg	1.04	4	2
vvl	0.97	-3	6

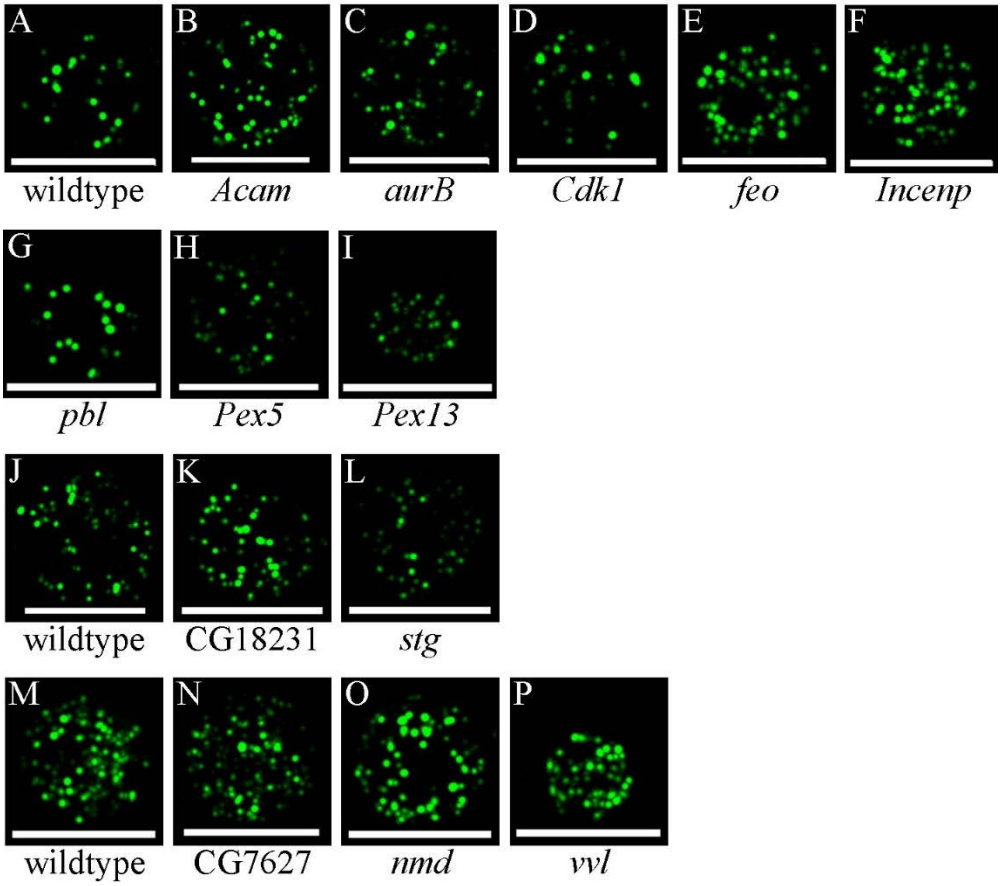

Figure 14. Qualitative effects of transient RNAi on peroxisome abundance. Potential regulators of peroxisome biogenesis identified by a prior high-throughput screen were knocked down via RNAi. The screen was conducted in three batches, presented here as panels A-I, J-L and M-P. The gene knocked down is named under each panel. All images are maximum intensity Z-projections. $n \geq 3$, scale bars = 5 μm.

4.3.2 Over-expression phenotypes for genes with novel effects on peroxisome abundance

Reporter fusions of twelve genes identified in the Magico screen were generated to explore the effects of transient over-expression (OE) upon, and potential co-localization with, the peroxisomal marker GFP-PTS1. The reporter fusions contained RFP at the N-terminus. The ratios of change in peroxisome abundance, calculated using data conforming to a 95 % confidence interval, and percent change in same are summarized in Table 8. There was only one over-expression plasmid used for each gene, with appropriate replicates, so there was only one mean value generated for comparison to the negative and positive control values to generate the final ratio and percent changes reported. Representative images of each gene's over-expression effect are presented in Figure 16. The transient over-expression of eleven genes had a significant effect on peroxisome abundance: *Androcam* (*Acam*), *aurora B* (*aurB*), *borealin-related* (*borr*), CG18231, *geminin*, *Inner centromere protein* (*Incenp*), *no mitochondrial derivative* (*nmd*), *pebble* (*pbl*), *spaghetti squash* (*sqh*), *string* (*stg*) and *ventral veins lacking* (*vvl*; Figure 15). This screen also identified five categories of cellular processes, apart from peroxisome biogenesis, that affected peroxisome abundance: motor protein regulation (*Acam*), mitosis (*aurB*, *borr*, *Incenp*, *pbl*, *sqh*, *stg*), mitochondrial function (*nmd*), transcription regulation (*geminin*, *vvl*), and collagen synthesis (CG18231).

a. The effect of Peroxin *over-expression*

Pex5 and *Pex13* over-expression increased peroxisome abundance by 66 and 36 %, respectively (Figure 15). The Pex13 observation complemented its knockdown data (Figure 13). The RFP-Pex13 reporter fusion overlapped almost perfectly with GFP-PTS1 (Figure 16R). The Pex5 observation complemented the portion of knockdown data that reported an effect (Figure 13). The RFP-Pex5 reporter appeared as puncta of the same approximate size as GFP-PTS1 puncta, and the signals were adjacent, however overlapping signal was not observed (Figure 16Q).

b. Genes with a canonical or predicted role in cell division

aurB over-expression resulted in a 36 % reduction in peroxisome abundance (Figure 15), complementary to its knockdown effect. A RFP-AurB reporter fusion had no specific pattern,

appearing as a cytosolic haze with several large puncta. The reporter did not overlap with GFP-PTS1, which appeared diminished in number and signal intensity (Figure 16D).

borr over-expression resulted in a 25 % increase in peroxisome abundance (Figure 15). Borr, like Incenp, is a targeting subunit for AurB in the chromosome passenger complex and is responsible for getting the complex to the centromere and cleavage furrow (Eggert *et al*., 2004; Hanson *et al*., 2005). At present there is no evidence for a direct interaction between Borr and any member of the *Peroxin* family. A RFP-Borr fusion reporter appeared as large puncta and a cytosolic haze that did not overlap with GFP-PTS1, which appeared more numerous than controls (Figure 16E). The apparent overlap (yellow signal) was an artifact of 3D → 2D image conversion.

Incenp over-expression resulted in an 8 % reduction in peroxisome abundance (Figure 15), which complemented the effect observed for its knockdown (Figure 13). A RFP-Incenp fusion reporter appeared as an aggregate of several large puncta with some adjacent haze (Figure 16J). The RFP signal did not overlap with GFP-PTS1.

pbl over-expression resulted in a 21 % increase in peroxisome abundance (Figure 15), complementing the effect observed for its knockdown (Figure 13). A RFP-Pbl reporter fusion formed several large puncta that appeared compartmentalized from GFP-PTS1, which had more and smaller puncta than controls (Figure 16K).

sqh over-expression resulted in a 24 % increase in peroxisome abundance (Figure 15). The function of Sqh is to directly regulate contraction of the cleavage furrow contractile ring during cytokinesis (Vasquez *et al*., 2014; Dean *et al*., 2005; Royou *et al*., 2002; Karess *et al*., 1991). *sqh* encodes the regulatory light chain of non-muscle type II myosin, which binds the heavy chain and activates myosin motor activity on the actin cytoskeleton when phosphorylated by the Rho-Rho kinase pathway. Thus, I consider *sqh* a cell cycle regulator instead of a cytoskeletal protein. A RFP-Sqh fusion reporter appeared as several puncta that did not overlap with GFP-PTS1 (Figure 16L).

stg over-expression resulted in an 84 % increase in peroxisome abundance, the highest change observed in this study (Figure 15). A RFP-Stg reporter fusion formed a few large puncta that appeared adjacent to large, numerous and aggregated GFP-PTS1 puncta (Figure 16S). The apparent overlap (yellow signal) was an artifact of 3D → 2D image conversion.

c. Genes encoding canonical or predicted motor protein regulators

Acam over-expression resulted in a 12 % increase in peroxisome abundance (Figure 15), the same trend as seen for *Acam* RNAi but lower in magnitude (Figure 13). A RFP-Acam fusion reporter appeared to concentrate around a large structure that may be the nucleus, with a few puncta and a general haze in the presumptive cytosol (Figure 16C). The RFP signal did not overlap with the GFP-PTS1 signal, which appeared as numerous puncta (Figure 16C).

d. Genes encoding canonical or predicted regulators of mitochondrial function

nmd over-expression resulted in an 18 % increase in peroxisome abundance (Figure 15), complementing the effect observed for its knockdown (Figure 13). A RFP-Nmd fusion reporter appeared as a few large puncta and aggregates predominantly at the cell periphery (Figure 16V). The RFP signal appeared to overlap somewhat with GFP-PTS1 (yellow signal), but that was an artifact of 3D → 2D image conversion.

e. Genes encoding canonical or predicted enzymes

CG18231 over-expression resulted in a 39 % increase in peroxisome abundance (Figure 15). This effect was the same trend as, but greater in magnitude than, the RNAi effects observed for this gene (Figure 13). A RFP-CG18231 reporter fusion formed appeared as a few large cytosolic puncta that did not overlap with GFP-PTS1 (Figure 16P). The apparent overlap of some CG18231 reporter signal with GFP-PTS1 (yellow signal) was an artifact of 3D → 2D image conversion. The signals did appear adjacent, suggesting the compartments were in close proximity.

f. Genes encoding canonical or predicted transcriptional regulators

geminin over-expression resulted in an 11 % increase in peroxisome abundance (Figure 15). Geminin is a negative regulator of DNA replication, and regulates the cell cycle of the

syncytial blastoderm as well as EGFR-Ras-MAPK signaling (Quinn *et al*., 2001; Mihaylov *et al*., 2002; Herr *et al*, 2010). In *Drosophila*, *geminin* over-expression resulted in ectopic differentiation of neural tissue and inhibited embryonic DNA replication (Quinn *et al*., 2001), implicating *geminin* as a cue for terminal differentiation in neurons. Similarly, vertebrate Geminin regulated the expression of the pluripotency factor Sox2 during neural plate development (Karamitros *et al*., 2010). A RFP-Geminin reporter fusion appeared as many cytosolic puncta and a cytosolic haze, none of which overlapped with GFP-PTS1 (Figure 16I).

vvl over-expression resulted in a 34 % increase in peroxisome abundance (Figure 15). This agreed with the results of two dsRNAs in the RNAi experiment, but not with the mean trend of overall *vvl* RNAi (Figure 13). A RFP-Vvl reporter fusion reported a single central punctum, with very light surrounding haze, in a cellular compartment presumed to be the nucleus (Figure 16M). The signal did not overlap with that of GFP-PTS1.

g. Genes with no observed effect in the present study

feo OE showed no effect on peroxisome abundance (Figure 15). To contrast, *feo* knockdown resulted in one of the highest increases in peroxisome abundance I observed (Figure 13). A RFP-Feo reporter fusion appeared as organized filamentous strands, matching its described function as a bundler of microtubules in the central spindle (Figure 16F; Wang *et al*., 2015; Verni *et al*., 2004). The RFP-Feo reporter appeared adjacent to puncta reported by GFP-PTS1 without overlapping.

4.3.3 Summary

Altogether, thirteen genes not previously associated with peroxisomes were assayed for their effects on peroxisome abundance. RNAi identified eight genes with an effect, OE identified eleven genes, and six were identified in both experiments. The genes were sorted into categories based on their canonical or predicted functions to identify cellular processes that impact peroxisome biogenesis. The RNAi and OE experiments each identified five cellular processes, four of which overlapped. For both experiments, half the genes had canonical roles in cell

division or mitosis. Notably, every gene associated with cell division/mitosis had been characterized previously while the genes in the other categories had not.

The OE experiment reported overlap with GFP-PTS1 only for RFP-Pex13 (Figure 16). Several RFP fusion reporters were adjacent to GFP-PTS1, sometimes leading to artifacts during the rendering process that resulted in false positive co-localization (yellow signal). The fusions that appeared adjacent to GFP-PTS1 were reporting *borr*, *feo*, *geminin*, *nmd*, *sqh* and CG18231 (Figure 16). RFP-Pex5 also appeared adjacent to GFP-PTS1 instead of overlapping. Previous experiments using the same GFP-PTS1-S2 cell line and the same OE/fusion reporter approach reported over 75 % co-localization between a FLAG-Pex5 reporter fusion and import-competent peroxisomes, suggesting the RFP tag used in the present study may have affected localization (Baron *et al*., 2016). The overlap between RFP-Pex13 and GFP-PTS1 suggests the RFP tag did not affect the localization of all reporters.

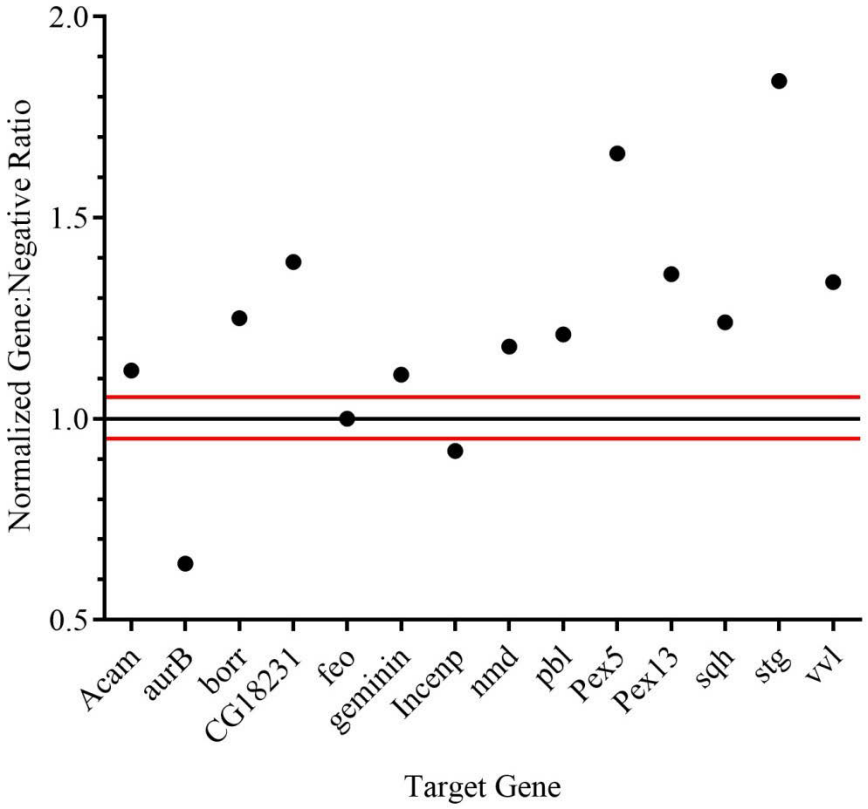

Figure 15. Quantitative effects of transient over-expression on peroxisome abundance. Each data point represents a ratio of means of n ≥ 3 replicates compared to a replicate-specific untreated control then compared to a replicate-specific positive transfection control. Ratios were calculated using data conforming to a 95 % confidence interval. The black horizontal line at ratio value 1.0 represents the null hypothesis, i.e. over-expression had no effect so the normalized ratio = 1. Red horizontal lines at 0.95 and 1.05 on the Y-axis represent 0.05 deviation in normalized mean ratio from the null hypothesis and define effect significance.

Table 8. Normalized changes in peroxisome abundance resulting from transient over-expression.

Gene	Ratio	Change (%)
Acam	1.12	12
aurB	0.64	-36
borr	1.25	25
CG18231	1.39	39
feo	1.00	0
geminin	1.11	11
Incenp	0.92	-8
nmd	1.18	18
pbl	1.21	21
Pex5	1.66	66
Pex13	1.36	36
sqh	1.24	24
stg	1.84	84
vvl	1.34	34

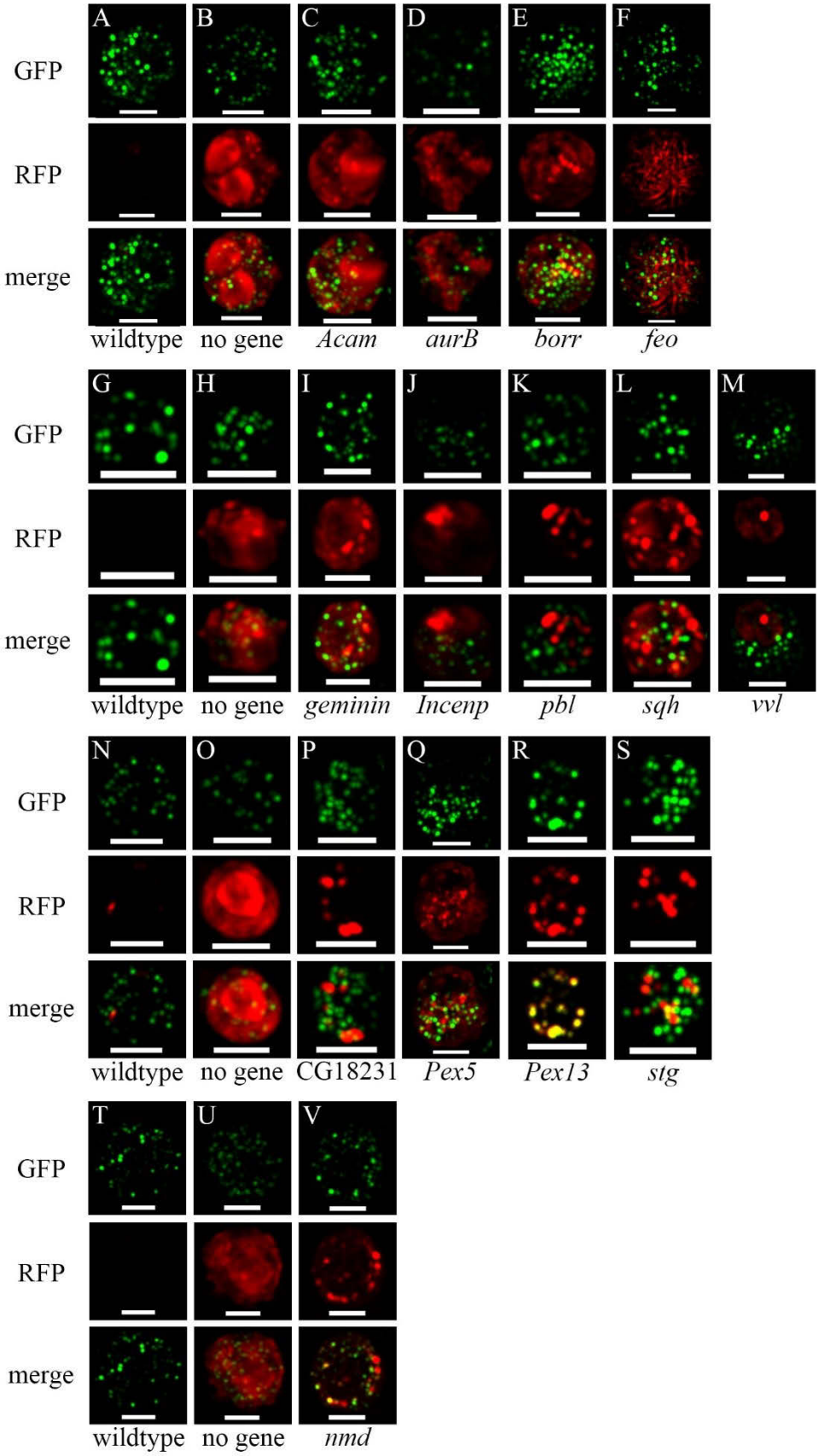
A
B
C
D
E
F
GFP
RFP
merge
wildtype
no gene
Acam
aurB
borr
feo
G
H
I
J
K
L
M
GFP
RFP
merge
wildtype
no gene
geminin
Incenp
pbl
sqh
vvl
N
O
P
Q
R
S
GFP
RFP
merge
wildtype
no gene
CG18231
Pex5
Pex13
stg
T
U
V
GFP
RFP
merge
wildtype
no gene
nmd

Figure 16. Qualitative effects of transient over-expression on peroxisome abundance. Plasmids containing N-terminal RFP reporter fusions of candidate peroxisome abundance regulator genes (red) were transiently transfected into S2 cells stably expressing GFP-PTS1 (green). The screen was conducted in four batches, presented here as columns A-F, G-M, N-S and T-V. The gene over-expressed is named under each column. All images are maximum intensity Z-projections. $n \geq 3$, scale bars = 2 μm.

Chapter 5 Discussion

5.1 The developmental *Drosophila Pex7* expression pattern and mutant phenotypes suggest a novel function

My observations of *Pex* transcription revealed most *Peroxin* mRNAs were found throughout the early embryo (Figure 4). Peroxin reporter fusions were observed previously to co-localize with peroxisomes in S2 cells (Baron *et al*., 2016). Together, these data support the hypothesis that *Drosophila Peroxins* conserve the localization, and thus the functions, of their mammalian homologs (Figure 1). The notable exception was *Pex7*. The identity of fly and human *Pex7* coding sequences, protein sequences and predicted domains (Figure 17A-B), suggested *Drosophila Pex7* conserved mammalian *PEX7* function. This hypothesis was supported by *Pex7* reporter fusion observations and experiments showing the ability of fly *Pex7* to restore human peroxisomal Thiolase localization in RCDP patient fibroblasts (Baron *et al*., 2016; Di Cara *et al*., 2017). Support for the *Pex7* conservation hypothesis was eroded by the loss of the PTS2 motif in the fly proteome (Faust *et* al., 2012). Some species, like *C. elegans*, have no PTS2 motif and no *Pex7* homolog in their genome (Motley *et al*., 2000). The loss of *Pex7* in organisms that do not use PTS2-mediated import seems logical from an evolutionary perspective because there is no need to retain a gene that carries out no function. Thus, the retention of Pex7 protein in flies suggested it had a purpose. In the present study I observed *Drosophila Pex7* mRNA and protein were extant, spatially restricted and had variable abundance during embryo development. *Drosophila Pex7* co-localized with peroxisomes, even though the PTS2 motif is absent, and is expressed only in specific cells during development (Chapter Three; Baron *et al*., 2016). *Pex7* mutant adult flies had affected lipid processing based on observations of altered lipid species abundance in total fatty acid content (Di Cara *et al*., 2019). My work determined loss of *Pex7* in post-mitotic neurons impaired hatching. I hypothesize *Pex7* performs a peroxisome-related function involving lipid metabolism that is essential to the developing nervous system. Future study into the potential role of *Pex7* in lipid processing, and whether that has a direct effect on peroxisome activity in *Drosophila* development and other life stages, will clarify the *Pex7*-peroxisome relationship and determine if *Drosophila* is a suitable RCDP model.

Continued characterization of *Pex7* may be useful to understanding the tissue-specific symptoms of RCDP, a human PBD caused by mutation in *PEX7* or one of its client enzymes.

RCDP causes skeletal defects, inappropriate or missing ossification of cartilage, and reduced plasmalogen (C16-C18 fatty acid) abundance (Braverman *et al.,* 2001; Irving *et al.*, 2008; Krakow *et al*., 2003). RCDP symptoms that manifest later in life include congenital cataracts, mild to severe mental retardation and recurrent respiratory tract infections due to neurologic compromise (Braverman *et al.,* 2001). The most severe RCDP symptoms are thought to be due to failed import of all PTS2 client enzymes, indicating loss of *PEX7* function. The specificity of RCDP symptoms suggest *PEX7*, and by extension the lipid metabolism functions it is necessary for, have an important role in nervous system development and homeostasis (Braverman *et al*., 1997; Braverman *et* al., 2001).

5.2 Early embryonic *Peroxin* mRNA localization suggests expression in all cell lineages

Previous characterization of *Drosophila Pex* genes focused on the characterization of larval and adult mutagenesis phenotypes. For example, third instar larvae with loss-of-function mutation in *Pex3* were smaller and contained less ceramide than their rescued counterparts (Faust *et al*., 2014). Muscle-specific knockdown of *Pex3* resulted in reduced survival to the adult stage by impairing eclosure (Faust *et al*., 2014). *Pex5* mutant adults displayed similar larval phenotypes, as well as highly disorganized neural, glial and muscular patterns during embryogenesis and altered larval abundance of VLCFA species (Di Cara *et al*., 2019). *Pex7* mutant larvae had reduced CNS size, and increased embryonic and larval neuro-specific apoptosis activity that was somewhat rescued by *nos>Pex7* (Di Cara *et al.,* 2019). As these examples illustrate, the expression of *Peroxins* during normal embryogenesis has yet to be explored systematically.

FISH analysis showed that *Pex* mRNAs had relatively equal prevalence in all areas of the embryo before cellularization, as would be expected were the canonical function of the cognate genes conserved. Supporting this hypothesis, there were some notable *Pex* mRNA observations that permitted functional inferences. *Pex1* and *Pex6* mRNA demonstrated similar FISH patterns at 4-8 h AEL. *Pex1* and *Pex6* are involved in similar aspects of peroxisome biogenesis in yeast and humans, so it was expected that they would both be expressed ubiquitously were that relationship preserved (Motley *et al*., 2015; Ciniawsky *et al*., 2015; Tamura *et al*., 2006). The

Pex3 FISH signal was also relatively equal in all gastrulating cells, suggesting Pex3 carries out an essential function apart from its role in muscle development. Said function may be the sorting of PMPs and Peroxins to ER-derived PPVs at the onset of *do novo* peroxisome biogenesis, as was observed in *S. cerevisiae* (Figure 4D; Faust *et al*., 2014; Hoepfner *et al*., 2005). The *Pex5* FISH signal was largely absent during gastrulation, matching its RNAseq temporal expression pattern (Graveley *et al*., 2011). Gastrulation is a period of co-ordinated changes in the morphology and division of primordial embryonic cells to generate two internal tissue layers, the mesoderm and the endoderm. Protein and mRNAs contributed by both the mother and the embryo are essential to the process (reviewed by Leptin, 1999). A lack of *Pex5* mRNA during gastrulation, within the context of its established necessity and conservation, suggests that sufficient Pex5 was either produced during the prior embryogenesis stage, the syncytial blastoderm, or was contributed maternally. The process of gastrulation also involves cell division and differentiation, necessitating synthesis of new plasma membrane and organelles (reviewed by Leptin, 1999). Therefore, it is reasonable to assume Pex5 is necessary during gastrulation because non-energetic lipid metabolism, a core function of peroxisomes, is essential to the production of new plasma membrane and Pex5 is essential to the proper localization of some of the necessary enzymes. It is possible that Pex5 accumulated by a sufficiency or checkpoint mechanism prior to gastrulation, permitting degradation of maternally-contributed *Pex5* mRNA during the MZT without replacement by zygotic *Pex5* mRNA. Transcript stability during early embryogenesis, and maternal vs embryonic mRNA source, could be determined empirically by measuring target mRNA abundance in fertilized and unfertilized *Drosophila* eggs (Semotok *et al*., 2008). This would disambiguate if *Pex5* mRNA abundance drops at the onset of gastrulation due to a lapse between maternal and embryonic *Pex5* transcription.

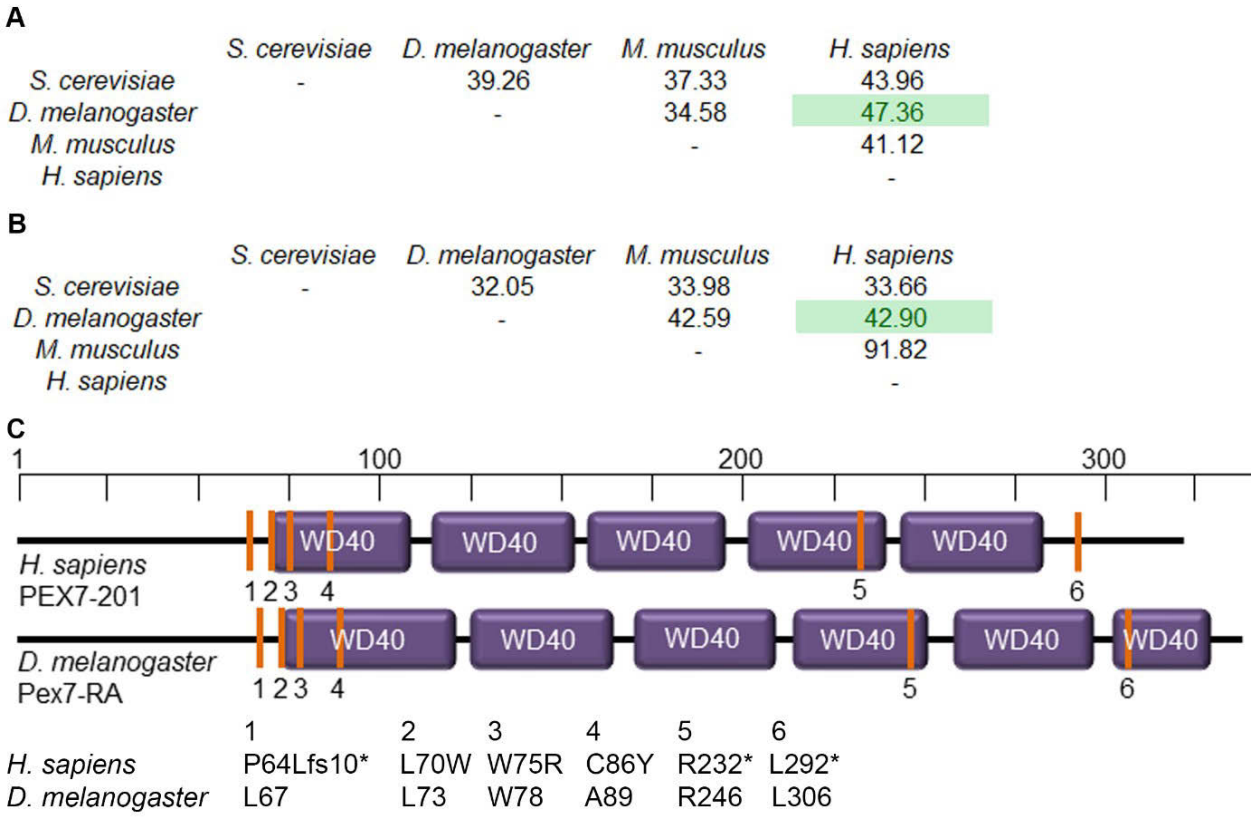

Figure 17. A comparison of *Pex7* sequence and domain identity. (A) Primary coding sequence percent identity matrix (PIM) revealed fly-human identity was higher than that of mouse-human. (B) Primary protein isoform PIM revealed fly-human protein sequence identity was within 5 % of their DNA sequence identity however it is less than half that of mouse-human protein sequence identity. (C) Human-*Drosophila* Pex7 protein domain comparison. Human disease-associated residues and alignment-predicted *D. melanogaster* equivalents are labeled (vertical orange bars). The specific lesions are detailed beneath.

Other *Pex* genes also showed unique spatial FISH patterns during gastrulation. The pattern of *Pex11* FISH was concentrated in the germ band and posterior midgut rudiment at 4-8 h AEL, suggesting fission-mediated peroxisome proliferation was occurring there. The overall spatial pattern of *Pex19* FISH signal 4-8 h AEL was similar to that of *Pex13*, which is interesting because their functions are not part of the same process. *Pex13*, though uncharacterized, may encode a conserved protein that is part of the import translocon at the peroxisome membrane that facilitates matrix protein import, along with *Pex14* (Table 1; Dias *et al*., 2017). The knockdown and over-expression experiments in my second project support the conservation of *Pex13* (Chapter Four). To contrast, mRNA FISH patterns differed for *Pex5*, *Pex13* and *Pex7* at 4-8 h AEL (Figure 4E, 3G and 3H, respectively), though this may be due to differences in developmental stage of the embryos imaged for each gene. *Pex19*, though also uncharacterized, may encode a chaperone protein that, together with Pex3, regulates the import of peroxisome membrane proteins into PPVs forming at the ER (Sacksteder *et al*., 2000). The striped pattern observed for *Pex19* FISH at 2-4 h AEL suggested it was regulated by a gap or pair rule gene, though no specific body pattern gene matched the observed *Pex19* transcription pattern (Nüsslein-Volhard and Wieschaus, 1980, flybase.org). At 4-8 h AEL the *Pex19* FISH signal accumulated in the midgut, the same temporal window that *Pex11* FISH signal was observed in the germ band and posterior midgut rudiment. These non-overlapping patterns suggested cells expressing *Pex11* were undergoing fission-mediated peroxisome proliferation, perhaps during the neural and gut organogenesis that follows mesoderm and endoderm differentiation, whereas gut cells expressing *Pex19* were undergoing *de novo* biogenesis (reviewed by Leptin, 1999). The inconsistent transcription patterns for other *Peroxins* in the 4-8 h AEL window, e.g. *Pex3* and *Pex5*, suggested peroxisome biogenesis occurs by both *de novo* and fission pathways during early *Drosophila* embryogenesis. This hypothesis is supported by the differing FISH patterns for *Pex11* and *Pex19* mRNA I observed. Alternatively, the temporal resolution of the 4 h collection window I used may have been too low, and overlapping patterns for various *Peroxins* may have been missed. Tighter collection windows, e.g. 30 min, may resolve this shortcoming.

The Berkeley Drosophila Genome Project (BDGP) maintains a curated database of embryonic expression patterns for genes from several genomic resources. The genes were characterized via high-throughput *in situ* hybridization of mRNA with complementary anti-sense

probes visualized by chromogenic staining. The FISH data presented in Figure 4 were compared with the BDGP data, where available. My data were in agreement for *wg*, *Pex1*, *Pex14* and *Pex19*. The data also agreed for *Pex11* and *Pex16* until stage 6 (~4 h AEL), after which the BDGP data reported nothing. In the case of *Pex11*, my 4-8 h AEL data may include background fluorescence due to tissue folding resultant of ventral nerve cord formation. In the case of *Pex16*, a faint signal was observed at 4-8 h AEL (stages 9-12; Figure 4L) that may have been below the detection threshold of the BDGP's chromogenic visualization method because the BDGP data reported no signal. *Pex5* had no signal until 8 h AEL in the BDGP data, contrary to the ubiquitous signal at 2-4 h AEL I observed (Figure 4E). Similarly, I observed a ubiquitous signal of *Pex7* mRNA until about stage 9 (about 8 h AEL), whereas the BDGP database reported no signal (Figure 4G). There is agreement between the data sets on *Pex7* mRNA patterns from about 8 h AEL until hatching. There was insufficient BDGP data to compare my observations for *Pex3*, *Pex6*, *Pex10*, or *Pex13* mRNA localization. Overall, differences in detection method provided greater resolution of the individual probe puncta in my study but weakened the patterns observed in the BDGP data.

Future improvements to FISH-based characterization of embryonic *Peroxin* mRNA localization include studying additional time points. For every *Peroxin* gene studied here except *Pex7*, data was only collected for 2-4 and 4-8 h AEL. Later time points may reveal novel mRNA localization patterns for other *Peroxins*, as was observed for *Pex7*. Second, my data set is missing observations for *Pex* translation. Classically, this would require validation of an antibody for each protein of interest. This approach is prohibitive in terms of cost, scale and labour for a whole gene family. Recent innovations using CRISPR-based genomic insertion, or "knock-in", permit tagging of endogenous genes with fluorescent reporters (Kina *et al*., 2019). This would permit observation of translation patterns at whole-organism and cellular resolutions *in vivo* and *in vitro*. Elaboration on my FISH data set could be achieved by generating cell-resolution expression data via single-cell transcriptome sequencing (scRNA-seq) or microarray analysis. For example, scRNA-seq could be used to identify the cell types expressing *Pex11* vs *Pex19* (Klein *et al*., 2015).

5.3 Comparing *Pex7* transcription and translation during *Drosophila* embryogenesis

A striking spatial expression pattern was revealed for *Drosophila Pex7* in developing embryos. Qualitative analyses confirmed *Pex7* mRNA and protein were present in a small subset of cells adjacent to neurons and glia. Quantitative analyses confirmed transcript and protein levels varied as the visual patterns changed. There were small differences observed in the patterns of *Pex7* mRNA and protein localization (Figures 4D-E and 6D-E). It is likely that in the cells where Pex7 was observed in the absence of its mRNA that the FISH signal intensity was below the detection threshold. More collection windows within each time point may identify transcription patterns that were not observed in the present study. I must also acknowledge the novel Pex7 antibody I used was not verified in *Pex7* mutant embryos. There are no true *Pex7* null mutant stocks available presently, although it is possible to generate a sufficient population of ubiquitous somatic *Pex7* knockouts using TRiP-KO to further test the specificity of anti-Pex7.

Identifying the cell type expressing *Pex7* was a goal of my project. Unfortunately, no neural lineage marker antibody overlapped with anti-Pex7, though anti-Pex7 did appear adjacent to anti-Elav and anti-Nrg (Figure 8). Microscope calibration determined the image layers were not displaced, ruling out false negative overlap. Cellular transcriptomic and proteomic profiling would be of excellent use in determining the neural cell type expressing *Pex7*. Transcriptomic profiling could be achieved by scRNA-seq and verified by microarray analysis (Klein *et al*., 2015). At present proteomic analysis has yet to reach single-cell resolution reliably, however tagging of endogenous *Pex7* and the neural markers used in this study, via CRISPR-mediated knock-in, could verify my IF findings and expand the data set to imaging *in vivo* (Kina *et al*., 2019).

5.4 *Pex7* is required in cells of the developing *Drosophila* nervous system

The results presented in Chapter Three suggested there were different functional requirements for *Pex7* in different subsets of embryonic nerve cells. Somatic CRISPR mutation via *elav>Pex7* TRiP-KO reduced viability by impairing hatching, whereas *pnr>Pex7* TRiP-KO did not (Figure 10). This suggested either the embryonic CNS required *Pex7*, or that embryonic

neurons required *Pex7* before acquiring their CNS/PNS fates. Either way, the effect of neuro-specific *Pex7* mutation on hatching suggested therere was a functional requirement for *Pex7* within embryonic neuronal cell lineages (Figure 10). Similar effects were observed when *Pex14* was mutated in neurons. *Pex14* encodes a conserved protein with a critical role in peroxisome matrix enzyme import, confirming a requirement for peroxisomal enzyme function in *Drosophila* neurons (Faust *et al*., 2012; Fujiki *et al*., 2014; Baron *et al*., 2016). Given previous results showing *Pex7* mutation caused brain defects in developing larvae (Di Cara *et al.* 2019), my observation that *Pex7* was required in embryonic neurons suggested the restricted spatio-temporal expression pattern observed for *Pex7* mRNA and protein at 16-20 h AEL (Figure 5G; Figure 7G), was due to a requirement for *Pex7* in those cells. Together, the data suggest that *Drosophila Pex7* is required by neurons for normal embryonic CNS development. Within the context of the literature, my data suggest *Pex7* has evolved a novel function that may not be related to the import of enzymes into the peroxisomal matrix. However, the function of *Pex7* remains related to lipid metabolism and ROS management in the cells in which it is expressed.

The knockout efficiency of the TRiP-KO system was not independently verified in my study. It is possible that the semi-lethal phenotype arose because the knockout was incomplete due to low efficiency. Alternatively, the indel generated by Cas9 may not have affected *Pex7* function consistently because the indel size may have been variable, resulting in a variable phenotype. Addressing these concerns, the consortium that created the TRiP-KO toolkit described how the strains were generated:

> *For all TRiP-CRISPR stocks, we used the DRSC Find CRISPR Tool (...) to pick the optimal sgRNA designs. With the knockout collection, we selected the sgRNAs targeting the first or second coding exons common to all isoforms with high efficiency scores and specificity scores. The efficiency scores we considered include the Housden efficiency score, which is based on a nucleotide position matrix (...), and the frameshift score, which predicts the likelihood of a frameshift happening based on microhomology sequences near the cutting site (...). At the same time, we also prioritize the designs with high specificity scores, including the seed score (the length of unique seed region) and off-target score* (Zirin *et al*., 2020).

Neuro-specific *Pex7* OE significantly reduced over-expressing:total adult ratios. This was different from phenotypes related to likewise-targeted *Pex1* OE, which had a stronger effect when over-expressed as directed by the *Act5C* enhancer (Figure 11). This suggested that *Pex7* was required in neurons whereas *Pex1* was required in multiple cell lineages. For the most part, non-specific effects were not observed in the transgenic lines used. An exception was the reduced egg counts in the *Pex7* OE assay (Figure 11C) although quantifiable defects in the fertility of the parent strains were not observed, i.e., neither parental strain was difficult to maintain. A similar but non-significant effect on egg counts was observed in TRiP-KO lines (Figure 10E). The control crosses also showed a similar effect even though they demonstrated a higher larva:egg ratio (Figure 10F), so the non-specific effect is probably not due to reduced parental fertility. The genetic elements of the OE experiment are designed to permit over-expression only when all elements are present, and neither parental strain had all the transgenes to permit that. The cause of the observed OE phenotype remains unknown. However, as both *Pex7* knockout and OE were semi-lethal when targeted to neurons it is possible there is a critical level of expression required for *Pex7* in those cells. This hypothesis is supported by the impaired hatching I observed in the *elav*-driven attempted rescue of homozygous *Pex7* mutants, which was similar in phenotype to that observed for *elav>Pex7* knockout. Alternatively, there may be a range of tolerable *Pex7* expression, especially considering the high relative level of expression of the *elav>Pex7* transgene (Figure 12G).

The specifics of the role of *Pex7* in peroxisome function remains unclear. Conserved *Peroxin* genes were used as positive controls in my knockout and OE experiments and reported similar phenotypes, although experimental design may have restricted phenotypic outcomes resulting in a false positive correlation between *Pex7* and either or both of the controls. Contrariwise, in the case of *Pex1*, ubiquitous OE resulted in a stronger phenotype than tissue-specific OE, reinforcing the tissue specificity of *Pex7* reported by my FISH and IF observations. The *Pex1* data also suggests *Pex1* was necessary in all cells, as is expected were it conserved. It is likely that Pex7 has a peroxisome-linked function because homozygous *Pex7* mutant larvae had altered lipid content, and expression of *Drosophila Pex7* rescued localization of thiolase in *PEX7* mutant fibroblasts from human RCDP patients (Di Cara *et al*., 2019). *Pex7* may therefore conserve some neuro-specific aspect of peroxisome cargo protein trafficking.

5.5 Altered expression of several genes not previously linked to peroxisomes influence peroxisome abundance in *Drosophila*

5.5.1 Overview of cell culture-based screens to identify genes involved in peroxisome biogenesis

Studies have used cell lines established from *Drosophila* tissues for over 50 years. These lines have been used for such diverse purposes as material sources for protein purification/ extraction, studies of basic cellular mechanisms, expression/investigation/purification of transgenes and their products, RNAi screening, pathogen and immune response studies, genomic analyses, and as bioreactors for secreted proteins and other factors (reviewed by Cherbas and Gong, 2014). Perhaps the best known *Drosophila* cell line is Schneider 2 (S2) cells. S2 cells are immortalized and in my hands take up plasmids easily, respond well to common transfection reagents like Effectene (Qiagen) and require no special culture conditions like CO_2 supplementation or media formulations. Studies of peroxisome-motor protein dynamics were also modeled in S2 cells, establishing the model's suitability to study peroxisomes in the context of other processes and pathways. That aside, the bulk of classical peroxisome biogenesis factor research was carried out using mammalian cell models such as CHO cells, PBD patient fibroblasts and various rat tissues. Challenges with the acquisition, use, maintenance and disposal of these models aside, the central theme of my work is the exploration of peroxisomes in *Drosophila*, which none of these alternative models permit. Translating cell study results into animal experiments is comparatively easy for *Drosophila* given the quality and availability of molecular tools, the high genetic tractability of the model, and the translatability of experimental approaches between cell and animal studies, for example the Gal4-UAS system, CRISPR-based mutagenesis approaches, and Gateway plasmids.

Using S2 cells has caveats. The cell line is derived from primary cultures isolated by crude homogenization of late-stage embryos, making determination of their tissue of origin difficult. Indeed, the original publication stated no effort was made to identify what tissue the culture came from (Schneider, 1972). However, their macrophage-like behaviour suggests S2 cells derive from a macrophage cell lineage such as haemocytes (reviewed by Cherbas and Gong, 2014). The genetic landscape of commercial S2 cells has not been characterized, apart from

determining their sex (DGRC.bio.indiana.edu), and it is unknown if successive passages of the current commercial stock have an effect on genomic stability as it did for the original culture, which incidentally was mixed-sex before becoming predominantly female by the sixteenth passage (Schneider, 1972). As a result, S2 cells may have altered proteomic, translatomic or genomic landscapes that could affect the applicability of data generated using cultured cells to whole animal studies. Thus, replicating the studies presented in Chapter Four in other cell types, e.g. Kc167 (the female equivalent of S2) and one or more of the CME lines, which are derived from various larval imaginal discs, may reveal different effects on peroxisomal abundance for the same candidate genes (DGRC.bio.indiana.edu).

Dating back to the first examinations of peroxisome biogenesis in PBD patient livers (Goldfischer *et al*., 1973), and perhaps even to the original "microbody" electron micrographs in Rhodin's dissertation (1954), the "gold standard" of peroxisome biogenesis study has been a visual assessment of changes in peroxisome abundance and morphology. Early reports indicated peroxisome size and counts varied by tissue in wildtype animals, making quantitative data generation difficult before the wide availability of computers and imaging software. Hence, assessment criteria remained principally qualitative. In the present study, image processing software was used to count GFP-labeled peroxisomes in 3D images of fields of cells. This approach provided a systematic and quantitative readout of changes in peroxisome abundance from qualitative data and allowed comparison between treatment types.

5.5.2 RNAi screen reveals cellular processes that affect peroxisome abundance

The RNAi-based genomic screen done by A. Magico that provided the preliminary data for the present study itself follows up on screens for novel *Peroxins* by J. Lacey and P. Drake (Drake, 2012; Lacey, 2015; A Magico, unpublished data). Drake's screens included a high-throughput RNAi analysis of *Drosophila* S2 cells transiently expressing GFP-PTS1 and a follow-up RNAi screen stably expressing the same reporter. The Drake screen reported that knockdown of *Drp1*, *Hsp83*, *nmd*, *Pex5*, *Pex7*, *Pex13*, *sqh* and *Tango11* resulted in altered GFP-PTS1 morphology (Drake, 2012). My study determined four of the genes from the Drake study also alter peroxisome abundance, namely *nmd*, *Pex5*, *Pex13* and *sqh*. Lacey followed up on *nmd* in

S2 cells and discovered its knockdown led to mislocalization of *Pex3*, a gene essential for PMP localization at ER subdomains during *de novo* peroxisome biogenesis (Lacey, 2015; Table 1). Nmd was also found to co-localize to both mitochondria and peroxisomes, supporting my observations of partial co-localization between RFP-Nmd and GFP-PTS1 (Figure 16V; Lacey, 2015). The results of these prior screens suggested there were genes besides the *Peroxins* that could affect peroxisome biogenesis and supported continued exploration for more candidates.

RNAi of eight genes resulted in altered peroxisome abundance using at least two different dsRNA molecules per gene. Knockdown of six resulted in increased peroxisome abundance: *Acam*, *aurB*, CG7627, CG18231, *feo*, and *Incenp*. The genes *feo* and *Incenp* are involved in mitotic spindle formation, *Acam* encodes a presumptive motor protein regulator, *aurB* is involved in chromosome segregation, and CG7627 and CG18231 are not characterized empirically. Knockdown of two genes reduced peroxisome abundance, *nmd* and *pbl*. *nmd* is involved in mitochondrial inheritance and may sort *Pex3* to ER subdomains. *pbl* regulates actin organization during cytokinesis. Thus, four genes are necessary for mitosis and another (*Acam*) may encode a homolog for a mitosis-specific regulator of cytoskeleton-peroxisome interaction and movement. Through the observed effects of individual gene knockdown, my RNAi screen revealed an indirect effect of certain perturbed cellular processes on peroxisome biogenesis, specifically the cell cycle and cytoskeleton-organelle interaction. Although these data were generated using multiple dsRNAs per gene, I acknowledge that further validation through qRT-PCR would increase my confidence in the effects I observed.

a. The effect of Peroxin *knockdown*

The knockdown of *Pex13* reduced peroxisome abundance (Figure 13, Table 7), validating the screen and suggesting the mechanism by which mitosis and cytoskeleton-organelle dynamics affect peroxisome abundance may be through interactions with, or effects on, Peroxins. This conclusion is supported by the nature of the GFP-PTS1 reporter I used, which only marks import-competent peroxisomes. Furthermore, as *Pex13* is not known to be involved in peroxisome proliferation or membrane assembly, this data suggests peroxisome abundance may ultimately be affected by impacting one or more categories of peroxisome biogenesis. The experimental design does not rule out the possibility that altered pexophagy may play a role in

the observed phenotypes. Pexophagy is not known to be directly regulated by Peroxins (Table 1) and no gene I investigated has a known role in the process, though pexophagy may be a confounding variable if peroxisome function is compromised such that the process is triggered.

b. Genes with a canonical or predicted role in cell division

Knockdown of *pbl* weakly reduced peroxisome abundance, barely exceeding the cutoff value (Table 1). Pbl is a RhoGEF with well-characterized roles in actin cytoskeleton organization and cytokinesis through its function as a Rho signal transduction regulator (flybase.org). The human *pbl* homolog, *ECT2*, is an oncogene that is considered a major regulator of mitosis and growth through its direct regulation of the actin-myosin contractile ring (Chen *et al*., 2019). Yeast relies on the actin cytoskeleton for organelle inheritance during mitosis, however *Drosophila* uses dynein and kinesin motors for peroxisome movement so it is unlikely that *pbl* knockdown exerted a direct effect on peroxisome abundance (Kural *et al*., 2005; reviewed by Knoblach and Rachubinski, 2015). In this context, *pbl* likely exerted an indirect effect on peroxisome abundance through its regulation of cytokinesis. Depletion of PDZ-RhoGEF and LARG, two classes of human RhoGEFs, resulted in reduced cholesterol efflux (Okuhira *et al*., 2010). Hypothetically, this would increase cellular cholesterol levels and reduce peroxisomal metabolic demands, which may lead to pexophagy and reduced peroxisome abundance. Knockdown of the *Drosophila* chaperone Hsc70-5 and its putative human homolog HSPA9 both resulted in reduced peroxisome abundance, which for the latter was traced to increased pexophagy and increased oxidative stress (Jo, Park *et al*., 2019). Thus, my hypothesis could be tested by measuring changes in cellular cholesterol and Hsc70-5 expression resultant of *pbl* mutagenesis.

c. Genes encoding canonical or predicted motor protein regulators

Acam knockdown resulted in increased peroxisome abundance, suggesting the loss of the myosin VI light-chain it putatively encodes caused dysregulated peroxisome dynamics and increased peroxisome proliferation. This result also ties *Drosophila* peroxisome dynamics to the actin cytoskeleton, as myosin motors interact specifically with actin filaments. The classical *Acam* phenotype was traced to the direct interaction of Acam with myosin VI located on the actin cone during spermiogenesis (Frank *et al*., 2006). These data challenge the dogma that

microtubules and dynein/kinesin motor proteins are solely responsible for *Drosophila* peroxisome dynamics, though there is a precedent for both cytoskeletal elements affecting peroxisomes in CHO cells (Kural *et al*., 2005; Rapp *et al*., 1996). *Acam* may encode a mitosis-related inhibitor of the myosin motor protein complex, such that when it is lost the result is increased organelle biogenesis. Alternatively, *Acam* may upregulate organelle biogenesis but require modification like phosphorylation to be activated. A third possibility is that *Acam* knockdown may have caused or permitted the upregulation or preferential binding of another factor to myosin motors that resulted in increased peroxisome proliferation, such as a mitosis-specific myosin regulator. Diminished or lost *Acam* may therefore arrest mitosis without directly affecting peroxisome biogenesis, resulting in a division-incompetent cell that has increased its peroxisome abundance in anticipation of division but cannot segregate them. The canonical *Acam* mutant phenotype is specific to males, and current commercial S2 cultures are also male (reviewed by Cherbas and Gong, 2014), so testing the peroxisome-related *Acam* knockdown phenotype in female cells such as Kc167 would determine if the effect is sex-specific. A study by Frank *et al*. (2006) determined Acam was a tissue-specific Calmodulin replacement, so assaying changes in *Cam* expression resultant of *Acam* knockdown would determine if Cam is involved, or is the hypothetical competitive Acam inhibitor that I proposed. CRISPR-mediated tagging of endogenous Acam and myosin VI with fluorescent reporters would permit observation of their co-localization with peroxisomes *in vivo*.

d. Genes encoding canonical or predicted transmembrane transport proteins

Knockdown of the putative ATPase CG7627 resulted in higher peroxisome abundance (Figure 13, Table 7). Explaining this result is challenging given the essential role of the ATPases Pex1 and Pex6 in recycling Pex5 to the cytosol, as well as the opposite phenotype being reported for knockout of either Peroxin (Figure 1, Table 1; Mast *et al*., 2011). The predicted human ortholog of CG7627, *ABCC4*, encodes a cellular detoxifier that pumps organic anions and prostaglandins across the plasma membrane called Multidrug resistance-associated protein 4 (flybase.org). Prostaglandins mediate the inflammatory response and interact with PPARs once secreted (Reid *et al*., 2003). *Drosophila* conserves prostaglandin synthesis and secretion but not PPARs (Tootle and Spradling, 2008; flybase.org). Hypothetically, loss of prostaglandin secretion via CG7627 knockdown could reduce inflammation, reducing peroxisome proliferation in

response to either as-yet unknown cues or the immune response. This hypothesis assumes conservation of autocrine/paracrine prostaglandin activity, and if correct would result in the opposite phenotype than reported here. Alternatively, if knockdown of CG7627 results in reduced organic anion efflux then cytosolic oxidative stress may accumulate because of increased ROS levels, resulting in increased peroxisome biogenesis. The second hypothesis agrees with my observations. An assay of cellular redox state and changes in Peroxin expression resultant of CG7627 knockdown would test the anion efflux hypothesis.

e. Genes encoding canonical or predicted regulators of mitochondrial function

Knockdown of *nmd* reduced peroxisome abundance (Figure 13, Table 7). The function of *nmd*, a predicted AAA ATPase, has yet to be fully explored however its loss resulted in spermatids without mitochondria, causing male sterility, and disrupted dorsal-ventral patterning in wings (Bejarano *et al*., 2008; Lindsley and Zimm, 1992). Lacey (2015) reported that loss of *nmd* resulted in mislocalization of Pex3, which in the context of its mammalian counterpart's role in sorting PMPs in the ER prior to *de novo* biogenesis (Table 1), suggested the function is conserved and that *Drosophila* employs both pathways of peroxisome biogenesis concurrently (Fakieh *et al*., 2013). Knockdown of *nmd* in my study appeared to mildly reproduce a loss-of-function phenotype reported previously (Lacey, 2015), which may have resulted in reduced peroxisome abundance by diminishing *de novo* biogenesis. Alternatively, because Nmd is predicted to contain an AAA ATPase domain, it may be essential to peroxisome import competence similar to *Pex1* (Table 1). RNAi of the AAA ATPase *Pex1* in S2 cells resulted in a similar loss of GFP-PTS1 puncta (Mast *et al*., 2011). Assaying the localization of FLAG-Pex5 resultant of *nmd* knockdown, which normally co-localizes about 70 % with GFP-PTS1 (Baron *et al*., 2016), would test my alternative hypothesis.

f. Genes encoding canonical or predicted enzymes

The effects of CG18231 knockdown are difficult to interpret, largely due to the lack of information about CG18231's function. Based on the domains found in its predicted primary sequence, the protein is an iron-binding oxidoreductase that contributes to peptidyl-proline hydroxylation, a central enzymatic function of collagen synthesis (flybase.org). CG18231 has three predicted human orthologues, *P4HA1*, *P4HA2* and *P4HA3*, all of which encode alpha

subunits of procollagen synthesis enzymes (flybase.org; Helaakoski *et al*., 1989; Annunen *et al*., 1997). *Drosophila* conserves collagen synthesis and uses procollagen IV as an essential component of the basement membrane, an extracellular matrix component (Lunstrum *et al*., 1988). A procollagen IV-like macromolecule, pericardin, is an essential component of the pericardium surrounding the *Drosophila* heart (Wilmes *et al*., 2018). Pericardial cells (PCs) use an altered redox state to regulate nearby cardiomyocytes (CMs; Lim *et al*, 2014). It is therefore possible that reduced procollagen synthesis, due to CG18231 knockdown, results in an altered cellular redox state and a subsequent increase in peroxisome biogenesis to mitigate increased ROS toxicity. Observation of cellular redox state, *Peroxin* expression and ROS enzyme expression resultant of CG18231 knockdown would test this hypothesis.

g. Genes with no observed effect in the present study

Knockdown of *Cdk1*, *stg* and *vvl* were not observed to have a significant effect on peroxisome biogenesis in this study. The dsRNA molecules I employed were designed to affect all splice variants of *Cdk1* mRNA. It is possible all the cells that underwent *Cdk1* RNAi failed to pass the M phase checkpoint of the cell cycle and died, leaving only unaffected cells to be counted and returning a false negative result. Alternatively, the knockdown effect may have been insufficient to overcome the redundancy of the Cdk1 family. It is also possible that a lack of cell cycle progression may have caused cell volumes to be abnormally large, skewing the automated determination of peroxisomes per unit area. However, *Cdk1* RNAi did not appear to alter cell size (Figure 14), suggesting the dsRNA effect, if any, was below the detection threshold rather than significant enough to alter cell cycle progression without inducing cell death. Measuring the transcript abundance of all *Cdk1* isoforms in cultures undergoing *Cdk1* knockdown via qRT-PCR would determine if my dsRNAs were effective.

Knockdown of *stg* did not appear to have an effect on peroxisome abundance. The importance of *stg* to centriole replication, and thus to cytoskeleton-organelle interactions, mitosis and ultimately to cell homeostasis in general, implied only unaffected cells remained alive following knockdown. Alternatively, no dsRNA molecule may have produced a strong enough phenotype to be detected. *stg* encodes two isoforms and has one paralog, *twe*, suggesting the redundancy mechanism proposed for the lack of a *Cdk1* RNAi phenotype does not necessarily

apply to *stg* (flybase.org). Cell size was not apparently altered in cells treated with *stg* dsRNA (Figure 14), which would be expected if cells had doubled everything in preparation for division that failed to occur. Verification of *stg* knockdown by qRT-PCR would resolve the redundancy hypothesis and determine the efficacy of my dsRNAs.

vvl knockdown may or may not have affected peroxisome abundance. *vvl* encodes a transcription factor that signals changes in cell fate by enhancing RNApolII recruitment to context-specific genes, depending on its binding partners (Junell *et al*., 2010; Anderson *et al*., 1995; Inbal *et al*., 2003; Certel *et al*., 1996; de Celis *et al*., 1995). Given the late embryonic stage from which S2 cells were originally isolated and the unknown genetic changes that the culture underwent leading to its immortalization, it is difficult to posit why *vvl* knockdown may diminish peroxisome abundance, but easy to understand why the data are ambiguous (Schneider, 1972; reviewed by Cherbas and Gong, 2014). My study reported two *vvl*-targeting dsRNAs had a significant effect while another two did not (Figure 13), although three dsRNAs were designed to target all *vvl* splice isoforms. Further characterization of *vvl* is required to elucidate how it is involved in peroxisome biogenesis, and to improve the reproducibility of its knockdown phenotype. Verification of each *vvl* dsRNA's effectiveness by qRT-PCR would disambiguate my data.

5.5.3 Transient over-expression reveals cellular processes that affect peroxisome abundance

While knockdown via RNAi may help elucidate a gene's function, as the gene product may become rate-limiting or otherwise insufficient to maintain a wildtype phenotype, classical genetic analysis maintains that it is also informative to observe the effects of additional gene product, or over-expression (OE). This approach has identified oncogenes, body patterning genes, and regulators of organelle abundance in *S. cerevisiae*, *A. thaliana*, *D. melanogaster* and cell lines from several organisms (reviewed by Prelich, 2012). I explored the transient OE of a cohort of genes identified previously to observe effects on peroxisome abundance (A Magico, unpublished data).

The OE of nine genes increased peroxisome abundance: *Acam*, *borr*, CG18231, *geminin*, *nmd*, *pbl*, *sqh*, *stg* and *vvl*; the OE of two genes, *aurB* and *Incenp*, reduced same (Figure 15, Table 8). I acknowledge there was only one over-expression plasmid used for each gene, with appropriate replicates. The ratios of change in peroxisome abundance were calculated using replicates conforming to a 95 % confidence interval. As a result, there was only one value generated for comparison to the negative and positive control values to generate the ratio and percent changes reported. As with my RNAi data, a pattern emerged of the cellular processes with which these genes were associated: organelle-cytoskeleton dynamics (*Acam*, *sqh*), cytokinesis/mitosis (*aurB, borr*, *geminin*, *Incenp*, *pbl*, *sqh*, *stg*), cell fate (*pbl*, *sqh*, *vvl*) and collagen synthesis (CG18231). Five genes are important to cytokinesis/mitosis, suggesting mitosis is a major influencer of peroxisome abundance. The OE data confirmed the findings of the RNAi screen for genes examined under both conditions by reporting complementary effects, with the exceptions of *Acam* and CG18231, and supported the hypothesis that these genes affected peroxisome biogenesis indirectly through their characterized or presumptive functions. In addition, OE of two *Peroxins* altered peroxisome abundance supporting the hypothesis that the other genes tested here ultimately affect peroxisome biogenesis by indirectly affecting the function of one or more *Peroxins*.

a. The effect of Peroxin *over-expression*

Over-expression of fusion reporters for the control genes *Pex5* and *Pex13* each resulted in increased peroxisome abundance (Figure 15). Notably, *Pex5* OE resulted in the second-highest increase in mean peroxisome abundance observed in this study (Table 8). A study of all potential *Drosophila Peroxin* orthologs using a similar approach, and the same imaging equipment, observed that FLAG-Pex5 co-localized about 70 % with GFP-PTS1 in fixed cells whereas my study using RFP-Pex5 in live cells reported adjacency without overlap (Figure 16; Baron *et al*., 2016). This suggested RFP-Pex5 was too large to enter the peroxisome. Interestingly, Baron *et al*. (2016) did not report a significant alteration in peroxisome numbers following transient FLAG-Pex5 OE, even though the reporter fusions used in that study were generated using the same Gateway system I employed. It is possible that the altered peroxisome abundance I observed was due to a cryptic confounding variable. Paired with my *Pex5* RNAi data, however, it is more likely that methodological differences, e.g. fixed vs. live cells and lack of a normalized

control in the OE experiments of the Baron *et al*. (2016) study, account for the differences. Both my data and that of Baron *et al*. (2016) support the candidacy of *Pex5* as a *bona fide Peroxin*. My data suggests peroxisome abundance correlates with that of Pex5.

The *Pex13* over-expression data complemented its RNAi data, and together suggest peroxisome abundance correlated with that of Pex13. Contrariwise, Baron *et al*. (2016) observed peroxisome number was reduced by about 17 % in S2 cells under transient Pex13 OE. They observed 72 ± 7.0 peroxisomes per untransfected cell vs. 60 ± 1.5 peroxisomes per cell reporting Pex13 OE. I was unable to determine which reporter fusion or imaging method was used to obtain the Pex13 OE data in the Baron *et al*. (2016) study. However, their report of about 64 % co-localization between their Pex13 reporter fusion and GFP-PTS1 is a good match for my observations of RFP-Pex13/GFP-PTS1 overlap (Figure 16). Together, these data suggest Pex13 conserves the peroxisomal localization of its mammalian ortholog and confirmed that my Pex13 reporter fusion did not have compromised peroxisomal targeting. My data supports a correlation between Pex13 abundance and that of peroxisomes using two differing experimental approaches and accounts for potential plasmid transfection effects, whereas the study by Baron *et al*. (2016) used only one approach and did not state a likewise consideration. Were *Pex13* conserved in *Drosophila*, it would be essential to peroxisome import and therefore its loss would result in fewer import-competent peroxisomes, reducing the counts of GFP-PTS1 puncta. Accordingly, an OE-induced increase in Pex13 abundance would increase peroxisome abundance, increasing the number of GFP-PTS1 puncta and indirectly promoting the expression of *Pex5* and *Pex14*, the other essential elements of the import translocon (Figure 1). This hypotheses is indirectly supported by my *Pex5* OE data. Knockout of *Pex5*, *Pex13* or *Pex14* by CRISPR/Cas9 mutagenesis would clarify the correlative relationships with peroxisome abundance for *Pex5* and *Pex13* that I observed.

b. Genes with a canonical or predicted role in cell division

Over-expression of *aurB* resulted in reduced peroxisome abundance. The *aurB* OE data complemented its RNAi data, and together suggested *aurB* indirectly downregulated peroxisome proliferation by regulating chromosome segregation. In mice, over-expression of the *aurB* homolog Aurora B resulted in aneuploidy, defective chromosome segregation, dysregulated

division leading to tumor growth and inhibition of the cell cycle inhibitor $p21^{Cip1}$ (González-Loyola *et al*., 2015). This suggested mammalian Aurora B promoted mitosis rather than inhibiting it, and were *Drosophila aurB* to function the same way then over-expressing it would hypothetically increase peroxisome abundance by promoting cell division and organelle biogenesis cues. Alternatively, were *aurB* OE to promote sufficiently rapid cell division then peroxisome abundance may be depleted as organelle biogenesis became outpaced by division. In *Drosophila*, the function of AurB in the chromosome complex is to coordinate the tubulin-based mitotic spindle via the centrosome (Giet and Glover, 2001; Radford *et al*., 2012; Mathieu *et al*., 2013). AurB loss resulted in premature abscission, suggesting AurB ensured chromosome segregation by pausing the final stages of mitosis (Mathieu *et al*., 2013). This knockout phenotype was similar to the mouse Aurora B over-expression phenotype, effectively casting the proteins as mitotic checkpoint proteins with opposite effects rather than homologs.

A direct interaction between AurB and an element of the peroxisome biogenesis pathway is unlikely, given the differing sub-cellular compartments the chromosome complex and the peroxisome occupy. The inhibitory effect of *aurB* OE on peroxisome abundance may therefore be an indirect effect of its role in mitosis. Specifically, because AurB pauses mitosis to ensure correct chromosome segregation, an excess of AurB may cue downregulation of organelle biogenesis, or an abandonment of mitosis altogether before peroxisome proliferation occurs. Alternatively, excess AurB may cue pexophagy in the course of effecting mitotic pause. The role of autophagy in AurB-mediated peroxisome proliferation could be examined using LysoTracker probes (ThermoFisher) and the same experimental approach used here, with validation of increased autophagy by qRT-PCR and IF of changes in *Atg8* expression, the *Drosophila* phagosome marker (reviewed by Mauvezin *et al*., 2014). Cell proliferation in cultures transiently over-expressing *aurB* could be assayed via incorporation of bromodeoxyuridine (BrdU).

Over-expression of *borr* resulted in increased peroxisome abundance. Borr is an AurB targeting subunit and constituent of the chromosome passenger complex (Eggert *et al*., 2004; Hanson *et al*., 2005). The chromosome passenger complex that AurB and Borr are part of resolves chromosome segregation issues and abscission at the end of mitosis, so the phenotype I observed suggested Borr upregulated peroxisome proliferation in the process of promoting

progress through the mitotic checkpoint that AurB regulates. Excess Borr may therefore also lead to abnormal chromosome segregation, premature abscission and aneuploidy, phenotypes reported for the OE of Aurora B kinase in mice (González-Loyola *et al*., 2015). All the homologs of *borr* have very low prediction scores, so drawing conclusions from the OE effects of *borr* and its closest potential mammalian homolog BOREALIN may not be informative (flybase.org, ncbi.nlm.nih.gov/gene). BOREALIN is necessary for chromosome segregation in humans, which it achieves through direct, and essential, interaction with nucleosomes (Abad *et al*., 2019). Over-expression of BOREALIN in tumor-derived primary cultures promoted growth and malignancy (Ci C *et al*., 2019; Bu Y *et al*., 2019). The underlying phenotype, increased cell proliferation, aligns with my *borr* OE data under the hypothesis that *borr* OE cues cell cycle progress, which would instruct the cell to proliferate organelles for inheritance. Complementing my current data with a *borr* mutagenesis experiment in S2 cells expressing GFP-PTS1 would determine if peroxisome abundance correlates with *borr* expression. Use of colchicine to disrupt microtubule formation under *borr* OE/knockout conditions would confirm if microtubules are involved in mediating the change in peroxisome abundance resulting from *borr* mutation.

geminin OE resulted in increased peroxisome abundance. This observation suggested *geminin* up-regulates peroxisome proliferation in its role as a mitosis regulator, which does not necessarily conflict with its function as a negative regulator of DNA replication (Quinn *et al*., 2001; Mihaylov *et al*., 2002). Alternatively, the role of *geminin* in regulating mitogen-activated protein kinase (MAPK) signaling may result in peroxisome proliferation through activation of an as-yet unidentified *Drosophila* PPAR, akin to the way the mammalian MAPK protein p38 activates PPARα (Herr *et al*, 2010; Barger *et al*., 2001). However, it is more likely that *geminin* indirectly affects peroxisome biogenesis through effects on mitosis. Embryonic *geminin* OE inhibited DNA replication and promoted apoptosis, and loss of *geminin* function resulted in anaphase defects in stage 16 *Drosophila* embryos (Quinn *et al*., 2001). This suggested *geminin* OE promoted peroxisome proliferation indirectly by arresting mitosis after organelle fission but before cytokinesis. Examining the effects of altered *geminin* expression on *Peroxin* expression, and the *Drosophila* p38 ortholog *p38a*, via qRT-PCR would elucidate which *Peroxin* gene may be involved in regulating peroxisome abundance in response to *geminin* and determine if MAPK signaling is involved.

Incenp OE reduced peroxisome abundance, which complemented its RNAi data and suggested *Incenp* expression correlated inversely with peroxisome proliferation. Like *borr*, *Incenp* encodes a targeting subunit for AurB. Unlike *borr*, the effects of altered *Incenp* expression on peroxisome abundance in this study matched those of AurB in direction, though not magnitude. Prior studies reported that *Incenp* OE in developing *Drosophila* eye tissue resulted in smaller adult eyes due to a reduced growth rate (Tseng and Hariharan, 2002). Likewise-targeted RNAi of *Incenp* resulted in populations of eye cells with 4n and 8n chromosome complements (Tseng and Hariharan, 2002). Thus, loss of *Incenp* upregulates cell cycle progression, resulting in polyploidy and organelle proliferation, and *Incenp* OE downregulates cell cycle progression, preventing organelle proliferation. Within this context, my data for *aurB*, *Incenp* and *borr* support a model in which AurB pauses mitosis when targeted by Incenp, an AurB activator, and permits mitosis to continue when targeted by Borr, inferred by its opposite effect on peroxisome proliferation to be an AurB inhibitor. The upregulation of peroxisome abundance when the abscission regulator *sqh* is over-expressed (Figure 15) supports this model. The chicken *Incenp* ortholog is found in several places during mitosis, beginning at the centromeres and moving to the spindle midzone during anaphase, then to the cleavage furrow during cytokinesis (Cooke *et al*., 1987). This suggests the chromosome passenger complex, or one or more of its constituents, may be found near peroxisomes at some point during the later stages of mitosis. Tagging endogenous Incenp with a fluorescent reporter via CRISPR may reveal if it, and by extension the chromosome passenger complex, co-localize with peroxisomes during mitosis.

pbl over-expression resulted in increased peroxisome abundance. This data complemented my *pbl* RNAi data and suggested Pbl upregulates peroxisome biogenesis through regulation of Rho signaling. Pbl has a sharp increase in abundance at the onset of cytokinesis and localizes to the cleavage furrow (Prokopenko *et al*., 1999). *pbl* loss-of-function mutant embryos had failed mitosis by embryo stages 14-16 (Prokopenko *et al*., 1999). Ectopic expression of *pbl* did not result in disorganized embryonic growth, though expression of PblΔ325–853 was embryo lethal and resulted in multinucleate cells (Prokopenko *et al*., 1999). The PblΔ325–853 mutation mimicked a similar mutation in the human ortholog ECT2 that correlated strongly with oncogenesis (Prokopenko *et al*., 1999). Thus, Pbl OE hypothetically cues increased peroxisome

proliferation by promoting cell division, and may do so through Rho signaling. Observing the effects of paired *pbl* and *rho* mutation in GFP-PTS1-S2 cells would conceptually validate this hypothesis, however there are six *rho* paralogs in *Drosophila* so practical examination would be somewhat labour intensive (flybase.org). A paired RNAi and OE screen of *pbl* in combination with the *rho* paralogs, one at a time, may also uncover the specific element of *rho* signaling that affects peroxisome proliferation in response to altered *pbl* expression.

sqh over-expression resulted in increased peroxisome abundance. The data for this gene make a strong case for the indirect effects of mitosis on peroxisome proliferation. *sqh* encodes a Rho kinase-dependent myosin light chain that activates closure of the actin contractile ring by myosin motors, concluding cytokinesis (Dean *et al*., 2005; Karess *et al*., 1991; Vasquez *et al*., 2014; Royou *et al*., 2002). Sqh is phosphorylated by Drok, a downstream regulator of the Fz/Dsh signal transduction pathway. Drok acts through Sqh to create a plane within the cell by directing asymmetrical cytoskeletal organization via non-muscle myosin II (Winter *et al*., 2001). Hypothetically, increased Sqh abundance may lead to increased myosin motor recruitment to the contractile ring and faster abscission, barring phosphorylation as the rate-limiting step. In mammalian cells, abscission does not complete until well into G_1 of the next mitotic cycle (Gershony *et al*., 2014). The timing, activation and abundance of elements of the abscission process, such as Sqh or phosphorylated Sqh, may therefore be considered G_1 cues. Accordingly, an increase in Sqh abundance may indirectly upregulate subsequent mitotic events like DNA replication and organelle proliferation. To determine if *sqh* phosphorylation state plays a role in peroxisome abundance, targeted *sqh* mutagenesis could be employed to create either phospho-mimetic (constitutively active) or un-phosphorylatable (constitutively inactive) Sqh variants in GFP-PTS1 cells, as described previously, but using CRISPR mutagenesis to target the endogenous *sqh* locus (Tan *et al*., 2003). This could be paired with an assay of *Drok* expression to see if it, and by extension the Fz/Dsh signal pathway, has an effect on peroxisome biogenesis, and if that effect is mediated by Sqh.

stg over-expression resulted in the strongest increase in peroxisome abundance observed in this study. *stg* regulates centriole replication, making it central to both cytoskeleton-peroxisome dynamics and mitosis. In the current study, both RNAi and OE experiments revealed

perturbation of either cellular process altered peroxisome abundance, so it is logical that perturbing a regulator of both processes would have a stronger and potentially synergistic effect. The strength of the *stg* phenotype was greater than the *Peroxin* controls (Figure 15, Table 8) suggesting *stg* regulated multiple facets of peroxisome biogenesis and, by extension, the function of more than one *Peroxin*. In the absence of evidence supporting direct interaction, the hypothetical mechanism is restricted to an indirect effect through the mitosis pathways *stg* regulates. This hypothesis is supported by the canonical function of Stg, which is to activate Cdk1 via de-phosphorylation to permit entry into M phase (flybase.org; ncbi.nlm.nih.gov/gene; Swaminathan and Pile, 2010). Ectopic *stg* OE rescued proliferation defects resultant of either diminished Extramacrochaetae (Emc) or increased Daughterless (Da), and induced mitosis in germline and cyst stem cells (Andrade-Zapata and Baonza, 2014; Inaba *et al*., 2011). These data indicate *stg* is not context-sensitive. It is reasonable to hypothesize that *stg* OE increased peroxisome abundance by promoting mitosis, which would indirectly cue organelle proliferation. Interestingly, RNAi of *Cdk1* did not alter peroxisome abundance in my study (Figure 13, Table 7). In the context of my *stg* data, this suggests merely knocking down *Cdk1*, instead of altering its functionality via *stg* over-expression, is not sufficient to alter the timing of mitotic entry and thereby induce peroxisome proliferation. This proposed mechanism could be examined by observing changes in phosphorylated Cdk1 resultant of *stg* mutation.

c. Genes encoding canonical or predicted motor protein regulators

Acam OE resulted in increased peroxisome abundance. This was a stronger version of the same phenotype observed for *Acam* knockdown. There is no prior record of *Acam* expression being detected outside the testis, where it is found decorating certain loops of the Y chromosome and binds specific sites on myosin VI different from those of its paralog *Cam* (Frank *et al*., 2006; Joshi *et al*., 2012; Lu and Beckingham, 2000). These findings suggest the effects I observed may be subject to the confounding variables of sex and unknown lineage of the S2 cells I used, particularly because of the canonical association of *Drosophila* peroxisomes with microtubules and associated motor proteins and not the actin-myosin cytoskeleton (Rapp *et al*., 1996; Kural *et al*., 2005). *Acam*'s ubiquitous paralog Calmodulin (Cam) is a calcium-sensing signal transduction protein that regulates many processes once it complexes with calcium ions (Scott *et al*., 1997). Null *Cam* alleles are larval lethal and loss-of-function mutations cause defects in

musculature, behaviour, the nervous system, flight, locomotion and mating (flybase.org). Defects in musculature, the nervous system, behaviour and larval lethality are also seen in *Peroxin* mutants (Chapter Three; Faust *et al*., 2014; Mast *et al*., 2011; Di Cara *et al*., 2019). A screen by Gregory *et al*. (2007) observed that *Cam* OE weakly suppressed a dominant negative eye phenotype resultant of inactive *pbl*. This suggested Cam, and perhaps Acam, could somewhat overcome *pbl* loss and signal the contextual cell division normally signaled by *pbl*. Accordingly, *Acam* OE may therefore cue mitosis in certain male cells or cultures derived from same, which would increase peroxisome abundance like I observed. Alternatively, if Acam is a phosphorylation-dependent regulator of myosin VI, as suggested by the predicted domains in its primary sequence, then it may preferentially bind when activated. The presence of phosphorylated Acam on myosin motors of the peroxisome-associated cytoskeleton may then aid recruitment of fission complexes (Pex11/Drp1/Fis1) and result in enhanced proliferation of peroxisomes. This hypothesis assumes phosphorylation activates Acam and that Acam activation is not the rate-limiting step in the proposed mechanism. Transient OE of phospho-mimetic and un-phosphorylatable versions of Acam may resolve the question of Acam activation, however further characterization of Acam is required beforehand to identify its phosphorylation sites. Determining if Acam is a cell proliferation cue, and if this function is restricted to male cells, could be achieved by observing BrdU incorporation in S2 and Kc167 cells over-expressing *Acam*.

d. Genes encoding canonical or predicted regulators of mitochondrial function

nmd over-expression resulted in increased peroxisome abundance. This observation complemented the gene's RNAi data, suggested *nmd* expression upregulated peroxisome biogenesis. My data also supported the hypothesis proposed by Lacey (2015) that Nmd sorted Pex3 to ER subdomains to permit the recruitment of PMPs necessary for PPV formation and subsequent *de novo* peroxisome biogenesis. Contrariwise, my data do not conclusively refute the possibility that *nmd* is otherwise essential to peroxisome function following biogenesis, depending on the interpretation of the weak overlap of RFP-Nmd and GFP-PTS1 that I observed (Figure 16V). My work, and that of others discussed herein, do support the hypothesis that *nmd* is not exclusively mitochondrial and instead regulates a function essential to both organelles, such as membrane synthesis or fission. A gain-of-function screen for suppressors of wing margin

defects discovered *nmd* OE suppressed the wing margin phenotype of the gain-of-function *Beadex* allele (Bejarano *et al*., 2008). Beadex (Bx) regulates the activity of Apterous (Ap) by direct interaction. Ap is a transcription factor involved in wing cell identity, neuronal pathfinding, embryonic muscle formation and juvenile hormone production (flybase.org; Bourgouin *et al*., 1992). To summarize, Ap promotes cell differentiation, Bx inhibits Ap and *nmd* suppresses *Bx*. Thus, Nmd may mediate cellular processes associated with asymmetric cell division such as the biogenesis of mitochondria and peroxisomes. A yeast two-hybrid assay would determine if Nmd interacts directly with *Drosophila* homologs of ER-PPV proteins, Peroxins, PMPs, Bx or Ap. This would clarify if Nmd is a direct regulator of peroxisome biogenesis or if it interacts with differentiation cues to promote organelle proliferation by prompting cell division.

e. Genes encoding canonical or predicted enzymes

Enigmatically, over-expression of CG18231 resulted in an increase in peroxisome abundance almost four times greater than the increase observed when it was knocked down (Tables 6 and 7). Assuming CG18231 encodes a procollagen synthesis subunit, this observation suggests the excess production of procollagen, or subsequent ECM accretion following procollagen secretion, indirectly cues peroxisome biogenesis. There is an alternative hypothesis. The closest human homolog to CG18231 is P4HA3 (flybase.org; ncbi.nlm.nih.gov/gene). P4HA3 was found to be significantly upregulated in gastric cancer, correlating with SNAI2 (Pearson r = 0.70; Song *et al*., 2018). The product of SNAI2, Slug, is a *snail* family transcriptional repressor that was found to bind efficiently to the P4HA3 promoter (Song *et al*., 2018). *Drosophila slug* is uncharacterized, but *snail* was discovered classically as the allele *Scutoid* and is a transcription factor that promotes asymmetric cell division, embryonic mesoderm development and the epithelial-mesenchymal transition (flybase.org; Reuter and Leptin, 1994). Thus, the cancer connection of its closest predicted human homolog suggests OE of CG18231, and thus procollagen synthesis, may be a cue for cell proliferation when *slug* can no longer repress it. This could be assayed by observing BrdU incorporation in cells over-expressing CG18231. Expanding on this hypothesis, the knockdown of CG18231 may promote asymmetric cell division over symmetric cell division. This would still require cells to replicate their organelles and may result in an increase in peroxisome abundance but at a slower pace,

which fits my observations for this gene. The involvement of *snail* could be tested by paired *snail*/CG18231 over-expression, RNAi and knockout experiments.

f. Genes encoding canonical or predicted transcriptional regulators

vvl over-expression resulted in increased peroxisome abundance. This finding complemented half the ambiguous *vvl* RNAi data I reported and suggests two of the four dsRNA molecules I employed were not significantly effective, rather than two having off-target effects. Peroxisomes are necessary for bacterial engulfment and mediating canonical innate immune responses, and loss of peroxisome function in the gut compromised the fly immune response by inducing epithelial instability via increased autophagy (Di Cara *et al*., 2017; Di Cara *et al*., 2018). Vvl OE activated antimicrobial peptide (AMP) genes independent of the Toll or IMD nuclear receptor pathways, which canonically upregulate AMP genes in response to microbial infection (Junell *et al*., 2010). Thus, *vvl* may promote a non-canonical innate immune response that triggers peroxisome proliferation. This hypothesis could be tested by ChIP of Vvl in S2 cells to see if Vvl promotes *Peroxins* or other peroxisome proliferation genes directly, or if it elicits responses from the canonical Toll/IMD pathways.

g. Genes with no observed effect in the present study

Over-expression of *feo* had no effect on peroxisome abundance. Feo binds central spindle microtubules and is essential for cytokinesis, and its knockdown resulted in one of the strongest RNAi phenotypes I observed (Figure 13; flybase.org). Many other genes that affected peroxisome abundance in my study are involved in the same processes as *feo*, so its OE was expected to strongly reduce peroxisome abundance. Prior observations of over-expressed Feo in S2 cells revealed extensive interphase microtubule bundling without affecting the cell cycle (Vernì *et al*., 2004). This phenotype was similar to that of over-expressed PRC1, the human *feo* ortholog, in HeLa cells except PRC1 was also found in the nucleus (Molinari *et al*., 2002). These observations suggest that *feo* operates by a sufficiency mechanism such that too little downregulated peroxisome abundance, because microtubules could not be bundled to permit proper cytokinesis, while excess had no effect on mitosis and merely upregulated microtubule bundling during interphase. Ablating endogenous *feo* expression via CRISPR/Cas9 mutagenesis would supplement my RNAi data. Ideally, replacing endogenous Feo with a version incapable of

binding microtubules would identify if this function is essential to its peroxisome-related behaviour, however *feo* requires further characterization to identify how it binds microtubules before that experiment is feasible.

5.6 Future directions

5.6.1 Additional functional characterization of Drosophila Peroxins

Active study of *PEROXINS* peaked in the 1990s and 2000s as a concerted effort to translate peroxisome assembly mutants from various yeast models to humans. The goal was to elucidate the cellular mechanisms behind Zellweger spectrum disorders and find the genes responsible for the complementation groups identified using PBD patient fibroblasts. Consequently, the peroxisome biogenesis factors in models besides yeast and mammals are poorly understood and most evidence of conservation involves assumptions of homology based on sequence analysis of expressed sequence tags and other public data (flybase.org). This has made functional analysis *of Drosophila Peroxins* difficult because algorithmic predictions of protein characteristics have not always agreed with the data from practical experiments. For example, Faust *et al*. (2012) determined the PTS2 tag *PEX7* used in other organisms was missing from the *Drosophila* proteome, and observed S2 cells could not localize reporter proteins bearing the canonical PTS2 motif. Contrariwise, Baron *et al*. (2016) observed over-expressed *Pex7* reporter fusions co-localized about 50 % with peroxisomes in S2 cells and Di Cara *et al*. (2019) demonstrated that transgenic *Drosophila Pex7* restored the localization of human thiolase, which has a canonical PTS2 motif, to peroxisomes in RCDP1 patient fibroblasts. Thus, my data support hypothesizing a novel, essential, peroxisome-associated role for *Pex7* in the nervous system during *Drosophila* embryogenesis. Contrariwise, this proposed novelty means *Drosophila* may not be an ideal model to explore RCDP until we know fly peroxisomes and *Pex7* better. In the context of similar CNS phenotypes observed for *Pex1* loss-of-function mutation (Mast *et al*., 2011) and *Pex5* knockdown (Di Cara *et al*., 2017), another hypothesis emerges proposing all *Peroxin* genes, and peroxisome biogenesis, are essential to nervous system development. This is of clear value to modeling PBDs in an organism as useful as *Drosophila*. Together, these studies support the continued investigation of *Drosophila Peroxins* to shed light on the tissue specificity

of, and treatment innovation for, peroxisome disorders. The continued exploration of *Peroxins* will benefit both fundamental and health research.

Work on *Pex7* is incomplete. There are many directions my work can go, apart from the improvements to the extant data set already discussed. The next step in characterizing *Pex7* is to identify its cellular function. IP experiments performed in the current study, using S2 cells and targeting either tagged or endogenous Pex7, failed to identify binding partners by mass spectrometry (MS) that could support inferring an associated pathway or mechanism. Use of other substrates may resolve this problem, such as homogenates of whole w^{1118} embryos, as they were confirmed to express Pex7 at detectable levels from 2-22 h AEL (Figure 6). IF of fixed, staged mutant embryos would permit further antibody validation and confirm *Pex7* loss. The innovation of CRISPR-based endogenous protein tagging enables tracking of genomic Pex7 via tag insertion and could be done with GFP/RFP to permit imaging at all life stages *in vivo*. This would validate my IF observations and expand the data set to larval and adult stages, improving our knowledge of the role of *Pex7* in nervous system development and the immune response (Pridie and Simmonds, 2020; Di Cara *et al*., 2017; Di Cara *et al*., 2019). Live imaging of CRISPR-tagged endogenous *Pex7* would also, in combination with established neurological assays such as the negative geotaxis (climbing) test and its derivative "bang" test, permit exploration of *Drosophila* as a model for the RCDP spectrum of PBDs by establishing an experimental protocol and, ultimately, a pipeline for low-cost, high-throughput screening of therapeutic interventions for PBDs. Should future research determine that *Drosophila Pex7* is not a *bona fide Peroxin* but rather carries out some other function necessary for neural development and immunity, the apparent functional overlap may be sufficient to model non-peroxisomal functions of human *PEX7.* This may help identify why certain tissues are more susceptible to *PEX7* loss than others within a genetic background of general loss of function, as observed for the symptoms of RCDP patients. Continued *Peroxin* research may also reveal novel functions for other *Drosophila Peroxins*, such as the discovery that *Pex14* associates with both lipid droplets and peroxisomes in a diet-dependent manner (M Anderson-Baron and A Simmonds, personal communication). The discoveries in *Drosophila* that increased longevity results from over-expressing human SOD1 in the CNS (Perkes *et al*., 1998) and that altered expression of the peroxisome-localized lipid metabolism gene ACOX1 causes neurodegeneration by axon loss

(Chung *et al*., 2020) suggest peroxisomes carry out tissue-specific functions. This implies peroxisome function is subject to tissue-specific regulation, and one or more *Peroxins* may be responsible for performing said regulation. Changes in gene expression resultant of altered *Pex7* expression could be performed via DNA microarray to identify the genes affected, and by inference the pathways, that *Pex7* regulates.

My work on *Pex7* identified gaps in our knowledge about how other *Drosophila Peroxins* work. To date, nine *Peroxins* have been studied empirically: *Pex1*, *Pex2*, *Pex3*, *Pex5*, *Pex7*, *Pex10*, *Pex14* and *Pex16* (see section 1.3.3). Data for *Pex1*, *Pex5* and *Pex14* suggest they are conserved *Pex* genes, hence the use of *Pex1* and *Pex14* as controls in my *Pex7* mutagenesis studies, yet no *Peroxins* have been studied in terms of impact on canonical peroxisomal enzyme localization or activity. The focus of *Drosophila Pex* research has been the acquisition of data using molecular and genetic approaches. This has produced data on transcript/protein/reporter localization, developmental and adult phenotypes resulting from mutation, and tissue-specific effects of altered expression, in a collective effort to generate new PBD models and augment extant ones. *Drosophila* stands as a premier model to explore developmental biology, and knowledge of the *Peroxin* family has benefited greatly by leveraging this strength, yet my data suggest one or more *Drosophila Pex* genes have evolved novel functions. In order to understand and categorize these novel functions, normal *Drosophila* peroxisome biology must first be elucidated in order to understand its differences from established PBD models. From this baseline, researchers can then identify those *Peroxin* functions that are truly novel from those that support normal *Drosophila* peroxisome function.

The establishment of a baseline for *Drosophila* peroxisome enzymatic activity and how *Peroxins* affect it can be achieved by using modern molecular and microscopy techniques. Expanding on work by Baron *et al*. (2016) and the OE screen of my second project, it is presently possible to engineer fluorescent reporters into endogenous gene sequences via CRISPR (Xue *et al*., 2014). It is obvious that this technique could be employed to perform a cell-based screen of all potential *Drosophila* peroxisome-associated proteins relative to a known endogenous peroxisome marker *in vivo* such as PMP70 or PMP34, or to exogenous GFP-PTS1. This approach may overcome the issues of functional impact and reporter detection that Baron *et*

al. (2016) and I experienced. CRISPR-based knock-in could also be used to mutate individual *Peroxins* and tag potential binding partners to observe changes in localization or other behaviour. For example, a potential relationship between *Pex5* and *Pex7* could be assayed by CRISPR-tagging both and using light microscopy to observe changes in their localization *in vivo*, then re-targeting the reporter knock-in to mutate either gene. This approach could be applied to the cargo proteins of both PTS pathways to confirm conservation, then to *Pex11* and its potential partners in the peroxisome fission pathway, and to *Pex3*/*Pex16*/*Pex19* in the *de novo* biogenesis pathway, all with the goal of verifying canonical *Peroxin* functions. Using this technique it would also be possible to perform IP of a tagged putative peroxisome enzyme of interest and assay its specific activity for similarity to its human ortholog, and observe its sub-cellular localization to confirm whether or not it is peroxisomal. Baron *et al*. (2016) performed localization experiments using transfected reporter constructs, however they reported the approach impacted fusion reporter localization depending on the reporter used. Their method, which I replicated in my second project, supplements wildtype gene expression rather than replacing it so every observation they reported was an over-expression phenotype. Tagging gDNA via CRISPR-mediated reporter insertion overcomes that design flaw. Finally, the CRISPR method could be used to observe changes in cellular ROS resultant of disrupted *Peroxin* expression by pairing gene-disrupting reporter knock-in with fluorescent, cell-permeable reagents that detect changes in general redox state (CellROX, ThermoFisher), lipid peroxidation (Image-iT, ThermoFisher), superoxide (MitoSOX Red, ThermoFisher), H_2O_2 (Premo Cellular H_2O_2 Detector, ThermoFisher) or glutathione (ThiolTracker, ThermoFisher). This would identify the elements of ROS production managed by *Drosophila* peroxisomes.

A highlight of the intersection between peroxisome and *Drosophila* research has been the ongoing development of PBD models in the course of exploring *Peroxin* function. Modern efforts have focused on phenotypic similarity to PBD symptoms for a given *Peroxin* mutant, which was successful for *Pex1* (Mast *et al*., 2011) but remains a challenge for other *Peroxins*; the present *Pex7* study is unfortunately an example of the latter. An initial goal of my *Pex7* project was to develop a RCDP model however it became apparent that *Pex7* had expression patterns at early stages of development different from those expected of a gene involved in a ubiquitous cellular process, so I refocused the project onto the effects of *Pex7* mutation during

embryogenesis. This means my project did not examine *Pex7* expression across the entire *Drosophila* life cycle, and that gap requires filling before continuing the development of the fly into a RCDP model. Even tissues that survive all developmental stages, like the brain and ventral nerve cord, are affected by the process of metamorphosis. The fly CNS must innervate larval tissues to permit instar feeding and movement behaviours, which develop during embryogenesis, and then restructure to innervate the adult structures differentiating within imaginal discs during pupariation. In addition, generation of a valid disease model requires comparison of analogous structures, and in the case of fly-human comparison it is the adult form of the fly that has the limbs, organs, tissues, body plan and behaviours analogous to those of humans. That said, the other *Drosophila* life stages should not be ignored because they do affect adulthood, as evidenced by studies on the effect of food availability on pupariation (Robertson, 1963). Expansion of *Pex7* research into all stages of the fly life cycle is therefore essential to understanding the gene's function.

Exploration of larval and adult tissues is facilitated by the extensive literature on dissection and preservation techniques suitable for microscopy (e.g., Lécuyer *et al*., 2008; Wilk *et al*., 2010; Krupp and Levine, 2010). This could be paired with direct, side-by-side comparison of homozygous mutant and phenotypically wildtype cells in the same tissue via mosaic analysis with a repressible cell marker (MARCM), which has been essential to the study of the developing nervous system (reviewed by Lee and Luo, 2001). This approach would permit observation of changes in the localization of peroxisomal enzymes *in vitro* in tissues analogous to human organs affected by peroxisome disorders, e.g. oenocytes (liver), Malpighian tubules (kidney) and nervous system resultant of *Pex7* mutation. Within the context of an animal expressing gene-specific fluorescent reporters, this approach may also be used as a backup to the *in vivo* CRISPR-mediated mutagenesis experiments I proposed earlier. Advances in targeted mutagenesis techniques have placed efficient and economical generation of disease-associated lesions within reach when paired with algorithmic sequence alignment. I used a modification of this approach to generate custom strains that conditionally over-express human or *Drosophila* versions of a disease-associated *PEX7* variant via inverse PCR and germline integration of an engineered plasmid (Figure 17C). These strains will permit screening for dominant-negative effects of disease-associated variant over-expression, and stand as proof-of-concept that

humanization of *Drosophila* with PBD-associated alleles is possible. The plasmids themselves can also be used to observe OE effects in cultured cells through transient transfection. CRISPR knock-in could be used to generate targeted, conditional mutants to complement the over-expression strains. This technique could also generate mutants, and truly "humanized" strains in which endogenous genes have been replaced with human orthologs, to explore the effects of other disease-associated *Peroxin* variants.

5.6.2 Explore factors with novel roles in peroxisome biogenesis and function

Of the thirteen genes that I verified had an effect on peroxisome biogenesis, half are involved in mitosis. Two, *Acam* and *sqh*, are potential and known non-muscle light-chain myosins, respectively, that regulate motor protein-organelle interactions. *sqh* is essential to cytokinesis, so I also categorized it as "involved in mitosis". In S2 cells, the direct interaction of transgenic human PEX26 and the similar, but non-homologous, *Drosophila* Unc104 with Kinesin-1 suggest that *Drosophila* has evolved means of peroxisome-motor protein interaction that do not involve *Peroxins* directly (De Rossi *et al*., 2017). In an approach similar to the one that I proposed to elucidate *Peroxin* gene function, CRISPR-mediated fluorescent reporter insertion into endogenous *Peroxins* in a cell line also stably expressing fluorescent Actin or Tubulin would permit observation of co-localization *in vivo*. Should co-localization be seen, IP-MS of the labeled *Peroxin* would identify other members of the protein complex such as the specific motor proteins and adaptors involved. Fluorescence resonance energy transfer (FRET) would identify adjacency of the candidates and confirm they form a complex, and a yeast two-hybrid screen would confirm direct interaction. In the absence of a positive finding, labeled PMP70 could be used as the bait for the IP-MS protocol. These data would then be compared to that of likewise-tagged *Acam* and *sqh*. This approach would identify the proteins involved in binding peroxisomes to the cytoskeleton, clarify the role of light-chain myosins, and determine if *Peroxins* are involved.

Proposing ways to explore the pathways by which the other genes I validated affect peroxisome proliferation, apart from the experiments proposed for *Acam* and *sqh*, is challenging because it is unlikely that the effects are due to direct interaction of a protein or associated

complex with peroxisomes or their proliferation proteins. For example, none of the cell cycle genes I identified are canonical transcription factors, ruling out direct promotion of *Peroxin* expression, and they do not necessarily function in the same sub-cellular compartment as peroxisomes, ruling out protein-protein interaction with Peroxins. Similarly, *vvl* is a transcription factor that is involved in cell fate, but not necessarily the cell cycle, and has no canonical role directly involving peroxisomes or *Peroxins*. Constructing hypothetical mechanisms or pathways by which these genes indirectly affect peroxisome proliferation through their established functions is likewise difficult, as is identifying a means to test the various associated pathways using a common approach. I propose a cell-based study with a workflow similar to the one I outlined for *Peroxin* exploration. The study would begin with DNA microarray analysis and qRT-PCR to determine the effects of altered non-*Peroxin* expression on that of *Peroxins*. This experiment would produce a list of candidate *Peroxin* targets for each gene I verified. Next, CRISPR-mediated knock-in of fluorescent reporters into a verified gene and a candidate *Peroxin* would permit observation of their cellular localization relative to each other *in vivo*. This may also reveal other organelles or structures that would merit further investigation. The gene pairs that co-localize would then be subject to IP-MS to identify other potential members of the protein complex, verifiable using FRET. This would refine the list of potential direct interactors for investigation via yeast two-hybrid screen. In the case of a localization mismatch, which I hypothesize to be the case for the majority of the genes I validated, IP-MS may identify intermediates for each gene of a pair that could then be iteratively tagged and studied using the same approach. Ultimately, the pathways mediating direct peroxisome interaction, likely through *Peroxin* interaction, as well as altering peroxisome proliferation would be discovered. The approach may also reveal the genes that have replaced PPAR family activity, if any. Alternatively, peroxisome-specific sub-pathways may be discovered within extant ones such as MAPK signal transduction, transcription regulation or any of the number of pathways governing mitochondrial or ER function. Finally, the proposed study may identify/verify the genes *Drosophila* uses to accomplish peroxisome fission and *de novo* biogenesis. The mutation effect of the genes I verified on peroxisome function could be tested in cultured S2 cells using cell-permeable fluorescent chemicals that detect ROS, which would indicate changes in oxidative stress and overall redox state. This is essential because changes in peroxisome abundance do not necessarily equate to changes in organelle function. I acknowledge this approach is similar to the

one I proposed to elucidate the function of the *Peroxin* family, however in this context the data would reveal if altered peroxisome proliferation, hypothetically a result of changes in the canonical cellular process associated with each gene, also has an effect on peroxisome function. If a given gene has a pathway to direct *Peroxin* interaction elucidated as a result of this study, then said gene may be proposed not only as a novel peroxisome proliferation regulator but also an accessory in the function of peroxisome biogenesis, and by extension a regulator of the cellular redox state. This would be valuable to determining if certain cellular processes, for example mitosis, differentiation or ECM synthesis, have a cognate altered cellular redox state that is mediated by peroxisome function. This has implications in the context of ROS as a signaling molecule, which was established in *Drosophila* as essential to proper cardiac function, and may present elsewhere as directed by the differentiation cues or cell cycle genes I verified (Lim *et al*., 2014). Alternatively, peroxisome proliferation may be decoupled its other functions and the observed proliferation effect could be a consequence of aberrant gene expression alone.

This project can be widened in scope to include animal studies. The value of this migration is attested by work on *Peroxins* demonstrating tissue-specific effects of altered peroxisome function that cannot be observed using cultured cells (Section 1.3.3; Chapter Three; Di Cara *et al*., 2019; Di Cara *et al*., 2017; Faust *et al*., 2014). *Drosophila* is an ideal choice for this approach. The principal aim of this study would be to assess the necessity of the genes to development, if not already known. The secondary aims would be to determine if peroxisome function is impacted, and if the changes in proliferation I observed at the cellular level were replicated. The BDSC and Vienna *Drosophila* research centre (VDRC) each maintain libraries of Gal4-UAS strains that would permit the ubiquitous and tissue-specific knockdown of the genes I verified by RNAi (bdsc.indiana.edu; stockcenter.vdrc.at). Preliminary fly work that I performed did not reveal novel adult phenotypes for RNAi of CG7627, *nmd* or *vvl* using ubiquitous (*tub*) or neuro-specific (*elav* or P{w$^{[+mW.hs]=GawB}$}T98) Gal4 drivers however there may be embryonic or larval phenotypes awaiting discovery. The TRiP-KO and TRiP-OE systems, available from the BDSC, could also be employed to examine targeted knockout or over-expression, respectively, of genes of interest *in vivo*. Screening of the genes I verified for developmental effects could be explored using an expanded version of approach I employed for *Pex7*. This would include examination of gene expression, meaning transcript and polypeptide, in staged embryo

collections of wildtype and mutant animals, larvae and adults. Targeted mutation, as informed by the gene expression profile, would permit examining effects on viability, development, sterility, lipid metabolism and climbing behaviour characteristic of impaired peroxisome function. For genes with known functions, I hypothesize the cells undergoing the associated process would be preferentially affected by aberrant expression of said gene. For example, embryogenesis involves frequent, sometimes co-ordinated mitosis in some tissues or the whole organism, and would therefore not only be susceptible to altered *borr* expression but would also hypothetically report altered peroxisome abundance in dividing cells compared to controls. As another example, embryos over-expressing the potential procollagen synthesis subunit CG18231 may have precocious or excessive ECM development during cellularization of the syncytial blastoderm. In addition to increased peroxisome proliferation, the overall oxidative stress of the blastoderm may be increased resultant of increased enzymatic and secretory activity, which may have signaling or viability effects. The issue of gene product characterization requiring novel antibodies could be overcome by tagging the endogenous protein via fluorescent reporter knock-in for *in vivo* observation, or an exogenous motif such as FLAG or Myc for work *in vitro*. Altering the knock-in target position could produce null or loss-of-function mutants, complementing knockdown and OE experiments to complete an altered expression profile for each gene. My present studies used confocal microscopy of live cells to acquire data, but high-resolution observation of fluorescent reporters in whole flies, at all life stages, requires light sheet fluorescence microscopy (LSFM). *In vivo* applications of LSFM are limited, so tissue dissection paired with standard light or confocal microscopy may be required, although this limitation also presents an opportunity for technique innovation (Pende *et al*., 2018; reviewed by Schmied and Tomancak, 2016).

Expanding the study of novel *Peroxin* regulators into animals may also benefit health research. A paired search of the *Drosophila* database and the NCBI human gene database for the thirteen genes I verified revealed that variants of the most supported human homologs for twelve of them were linked to some form of cancer (flybase.org; ncbi.nlm.nih.gov/gene). The exception was *Acam*, whose three weakly-supported homologs CALMODULIN 1/2/3 were a much closer match to *Drosophila Calmodulin* (*Cam*). The use of *Drosophila* as a cancer model is evolving. Presently it is possible to model some basic elements of cancer biology in flies such as drug resistance, tumor microenvironment and clonal evolution using MARCM (reviewed by Enamoto

et al., 2018). Combined with CRISPR-mediated knock-in, MARCM would permit observation of the effects of altered peroxisome proliferation by genes affiliated with the relevant element of the cancer model under normal and disease states in the same tissue. For example, using MARCM to genetically simulate the drug resistance condition common to many cancers, the effects of altered CG7627 expression (the potential fly homolog of the drug-resistance gene ABCC4) could be observed in clones of affected and unaffected oenocytes in the same animal. It is unclear if exploring peroxisome biology in a *Drosophila* cancer model would also provide novel cancer therapeutic targets because the canonical functions of peroxisomes all involve oxygen. Cancer cells frequently forego aerobic respiration in favour of modified glycolysis and aerobic fermentation, a change termed the Warburg effect (reviewed by Alfarouk *et al*., 2014). Contrariwise, peroxisomes are not the site of oxidative phosphorylation and a hallmark characteristic of cancer is cell division, which requires peroxisomal enyme products for membrane synthesis. Thus, exploring the role of peroxisome biogenesis and its regulatory factors in the context of cancer may offer insights into the disease and the function of the gene being examined.

References

Abad MA, Ruppert JG, Buzuk L, (…), Jeyaprakash AA. 2019. Borealin-nucleosome interaction secures chromosome association of the chromosomal passenger complex. J Cell Biol 218(12):3912-3925. doi:10.1083/jcb.201905040.

Adams RR, Maiato H, Earnshaw WC, Carmena M. 2001. Essential roles of *Drosophila* inner centromere protein (INCENP) and Aurora B in Histone H3 phosphorylation, metaphase chromosome alignment, kinetochore disjunction, and chromosome segregation. J Cell Biol 153(4):865-80.

Albertini M, Rehling P, Erdmann R, Girzalsky W, Kiel JAKW, Veenhuis M, Kunau WH. 1997. Pex14p, a peroxisomal membrane protein binding both receptors of the two PTS-dependent import pathways. Cell 89(1):83-92.

Alfarouk KO, Verduzco D, Rauch C, (…), Harguindey S. 2014. Glycolysis, tumor metabolism, cancer growth and dissemination. A new pH-based etiopathogenic perspective and therapeutic approach to an old cancer question. Oncoscience 1(12):777–802. doi:10.18632/oncoscience.109.

Ally S, Larson AG, Barlan K, Rice SE, Gelfand VI. 2009. Opposite-polarity motors activate one another to trigger cargo transport in live cells. J Cell Biol 187(7):1071-82.

Anderson MG, Perkins GL, Chittick P, Shrigley RJ, Johnson WA. 1995. drifter, a *Drosophila* POU-domain transcription factor, is required for correct differentiation and migration of tracheal cells and midline glia. Genes Dev 9(1):123-37.

Andrade-Zapata I, Baonza A. 2014. The bHLH factors Extramacrochaetae and Daughterless control cell cycle in *Drosophila* imaginal discs through the transcriptional regulation of the *cdc25* phosphatase *string*. PLoS Genetics. https://doi.org/10.1371/journal.pgen.1004233.

Annunen P, Helaakoski T, Myllyharju J, Veijola J, Pihlajaniemi T, Kivirikko KI. 1997. Cloning of the human prolyl 4-hydroxylase alpha subunit isoform alpha(II) and characterization of the type II enzyme tetramer. The alpha(I) and alpha(II) subunits do not form a mixed alpha(I)alpha(II)beta2 tetramer. J Biol Chem 272(28):17342-8.

Antonenkov VD, van Veldhoven PP, Waelkens E, Mannaerts GP. 1997. Substrate specificities of 3-oxoacyl-CoA thiolase A and sterol carrier protein 2/3-oxoacyl-CoA thiolase purified from normal rat liver peroxisomes. J Biol Chem 272(41):26023-31.

Ashburner M, Golic KG, Hawler RS. 2005. *Drosophila*: a laboratory handbook, 2nd edition. Cold Spring Harbor Laboratory Press. ISBN 978-0-87969-706-8.

Assia Batzir NA, Bhagwat PK, Eble TN, Liu P, Eng CM, Elsea SH, Robak LA, Scaglia F, Goldman AM, Dhar SU, Wangler MF. 2019. De novo missense variant in the GTPase effector domain (GED) of *DNM1L* leads to static encephalopathy and seizures. Cold Spring Harb Mol Case Stud 5: a003673. doi:10.1101/mcs.a003673.

Avers CJ, Federman M. 1968. The occurrence in yeast of cytoplasmic granules which resemble microbodies. J Cell Biol 37(2):555-9.

Baes M, Van Veldhoven PP. 2012. Mouse models for peroxisome biogenesis defects and β-oxidation enzyme deficiencies. Bioch Biophys Acta 1822(9): 1489-1500. https://doi.org/10.1016/j.bbadis.2012.03.003.

Bainbridge SP, Bownes M. 1981. Staging the metamorphosis of *Drosophila melanogaster*. J Embryol Exp Morphol 66:57-80.

Baker NE. 1988. Localization of transcripts from the *wingless* gene in whole *Drosophila* embryos. Development 103:289-298.

Barger PM, Browning AC, Garner AN, Kelly DP. 2001. p38 mitogen-activated protein kinase activates peroxisome proliferator-activated receptor alpha: a potential role in the cardiac metabolic stress response. J Biol Chem 276(48):44495-501.

Baron MN, Klinger CM, Rachubinski RA, Simmonds AJ. 2016. A systematic cell-based analysis of localization of predicted *Drosophila* peroxisomal proteins. Traffic 17:536-53. doi:10.1111/tra.12384.

Bateman JR, Lee AM, Wu CT. 2006. Site-specific transformation of Drosophila via phiC31 integrase-mediated cassette exchange. Genetics 173(2):769-77.

Baudhuin P, Beaufay H, de Duve C. 1965b. Combined biochemical and morphological study of particulate fractions from rat liver. Analysis of preparations enriched in lysosomes or in particles containing urate oxidase, D-amino oxidase, and catalase. J Cell Biol 26:219-43.

Baudhuin P, Müller M, Poole B, de Duve C. 1965a. Non-mitochondrial oxidizing particles (microbodies) in rat liver and kidney and in *Tetrahymena pyriformis*. Bioch Biophys Res Comm 20(1):53-9.

Beard ME, Holtzman E. 1987. Peroxisomes in wild-type and rosy mutant *Drosophila melanogaster*. Proc Natl Acad Sci USA 84:7433-7.

Beard ME, Sapirstein V, Kolodny EH, Holtzman E. 1985. Peroxisomes in fibroblasts from skin of Refsum's Disease patients. J Histochem Cytochem 33(5):480-4.

Beira JV, Paro R. 2016. The legacy of *Drosophila* imaginal discs. Chromosoma 125(4):573–592. doi:10.1007/s00412-016-0595-4.

Bejarano F, Luque CM, Herranz H, Sorrosal G, Rafel N, Pham TT, Milán M. 2008. A gain-of-function suppressor screen for genes involved in dorsal-ventral boundary formation in the *Drosophila* wing. Genetics 178(1):307-23.

Bellen HJ, Levis RW, Liao G, He Y, Carlson JW, *et al*. 2004. The BDGP gene disruption project: single transposon insertions associated with 40% of *Drosophila* genes. Genetics 167:761–781.

Ben-David G, Miller E, Steinhauer J. 2015. *Drosophila* spermatid individualization is sensitive to temperature and fatty acid metabolism. Spermatogenesis 5(1): e1006089. doi:10.1080/21565562.2015.1006089.

Benzer S. 1971. From the gene to behavior. JAMA 218:1015–1022.

Berthet J, de Duve C. 1951. Tissue fraction studies. 1. The existence of a mitochondria-linked enzymically (sic) inactive form of acid phosphatase in rat-liver tissue. Biochem J 50(2):174-81.

Bischof J, Maeda RK, Hediger M, Karch F, Basler K. 2007. An optimized transgenesis system for Drosophila using germ-line-specific phiC31 integrases. Proc Natl Acad Sci USA 104(9):3312-7.

Bodnar AG, Rachubinski RA. 1990. Cloning and sequence determination of cDNA encoding a second rat liver peroxisomal 3-ketoacyl-CoiA thiolase. Gene 91:193-99.

Bourgouin C, Lundgren SE, Thomas JB. 1992. Apterous is a *Drosophila* LIM domain gene required for the development of a subset of embryonic muscles. Neuron 9(3): 549-561. https://doi.org/10.1016/0896-6273(92)90192-G.

Brand AH, Perrimon N. 1993. Targeted gene expression as a means of altering cell fates and generating dominant phenotypes. Development 118:401–415

Braverman N, Dodt G, Gould SJ, Valle D. 1998. An isoform of Pex5p, the human PTS1 receptor, is required for the import of PTS2 proteins into peroxisomes. Hum Mol Genet 7(8):1195.1205.

Braverman N, Steel G, Obie C, Moser A, Moser H, Gould SJ, Valle D. 1997. Human *PEX7* encodes the peroxisomal PTS2 receptor and is responsible for rhizomelic chondrodysplasia punctata. Nat Genet 15:369-76.

Braverman NE, Moser AB, Steinberg SJ. 2001, updated 2012. Rhizomelic Chondrodysplasia Punctata Type 1. GeneReviews® [Internet]. Seattle (WA): University of Washington, Seattle.

Breidenbach RW, Beevers H. 1967. Association of the glyoxylate cycle enzymes in a novel subcellular particle from castor bean endosperm. Biochem Bioph Res Co 27(4):462-9.

Brocard C, Hartig A. 2006. Peroxisome targeting signal 1: is it really a simple tripeptide? Biochim Biophys Acta 1763(12):1565-73.

Bu Y, Shi L, Yu D, Liang Z, Li W. 2019. CDCA8 is a key mediator of estrogen-stimulated cell proliferation in breast cancer cells. Gene 703:1-6. doi:10.1016/j.gene.2019.04.006.

Bülow MH, Wingen C, Senyilmaz D, (...), Sellin J. 2017. Unbalanced lipolysis results in lipotoxicity and mitochondrial damage in peroxisome-deficient *Pex19* mutants. Mol Biol Cell 29:396-407. doi:10.1091/mbc.E17-08-0535.

Burdett K, Larkins LK, Das AK, Hajra AK. 1991. Peroxisomal localization of acyl-coenzyme A reductase (long chain alcohol forming) in guinea pig intestine mucosal cells. J Biol Chem 266(19):12201-06.

Campos-Ortega JA, Hartenstein V. 1985. *The embryonic development of* Drosophila melanogaster. Springer-Verlag: Berlin. ISBN (2nd edition): 978-3-662-22491-5.

Certel K, Anderson MG, Shrigley RJ, Johnson WA. 1996. Distinct variant DNA-binding sites determine cell-specific autoregulated expression of the Drosophila POU domain transcription factor drifter in midline glia or trachea. Mol Cell Biol 16(4):1813-23.

Chang CC, Warren DS, Sacksteder KA, Gould SJ. 1999. Pex12 interacts with Pex5 and Pex10 and acts downstream of receptor docking in peroxisomal matrix protein import. J Cell Biol 147(4):761-74. https://doi.org/10.1083/jcb.147.4.761.

Chang CJ, Goulding S, Adams RR, Earnshaw WC, Carmena M. 2006. *Drosophila* Incenp is required for cytokinesis and asymmetric cell division during development of the nervous system. J Cell Sci 119(6):1144-53.

Chao Y, Robak LA, Xia F, (...), Wangler MF. 2016. Missense variants in the middle domain of *DNM1L*in cases of infantile encephalopathy alter peroxisomes and mitochondria when assayed in *Drosophila*. Hum Mol Genet 25(9):1846-56.

Chen H, Liu Z, Huang X. 2009. *Drosophila* models of peroxisomal biogenesis disorder: Peroxins are required for spermatogenesis and very-long-chain fatty acid metabolism. Hum Mol Genet 19(3):494-505. doi:10.10.93/hmg/ddp518.

Chen M, Pan H, Sun L, (...), Chen Z. 2019. Structure and regulation of human Epithelial Cell Transforming 2 protein. Proc Natl Acad Sci USA 117(2):1027-1035. doi:10.1073/pnas.1913054117.

Cherbas L, Gong L. 2014. Cell lines. Methods 68(1):74–81.

Chiang, JYL. 2009. Bile acids: regulation of synthesis. J Lipid Res 50:1955-66.

Chung H, Wangler MF, Marcogliese PC, (...), Bellen HJ. 2020. Loss- or gain-of-function mutations in ACOX1 cause axonal loss via different mechanisms. Neuron 106(4):589-606. https://doi.org/10.1016/j.neuron.2020.02.021.

Ci C, Tang B, Lyu D, (...), Ding W. 2019. Overexpression of CDCA8 promotes the malignant progression of cutaneous melanoma and leads to poor prognosis. Int J Mol Med 43(1):404-412. doi:10.3892/ijmm.2018.3985.

Ciniawsky S, Grimm I, Saffian D, Girzalsky W, Erdmann R, Wendler P. 2015. Molecular snapshots of the Pex1/6 AAA+ complex in action. Nat Commun 6:7331. doi:10.1038/ncomms8331.

Connock M, Pover W. 1970. Catalase particles in the epithelial cells of the guinea-pig small intestine. Histochem J 2:371-80.

Cooke CA, Heck MM, Earnshaw WC. 1987. The inner centromere protein (INCENP) antigens: movement from inner centromere to midbody during mitosis. J Cell Biol 105:2053–2067.

CSH Protocols. 2006. Phosphate-buffered saline (PBS). Cold Spring Harb Protoc. doi:10.1101/pdb.rec8247.

CSH Protocols. 2011. *Drosophila* apple juice-agar plates. Cold Spring Harb Protoc. doi:10.1101/pdb.rec065672.

de Celis JF, Llimargas M, Casanova J. 1995. *ventral veinless*, the gene encoding the Cf1a transcription factor, links positional information and cell differentiation during embryonic and imaginal development in *Drosophila melanogaster*. Development 121(10):3405-16.

de Duve C, Baudhuin P. 1965. Peroxisomes (microbodies and related particles). Review. Physiol Rev 46(2):323-57.

de Duve C, Beaufay H, Jacques P, (...), de Coninck S. 1960. Intracellular localization of catalase and of some oxidases in rat liver. Biochim Biophys Acta 40:186-7.

De Rossi MC, Wetzler DE, Benseñor L, (...), Levi V. 2017. Mechanical coupling of microtubule-dependent motor teams during peroxisome transport in *Drosophila* S2 cells. Biochim Biophys Acta 1861:3178-89.

de Vet ECJM, Ijlst L, Oostheim W, Wanders RJA, van den Bosch H. 1998. Alkyl-dihydroxyacetonephosphate synthase. Fate in peroxisome biogenesis disorders and identification of the point mutation underlying a single enzyme deficiency. J Biol Chem 273(17):10296-301.

Dean JM, Lodhi IJ. 2017. Structural and functional roles of ether lipids. Protein Cell 9(2):196-206.

Dean SO, Rogers SL, Stuurman N, Vale RD, Spudich JA 2005. Distinct pathways control recruitment and maintenance of myosin II at the cleavage furrow during cytokinesis. Proc Natl Acad Sci USA 102(38):13473-8.

DiAngelo JR, Birnbaum MJ. 2009. Regulation of fat cell mass by insulin in *Drosophila melanogaster*. Mol Cell Biol 29(24):6341-6352. doi:10.1128/MCB.00675-09.

Di Cara F, Bülow MH, Simmonds AJ, Rachubinski RA. 2018. Dysfunctional peroxisomes compromise gut structure and host defense by increased cell death and Tor-dependent autophagy. Mol Biol Cell 29:2766-83.

Di Cara F, Rachubinski RA, Simmonds AJ. 2019. Distinct Roles for Peroxisomal Targeting Signal Receptors Pex5 and Pex7 in *Drosophila*. Genetics 211(1):141-149. doi:10.1534/genetics.118.301628.

Di Cara F, Sheshachalam A, Braverman NE, Rachubinski RA, Simmonds AJ. 2017. Peroxisome mediated metabolism is required for immune response to microbial infection. Immunity 47:93-106.

Dias AF, Rodrigues TA, Pedrosa AG, Barros-Barbosa A, Francisco T, Azevedo JE. 2017. The peroxisomal matrix protein translocon is a large cavity-forming protein assembly into which PEX5 protein enters to release its cargo. J Biol Chem 292:15287-15300. doi:10.1074/jbc.M117.805044.

Distel B, Erdmann R, Gould SJ, Blobel G, Crane DI, *et al*. 1996. A unified nomenclature for peroxisome biogenesis factors. J Cell Biol 135:1-3.

Drake P. 2012. The first genome-wide screen for animal Peroxins using RNAi in Drosophila melanogaster (sic). Thesis. Department of Molecular Biology and Biotechnology, University of Sheffield, UK.

Dreyer C, Krey K, Keller H, Givel F, Helftenbein G, Wahli W. 1992. Control of the peroxisomal β-oxidation pathway by a novel family of nuclear hormone receptors. Cell 68(5):879-87.

Dunphy WG, Kumagai A. 1991. The cdc25 protein contains an intrinsic phosphatase activity. Cell 67(1):189-96.

Echalier G, Ohanessian A. 1969. [Isolation, in tissue culture, of *Drosophila melangaster* (sic) cell lines]. C R Acad Hebd Seances Acad Sci D 268(13):1771-3.

Edgar BA, O'Farrell PH. 1989. Genetic control of cell division patterns in the *Drosophila* embryo. Cell 57(1):177-87.

Eggert US, Kiger AA, Richter C, Perlman ZE, Perrimon N, Mitchison TJ, Field CM. 2004. Parallel Chemical Genetic and Genome-Wide RNAi Screens Identify Cytokinesis Inhibitors and Targets. PLoS Biol 2(12):e379.

Emmanouilidis L, Gopalswamy M, Passon DM, Wilmanns M, Sattler M. 2015. Structural biology of the import pathways of peroxisomal matrix proteins. Biochim Biophys Acta 1863(5):804-13. doi:10.1016/j.bbamcr.2015.09.034.

Enamoto M, Siow C, Igaki T. 2018. *Drosophila* as a cancer model. Adv Exp Med Biol 1076:173-94. doi:10.1007/978-981-13-0529-0_10.

Erdmann R, Veenhuis M, Mertens D, Kunau WH. 1989. Isolation of peroxisome-deficient mutants of *Saccharomyces cerevisiae*. Proc Natl Acad Sci USA 86:5419-23.

Erdmann R, Wiebel FF, Flessau A, (...), Kunau WH. 1991. *PAS1*, a yeast gene required for peroxisome biogenesis, encodes a member of a novel family of putative ATPases. Cell 64:499-510.

Fabian L, Brill JA. 2012. *Drosophila* spermiogenesis. Big things come from little packages. Spermatogenesis 2(3): 197–212. doi:10.4161/spmg.21798.

Fagarasanu A, Fagarasanu M, Eitzen GA, Aitchison JD, Rachubinski RA. 2006. The peroxisomal membrane protein Inp2p is the peroxisome-specific receptor for the myosin V

motor Myo2p of *Saccharomyces cerevisiae*. Dev Cell 10(5):587-600. doi:10.1016/j.devcel.2006.04.012.

Fakieh MH, Drake PJM, Lacey J, Munck JM, Motley AM, Hettema EH. 2013. Intra-ER sorting of the peroxisomal membrane protein Pex3 relies on its luminal domain. Biol Open 2:829-37. doi:10.1242.bio.20134788.

Falany CN, Johnson MR, Barnes S, Diasio RB. 1994. Glycine and taurine conjugation of bile acids by a single enzyme. Molecular cloning and expression of human liver bile acid CoA:amino acid *N*-acyltransferase. J Biol Chem 269(30):19375-9.

Faust JE, Manisundaram A, Ivanova PT, (...), McNew JA. 2014. Peroxisomes are required for lipid metabolism and muscle function in *Drosophila melanogaster*. PLoS One 9(6):e100213. doi:10.1371/journal.pone.0100213.

Faust JE, Verma A, Peng C, McNew JA. 2012. An inventory of peroxisomal proteins and pathways in *Drosophila melanogaster*. Traffic 13:1378-92.

Ferdinandusse S, Deni S, Faust PL, Wanders RJA. 2009. Bile acids: the role of peroxisomes. J Lipid Res 50:2139-47. doi:10.1194.jlr.R900009-JLR200.

Foley E, O'Farrell PH. 2004. Functional dissection of an innate immune response by a genome wide RNAi screen. PLoS Biol 2(8):E203. doi:10.1371/journal.pbio.0020203.

Frank DJ, Martin SR, Gruender BNT, (...), Beckingham KM. 2006. Androcam is a tissue-specific light chain for myosin VI in the *Drosophila* testis. J Biol Chem 281(34):24728-36.

Fransen M, Nordgren M, Wang B, Apanasets O. 2011. Role of peroxisomes in ROS/RNS metabolism: Implications for human disease. Biochim Biophys Acta 1822:1363-73.

Fujiki Y, Rachubinski RA, Lazarow PB. 1984. Synthesis of a major rat integral membrane polypeptide of rat liver peroxisomes on free polysomes. Proc Natl Acad Sci USA 81:7127-31.

Fujiki Y. 2016. Peroxisome biogenesis and human peroxisome-deficiency disorders. Proc Jpn Acad Ser B 92(10):463-477.

Gabaldón T. 2010. Review: peroxisome diversity and evolution. Philos Trans R Soc Lond B Biol Sci 365(1541): 765–773. doi:10.1098/rstb.2009.0240.

Gandre-Babbe S, van der Bliek AM. 2008. The novel tail-anchored membrane protein Mff controls mitochondrial and peroxisomal fission in mammalian cells. Mol Biol Cell 19:2402 12.

Gautama NK, Verma P, Tapadia MG. 2017. *Drosophila* Malpighian tubules: a model for understanding kidney development, function, and disease. Results Probl Cell Differ 60:3-25. doi:10.1007/978-3-319-51436-9_1.

Geer LY, Marchler-Bauer A, Geer RC, (...), Bryant SH. 2010. The NCBI BioSystems database. Nucleic Acids Res 38(Database issue):D492-6. doi:10.1093/nar/gkp858.

Geisbrecht BV, Collins CS, Reuber BE, Gould SJ. 1998. Disruption of a PEX1-PEX6 interaction is the most common cause of the neurologic disorders Zellweger syndrome, neonatal adrenoleukodystrophy, and infantile Refsum disease. Proc Natl Acad Sci USA 95:8630-5.

Gershony O, Pe'er T, Noach-Hirsch M, Elia N, Tzur A. 2014. Cytokinetic abscission is an acute G1 event. Cell Cycle 13(21):3436-41.

Ghys K, Fransen M, Mannaerts GP, van Veldhoven PP. 2002. Functional studies on human Pex7p: subcellular localization and interaction with proteins containing a peroxisome-targeting signal type 2 and other peroxins (sic). Biochem J 1:(365, Pt 1):41-50. doi:10.1042/BJ20011432.

Giet R, Glover DM. 2001. Drosophila aurora B kinase is required for histone H3 phosphorylation and condensin recruitment during chromosome condensation and to organize the central spindle during cytokinesis. J Cell Biol 152(4):669-81.

Giordiano FJ. 2005. Oxygen, oxidative stress, hypoxia, and heart failure. J Clin Invest 115:500-508.

Goldfischer S, Moore CL, Johnson AB, (...), Gartner LM. 1973. Peroxisomal and mitochondrial defects in the cerebro-hepato-renal syndrome. Science 182:62-4.

Goldfischer SL, Collins J, Rapin I, *et al*. 1986. Pseudo-Zellweger syndrome: deficiencies in several peroxisomal oxidative activities. J Pediatr 108:25-32.

Gonzalez NH, Felsner G, Schramm FD, Klingl A, Maier UG, Bolte K. 2011. A single peroxisomal targeting signal mediates matrix protein import in diatoms. PLoS One 6(9):e25316. doi:10.1371/journal.pone.0025316.

González-Loyola A, Fernández-Miranda G, Trakala M, (...), Malumbres M. 2015. Aurora B overexpression causes aneuploidy and $p21^{Cip1}$ repression during tumor development. Mol Cell Biol 35(20):3566–3578. doi:10.1128/MCB.01286-14.

Gordon JA, Figard PH, Spector AA. 1990. Hydroxyeicosatetraenoic acid metabolism in cultured human skin fibroblasts. Evidence for peroxisomal β-oxidation. J Clin Invest 85:1173-81.

Gould SJ, Kalish JE, Morrell JC, Bjorkman J, Urquhart AJ, Crane DI. 1996. Pex13p is an SH3 protein of the peroxisome membrane and a docking factor for the predominantly cytosolic PTS1 receptor. J Cell Biol 135(1):85-95.

Gould SJ, Keller G-A, Scheider M, (...), Subramani S. 1990. Peroxisomal protein import is conserved between yeast, plants, insects and mammals. EMBO J 9(1):85-90.

Gould SJ, Keller GA, Subramani S. 1988. Identification of peroxisomal targeting signals located at the carboxy terminus of four peroxisomal proteins. J Cell Biol 107:897-905.

Gratz SJ, Rubinstein CD, Harrison MM, Wildonger J, Connor-Giles KM. 2015. CRISPR-Cas9 genome editing in *Drosophila*. Curr Protoc Mol Biol 111:311-20. doi:10.1002/0471142727.mb3102s111.

Graveley BR, Brooks AN, Carlson JW, Duff MO, (...), Oliver B, Celniker SE. 2011. The developmental transcriptome of *Drosophila melanogaster*. Nature 471(7339):473-479.

Graves HK, Jangam S, Tan KL, (...), Wangler MF. 2020. A genetic screen for genes that impact peroxisomes in *Drosophila* identifies candidate genes for human disease. G3 (Bethesda) 10:69-77. https://doi.org/10.1534/g3119.400803.

Greer ER, Chao AT, Bejsovec A. 2013. Pebble/ECT2 RhoGEF negatively regulates the Wingless/Wnt signaling pathway. Development 140(24):4937-46.

Gregory SL, Shandala T, O'Keefe L, Jones L, Murray MJ, Saint RB. 2007. A *Drosophila* overexpression screen for modifiers of Rho signalling in cytokinesis. Fly 1(1):13-22. doi:10.4161/fly.3806.

Groth AC, Fish M, Nusse R, Calos MP. 2004. Construction of transgenic *Drosophila* by using the site-specific integrase from phage phiC31. Genetics 166:1775–1782.

Hales KG, Korey CA, Larracuente AM, Roberts DM. 2015. Genetics on the fly: a primer on the *Drosophila* model system. Genetics 201:815-42.

Hanson KK, Kelley AC, Bienz M. 2005. Loss of *Drosophila* borealin causes polyploidy, delayed apoptosis and abnormal tissue development. Development 132(21):4777-87.

Hanukoglu I, Rapoport R, Weiner L, Sklan D. 1993. Electron leakage from the mitochondrial NADPH-adrenodoxin reductase-adrenodoxin-P450scc (cholesterol side chain cleavage) system. Arch Biochem Biophys 305(2):489-98.

Hartenstein V. 1993. *Atlas of Drosophila Development*. Cold Spring Harbor Laboratory Press. https://www.sdbonline.org/sites/fly/atlas/00atlas.htm.

Heiland I, Erdmann R. 2005. Biogenesis of peroxisomes. Topogenesis of the peroxisomal membrane and matrix proteins. FEBS J 272:2362-72.

Helaakoski T, Vuori K, Myllylä R, Kivirikko KI, Pihlajaniemi T. 1989. Molecular cloning of the alpha-subunit of human prolyl 4-hydroxylase: the complete cDNA-derived amino acid sequence and evidence for alternative splicing of RNA transcripts. Proc Natl Acad Sci USA 86(12):4392-6.

Herr A, McKenzie L, Suryadinata R, (...), Richardson HE. 2010. Geminin and Brahma act antagonistically to regulate EGFR-Ras-MAPK signaling in *Drosophila*. Dev Biol 344(1):36-51.

Hillebrand M, Gersting SW, Lotz-Havla AS, (...), Gärtner J. 2012. Identification of a new fatty acid synthesis-transport machinery at the peroxisomal membrane. J Biol Chem 287(1):210-21.

Hirabayashi S. 2016. The interplay between obesity and cancer: a fly view. Dis Mod Mech 9: 917-26. doi:10.1242/dmm.025320.

Hoefler G, Hoefler S, Watkins PA, (...), Moser HW. 1987. Biochemical abnormalities in rhizomelic chondrodysplasia punctata. J Pediatr 112(5):726-33.

Hoepfner D, Schildknegt D, Braakman I, Philippsen P, Tabak HF. 2005. Contribution of the endoplasmic reticulum to peroxisome formation. Cell 122(1): 85-95. doi:10.1016/j.cell.2005.04.025.

Höhfeld H, Veenhuis M, Kunau WH. 1991. PAS3, a *Saccharomyces cerevisiae* gene encoding a peroxisomal integral mem brane protein essential for peroxisome biogenesis. J Cell Biol 114(6):1167-78.

Honsho M, Asaoku S, Fukumoto K, Fujiki Y. 2013. Topogenesis and homeostasis of fatty acyl-CoA reductase 1. J Biol Chem 288(48):34588-98. doi:10.1074/jbc.M113.498345.

Houten SM, Wanders RJ. 2010. A general introduction to the biochemistry of mitochondrial fatty acid β-oxidation. J Inh Metab Dis 33(5):469–77.

Hruban Z, Swift H. 1964. Uricase: localization in hepatic microbodies. Science 146:1316-18.

Hu Y, Sopko R, Foos M, (...), Mohr SE. 2013. FlyPrimerBank: an online database for Drosophila melanogaster gene expression analysis and knockdown evaluation of RNAi reagents. G3 (Bethesda) 3(9):1607 16. doi:10.1534/g3.113.007021.

Huang Y, Huang S, Lam SM, Liu Z, Shui G, Zhang YQ. 2016. Acsl, the *Drosophila* ortholog of intellectual-disability-related ACSL4, inhibits synaptic growth by altered lipids. J Cell Sci 129:4034-45. doi:10.1242/jcs.195032.

Hughes SC, Saulier-Le Drean B, Livne-Bar I, Krause HM. 1996. Fluorescence in situ hybridization in whole-mount *Drosophila* embryos. Biotechniques 20(5):748-50. doi:10.2144/96205bm01.

Hutton D, Stumpf PK. 1969. Fat metabolism in higher plants XXXVII. Characterization of the β-oxidation systems from maturing and germinating castor bean seeds. Plant Physiol 44:508-16.

Imanaka T, Small GM, Lazarow PB. 1987. Translocation of Acyl-CoA oxidase into peroxisomes requires ATP hydrolysis but not a membrane potential. J Cell Bio 105(6):2915-22.

Inaba M, Yuan H, Yamashita YM. 2011. String (Cdc25) regulates stem cell maintenance, proliferation and aging in *Drosophila* testis. Development 138:5079-86. doi:10.1242/dev.072579.

Inbal A, Levanon D, Salzberg A. 2003. Multiple roles for u-turn/ventral veinless in the development of *Drosophila* PNS. Development 130(11):2467-78.

Inoue H, Nojima H, Okayama H. 1990. High efficiency transformation of *Escherichia coli* with plasmids. Gene 96:23-8.

Irving MD, Chitty LS, Mansour S, Hall CM. 2008. Chondrodysplasia punctata: a clinical diagnostic and radiological review. Clin Dysmorphol 17(4):229-41. doi:10.1097/MCD.0b013e3282fdcc70.

Ishii H, Fukumori N, Horie S, Suga T. 1980. Effects of fat content in the diet on hepatic peroxisomes of the rat. Bioch Biophys Acta 617:1-11.

Jan YN, Ghysen A, Christoph I, Barbel S, Jan LY. 1985. Formation of neuronal pathways in the imaginal discs of *Drosophila melanogaster*. J Neurosci 5(9):2453-64.

Jiang LL, Kurosawa T, Sato M, Suzuki Y, Hashimoto T. 1997. Physiological role of D-3-hydroxyacyl-CoA dehydratase/D-3-hydroxyacyl-CoA dehydrogenase bifunctional protein. J Biochem 121:506-13.

Jo SJ, Park J, Kim A, (...), Cho D. 2019. Loss of HSPA9 induces peroxisomal degradation by increasing autophagy. Autophagy. doi:10.1080/15548627.2020. 1712812.

Johnson SA, Milner MJ. 1987. The final stages of wing development in *Drosophila melanogaster*. Tissue Cell 19:505-13.

Joshi MK, Moran S, Beckingham KM, MacKenzie KR. 2012. Structure of androcam supports specialized interactions with myosin VI. Proc Natl Acad Sci USA 109(33):13290-5. doi:10.1073/pnas.1209730109.

Junell A, Uvell H, Davis MM, (...), Engström Y. 2010. The POU transcription factor Drifter/Ventral veinless regulates expression of *Drosophila* immune defense genes. Mol Cell Biol 30(14):3672-84.

Karamitros D, Kotantaki P, Lygerou Z, (...), Taraviras S. 2010. Differential Geminin requirement for proliferation of thymocytes and mature T cells. J Immunol 184(5):2432-2441. https://doi.org/10.4049/jimmunol.0901983.

Karess RE, Chang XJ, Edwards KA, Kulkarni SJ, Aguilera I, Kiehart DP. 1991. The regulatory light chain of nonmuscle myosin is encoded by spaghetti-squash, a gene required for cytokinesis in *Drosophila*. Cell 65(7):1177-89.

Karnik SK, Trelease RN. 2005. Arabidopsis Peroxin 16 coexists at steady state in peroxisomes and endoplasmic reticulum. Plant Physiol 138:1967-81.

Kim PK, Mullen RT, Schumann U, Lippincott-Schwartz J. 2006. The origin and maintenance of mammalian peroxisomes involves a de novo PEX16-dependent pathway from the ER. J Cell Biol 173:521-32.

Kina H, Yoshitani T, Hanyu-Nakamura K, Nakamura A. 2019. Rapid and efficient generation of GFP-knocked-in *Drosophila* by the CRISPR-Cas9-mediated genome editing. Dev Growth Differ 61(4):265-275. doi:10.1111/dgd.12607.

Klein AM, Mazutis L, Tallapragada N, (...), Kirschner MW. 2015. Droplet barcoding for single cell transcriptomics applied to embryonic stem cells. Cell 161(5):1187-1201. doi:10.1016/j.cell.2015.04.044.

Klingensmith J, Nusse R. 1994. Signaling by wingless in *Drosophila*. Dev Biol 166(2):396-414.

Knoblach B, Rachubinski RA. 2015. Sharing the cell's bounty – organelle inheritance in yeast. Commentary. J Cell Sci 128:621-630. doi:10.1242/jcs.151423.

Koch J, Pranjic K, Huber A, (...), Brocard C. 2010. PEX11 family members are membrane elongation factors that coordinate peroxisome proliferation and maintenance. J Cell Sci 123:3389-3400. doi:10.1242/jcs.064907.

Krakow D, Williams J 3rd, Poehl M, Rimoin DL, Platt LD. 2003. Use of three-dimensional ultrasound imaging in the diagnosis of prenatal-onset skeletal dysplasias. Ultrasound Obstet Gynecol 21(5):467-72.

Krisans SK, Thompson SL, Pena LA, Kok E, Javitt NB. 1985. Bile acid synthesis in rat liver peroxisomes: metabolism of 26-hydroxycholesterol to 3β-hydroxy-5-cholenoic acid. J Lipid Res 26:1324-32.

Krupp JJ, Levine JD. 2010. Dissection of oenocytes from adult *Drosophila melanogaster*. J Vis Exp 41:2242. doi:10.3791/2242.

Kuff EL, Schneider WC. 1954. Intracellular distribution of enzymes. XII. Biochemical heterogeneity of mitochondria. J Biol Chem 206:677.

Kulić IM, Brown AEX, Kim H, (...), Gelfand VI. 2008. The role of microtubule movement in bidirectional organelle transport. Proc Natl Acad Sci USA 105(29):10011-6.

Kunze M, Malkani N, Maurer-Stroh S, Wiesinger C, Schmid JA, Berger J. 2015. Mechanistic insights into PTS2-mediated peroxisomal protein import: the co-receptor PEX5L drastically increases the interaction strength between the cargo protein and the receptor PEX7. J Biol Chem 290:4928-40. doi:10.1074/jbc.M114.601575.

Kural C, Kim H, Syed S, Goshima G, Gelfand VI, Selvin PR. 2005. Kinesin and Dynein move a peroxisome in vivo: a tug-of-war or coordinated movement? Science 308:1469-72.

Lacey J. 2015. Characterisation of a novel Peroxin in *Drosophila melanogaster.* Thesis. Department of Molecular Biology and Biotechnology, University of Sheffield, UK.

Lawarow PB, Fujiki Y. 1985. Biogenesis of peroxisomes. Annu Rev Cell Biol 1:489-530.

Lazarow PB, Black V, Shio H, (...), Dancis J. 1985. Zellweger syndrome: biochemical and morphological studies on two patients treated with clofibrate. Pediatr Res 19(12):1356-64.

Lazarow PB, de Duve C. 1976. A fatty acyl-CoA oxidizing system in rat liver peroxisomes; enhancement by clofibrate, a hypolipidemic drug. Proc Natl Acad Sci USA 73(6):2043-6.

Lazarow PB, Fujiki Y, Small GM, Watkins P, Moser H. 1986. Presence of the peroxisomal 22-kDa integral membrane protein in the liver of a person lacking recognizable peroxisomes (Zellweger syndrome). Proc Natl Acad Sci USA 83:9193-6.

Lazarow PB. 1978. Rat liver peroxisomes catalyze fatty acid β oxidation. J Biol Chem 253(5):1522-8.

Lazarow PB. 2003. Peroxisome biogenesis: advances and conundrums. Curr Opin Cell Biol 15:489-97.

Lécuyer E, Parthasarathy N, Krause HM. 2008. Fluorescent in situ hybridization protocols in Drosophila embryos and tissues. Methods Mol Biol 420:289-302. doi:10.1007/978-1-59745-583-1_18.

Lee T, Luo L. 2001. Mosaic analysis with a repressible cell marker (MARCM) for *Drosophila* neural development. Trends Neurosci 24(5):251-4. doi:10.1016/s0166-2236(00)01791-4. Erratum in Trends Neurosci 2001, 24(7):385.

Leighton F, Poole B, Beaufay H, (...), de Duve C. 1968. The large-scale separation of peroxisomes, mitochondria, and lysosomes from the livers of rats injected with Triton WR-1339. J Cell Biol 37:482-513.

Leighton F, Poole B, Lazarow PB, de Duve C. 1969. The synthesis and turnover of rat liver peroxisomes. I. Fractionation of peroxisome proteins. J Cell Biol 41:521-35.

Leptin M. 1999. Gastrulation in *Drosophila*: the logic and the cellular mechanisms. EMBO J 18:3187-92. https://doi.org/10.1093/emboj/18.12.3187.

Lewin TM, van Horn CG, Krisans SK, Coleman RA. 2002. Rat liver acyl-CoA synthetase 4 is a peripheral-membrane protein located in two distinct subcellular organelles, peroxisomes, and mitochondrial-associated membrane. Arch Biochem Biophys 404:263-70.

Li W, Cowley A, Uludag M, (...), Lopez R. 2015. The EMBL-EBI bioinformatics web and programmatic tools framework. Nucleic Acids Res 43(W1):W580-4. doi:10.1093/nar/gkv279.

Li X, Fang P, Choi ET, Wang H, Yang X. 2013. Targeting mitochondrial reactive oxygen species as novel therapy for inflammatory diseases and cancers. J Hematol Oncol 6:19. doi:10.1186/1756-8722-6-19.

Lim H, Wang W, Chen J, Ocorr K, Bodmer R. 2014. ROS regulate cardiac function via a distinct paracrine mechanism. Cell Rep 7:35-44. http://dx.doi.org/10.1016/j.celrep.2014.02.029.

Lin S, Ewen-Campen B, Ni X, Housden BE, Perrimon N. 2015. *In vivo* transcriptional activation using CRISPR/Cas9 in *Drosophila*. Genetics 201(2):433-42. doi:10.1534/genetics.115.181065.

Linderman JA, Chambers MC, Gupta AS, Schneider DS. 2012. Infection-related declines in chill coma recovery and negative geotaxis in Drosophila melanogaster. PLoS One 7(9):e41907. doi:10.1371/journal.pone.0041907.

Lindsley DL, Zimm GG. 1992. The Genome of *Drosophila melanogaster* (aka The Red Book). : viii + 1133pp. ISBN 9780124509900.

Livak KJ, Schmittgen TD. 2001. Analysis of relative gene expression data using real-time quantitative PCR and the 2(-Delta Delta C(T)) Method. Methods 25(4):402-8.

Lu AQ, Beckingham K. 2000. Androcam, a *Drosophila* calmodulin-related protein, is expressed specifically in the testis and decorates loop kl-3 of the Y chromosome. Mech Dev 94(1-2):171-81. doi:10.1016/S0925-4773(00)00262-8.

Lunstrum GP, Bachinger H, Fessler LI, Duncane KG, Nelson RE, Fessler JH. 1988. *Drosophila* basement membrane procollagen IV. I. Protein characterization and distribution. J Biol Chem 263(34):18318-27.

Madeira F, Park YM, Lee J, (...), Lopez R. 2019. The EMBL-EBI search and sequence analysis tools APIs in 2019. Nucleic Acids Res 47(W1):W636-W641. doi:10.1093/nar/gkz268.

Makki R, Cinnamon E, Gould AP. 2014. The development and function of oenocytes. Annu Rev Entymol 59:405-425. https://doi.org/10.1146/annurev-ento-011613-162056.

Manning A. 1962. A sperm factor affecting the receptivity *Drosophila melanogaster* females. Nature 194:252-3.

Marchler-Bauer A, Bo Y, Han L, (...), Bryant SH. 2017. CDD/SPARCLE: functional classification of proteins via subfamily domain architectures. Nucleic Acids Res 45(D1):D200-D203. doi:10.1093/nar/gkw1129.

Martin SR, Lu AQ, Xiao J, Kleinjung J, Beckingham K, Bayley PM. 1999. Conformational and metal-binding properties of androcam, a testis-specific, calmodulin-related protein from *Drosophila*. Protein Sci 8(11):2444-54.

Marzioch M, Erdmann R, Veenhuis M, Kunau W-H. 1994. PAS7 encodes a novel yeast member of the WD-40 protein family essential for import of 3-oxoacyl-CoA thiolase, a PTS2-containing protein, into peroxisomes. EMBO J 13(20):4908-18.

Mast F, Li J, Virk MK, Hughes SC, Simmonds AJ, Rachubinski RA. 2011. A *Drosophila* model for the Zellweger spectrum of peroxisome biogenesis disorders. Dis Mod Mech 4:659-72. doi:10.1242/dmm.007419.

Mathieu J, Cauvin C, Moch C, (...), Huynh JR. 2013. Aurora B and cyclin B have opposite effects on the timing of cytokinesis abscission in *Drosophila* germ cells and in vertebrate somatic cells. Dev Cell 26(3):250-65.

Mauvezin C, Ayala C, Braden CR, Kim J, Neufeld TP. 2014. Assays to monitor autophagy in *Drosophila*. Methods 68(1):134-9. doi:10.1016/j.ymeth.2014.03.014.

Mears JA, Lackner LL, Fang S, Ingerman E, Nunnari J, Hinshaw JE. 2011. Conformational changes in Dnm1 support a contractile mechanism for mitochondrial fission. Nat Struct Mol Biol 18:20-6. doi:10.1038/nsmb.1949.

Mehtälä ML, Haataja TJK, Blanchet CE, Hiltunen JK, Svergun DI, Glumoff T. 2013. Quaternary structure of human, *Drosophila melanogaster* and *Caenorhabditis elegans* MFE-2 in solution from synchrotron small-angle X-ray scattering. FEBS Letters 587:305-10.

Meinecke M, Cizmowski C, Schliebs W, Krüger V, Beck S, Wagner R, Erdmann R. 2010. The peroxisomal importomer constitutes a large and highly dynamic pore. Nat Cell Biol 12(3):273-7. doi:10.1038/ncb2027.

Mihaylov IS, Kondo T, Jones L, (...), Zhang H. 2002. Control of DNA replication and chromosome ploidy by geminin and cyclin a. Mol Cell Biol 22(6):1868-80.

Mindell D P. 2013. The Tree of Life: Metaphor, Model, and Heuristic Device. Syst Biol 62(3):479-89. https://doi.org/10.1093/sysbio/sys115.

Miura S, Kasuya-Arai I, Hitoshi Mori, (...), Fujiki Y. 1992. Carboxy-terminal consensus Ser-Lys-Leu-related tripeptide of peroxisomal proteins functions *in vitro* as a minimal peroxisome-targeting signal. J Biol Chem 267(20):14405-11.

Miyata N, Hosoi K, Mukai S, Fujiki Y. 2009. In vitro import of peroxisome-targeting signal type 2 (PTS2) receptor Pex7p into peroxisomes. Biochim Biophys Acta 1793(5):860-70. doi:10.1016/j.bbamcr.2009.02.007.

Miyazawa S, Osumi T, Hashimoto T, Ohno K, Miura S, Fujiki Y. 1989. Peroxisome targeting signal of rat liver Acyl-Coenzyme A oxidase resides at the carboxy terminus. Mol Cell Biol 9:83-91.

Mockett RJ, Bayne AV, Kwong LK, Orr WC, Sohal RS. 2003. Ectopic expression of catalase in *Drosophila* mitochondria increases stress resistance but not longevity. Free Radic Biol Med 34(2):207-17. doi:10.1016/s0891-5849(02)01190-5.

Moffit JS, Aleksunes LM, Maher JM, Scheffer GL, Klaasen CD, Manautou JE. 2006. Induction of hepatic transporters multidrug resistance-associated proteins (Mrp) 3 and 4 by clofibrate is regulated by peroxisome proliferator-activated receptor alpha. J Pharmacol Exp Ther 317(2):537-45. doi:10.1124/jpet.105.093765.

Molinari C, Kleman J-P, Jiang W, Schoehn G, Hunter T, Margolis RL. 2002. PRC1 is a microtubule binding and bundling protein essential to maintain the mitotic spindle midzone. J Cell Biol 157(7): 1175–86. doi:10.1083/jcb.200111052.

Morgan TH, Bridges CB. 1916. Sex-linked inheritance in *Drosophila*. Carnegie Institution of Washington: Washington, DC, USA.

Morgan TH. 1940. Biographical memoir of Calvin Blackman Bridges. Proc Natl Acad Sci USA 22.

Moser AE, Singh I, Brown FR, (...), Moser HW. 1984. The cerebro-hepatorenal (Zellweger) syndrome. Increased levels and impaired degradation of very-long-chain fatty acids and their use in prenatal diagnosis. N Engl J Med 310(18):1141-6.

Motley AM, Galvin PC, Ekal L, Nuttall JM, Hettema EH. 2015. Reevaluation of the role of Pex1 and dynamin-related proteins in peroxisome membrane biogenesis. J Cell Biol 211(5):1041 56. doi:10.1083/jcb.201412066.

Motley AM, Hettema EH, Ketting R, Plasterk R, Tabak HF. 2000. *Caenorhabditis elegans* has a single pathway to target matrix proteins to peroxisomes. EMBO Rep 1(1):40-6.

Motley AM, Hettema EH. 2007. Yeast peroxisomes multiply by growth and division. J Cell Biol 178(3):399-410.

Mozer BA, Easwarachandran K. 1999. Pattern formation in the absence of cell proliferation: tissue-specific regulation of cell cycle progression by string (stg) during *Drosophila* eye development. Dev Biol 213(1):54-69.

Mu Y, Maharjan Y, Dutta RK, (...), Park R. 2020. Dimethyloxaloylglycine induces pexophagy in a HIF-2α dependent manner involving autophagy receptor p62. Biochem Biophys Res Comm 525(1):46-52. https://doi.org/10.1016/j.bbrc.2020.02.051.

Mukai S, Ghaedi K, Fujiki Y. 2002. Intracellular localization, function, and dysfunction of the peroxisome-targeting signal type 2 receptor, Pex7p, in mammalian cells. J Biol Chem 277(11):9548-61.

Mullen RT, Lisenbee CS, Miernyk JA, Trelease RN. 1999. Peroxisomal membrane ascorbate peroxidase is sorted to a membranous network that resembles a subdomain of the endoplasmic reticulum. The Plant Cell 11:2167-85.

Muller HJ. 1928. The production of mutations by X-rays. Proc Natl Acad Sci USA 14:714–726.

Müller M, Hogg JF. 1967. Fed Proc Amer Soc Exp Biol 26(2):284. Original article not found; referenced in Breidenbach and Beevers, 1967.

Müller M, Hogg JF, de Duve C. 1968. Distribution of tricarboxylic acid cycle enzymes and glyoxylate cycle enzymes between mitochondria and peroxisomes in *Tetrahymena pyriformis*. J Biol Chem 243(20):5385-95.

Nagarkar-Jaiswal S, Lee PT, Campbell ME, (...), Bellen HJ. 2015. A library of MiMICs allows tagging of genes and reversible, spatial and temporal knockdown of proteins in Drosophila. eLife 4: e05338. doi:10.7554/eLife.05338.

Nair DM, Purdue PE, Lazarow PB. 2004. Pex7p translocates in and out of peroxisomes in *Saccharomyces cerevisiae*. J Cell Biol 176(4):599-604.

Nakayama M, Sato H, Okuda T, (...), Matsuno K. 2011. *Drosophila* carrying *Pex3* or *Pex16* mutations are models of Zellweger syndrome that reflect its symptoms associated with the absence of peroxisomes. PLoS One 6(8):e22984.

Nathan C, Ding A. 2010. SnapShot: reactive oxygen intermediates (ROI). Cell 140:951.

Niesel DW, Bewley GC, Miller SG, Armstrong FB, Lee CY. 1980. Purification and structural analysis of the soluble sn-glycerol-3-phosphate dehydrogenase isozymes in *Drosophila melanogaster*. J Biol Chem 255(9):4073-80.

Novikoff AB, Podber E, Ryan J, Noe E. 1952. Biochemical heterogeneity of the cytoplasmic particles isolated from rat liver homogenate. J Histochem and Cytochem 1:27.

Novikoff AB, Shin W-Y. 1964. The endoplasmatic (sic) reticulum in the Golgi zone and its relations to microbodies, Golgi apparatus and autophagic vacuoles in rat liver cells. J Mikros Oxford 3:187–206.

Novikoff PM, Novikoff AB. 1972. Peroxisomes in absorptive cells of mammalian small intestine. J Cell Biol 52:532-60.

Novokov D, Dieuaide-Noubhani M, Vermeesch JR, Fournier B, Mannaerts GP, van Veldhoven PP. 1997. The human peroxisomal multifunctional protein involved in bile acid synthesis:

activity measurement, deficiency in Zellweger syndrome and chromosome mapping. Bioch Biophys Acta 1360:229-40.

Nüsslein-Volhard C, Wieschaus E. 1980. Mutations affecting segment number and polarity in *Drosophila*. Nature 287:795–801.

O'Brien SJ, Macintyre RJ. 1972. The α-glycerophosphate in Drosophila melanogaster. II. Genetic aspects. Genetics 71(1):127-38.

Ofman R, Hettema EH, Hogenhout EM, Caruso U, Muijsers AO, Wanders RJA. 1998. Acyl-CoA:dihydroxyacetonephosphate acyltransferase: cloning of the human cDNA and resolution of the molecular basis in rhizomelic chondrodysplasia punctata type 2. Hum Mol Genet 7(5):847-53.

Okuhira K, Fitzgerald ML, Tamehiro N, (...), Nishikami Mogami T. 2010. Binding of PDZ-RhoGEF to ATP-binding cassette transporter A1 (ABCA1) induces cholesterol efflux through RhoA activation and prevention of transporter degradation. J Biol Chem 285:16369-77. doi:10.1074/jbc.M109.061424.

Okumoto K, Misono S, Miyata N, Matsumoto Y, Mukai S, Fujiki Y. 2011. Cysteine ubiquitination of PTS1 receptor Pex5p regulates Pex5p recycling. Traffic 12(8):1067-83. doi:10.1111/j.1600-0854.2011.01217.x.

Orr WC, Sohal RS. 1994. Extension of life-span by overexpression of superoxide dismutase and catalase in *Drosophila melanogaster*. Science 263:1128-30.

Palade GE, Siekevitz P. 1956. Liver microsomes. An integrated morphological and biochemical study. J Biophys Biochem Cytol 2(2): 171–200. doi:10.1083/jcb.2.2.171.

Pan D, Nakatsu T, Kato H. 2013. Crystal structure of peroxisomal targeting signal-2 bound to its receptor complex Pex7p-Pex21p. Nat Struct Mol Biol 20(8):987-93. doi:10.1038/nsmb.2618.

Parkes TL, Elia AJ, Dickinson D, (...), Boulianne GL. 1998. Extension of *Drosophila* lifespan by overexpression of human *SOD1*in motorneurons. Nat Genet 19:171-4.

Patel NH, Schafer B, Goodman CS, Holmgren R. 1989. The role of segment polarity genes during Drosophila neurogenesis. Genes Dev 3(6):890-904.

Pende M, Becker K, Wanis M, (...), Dodt H-U. 2018. High-resolution ultramicroscopy of the developing and adult nervous system in optically cleared *Drosophila melanogaster*. 2018. Nat Commun 9:4371. https://doi.org/10.1038/s41467-018-07192-z.

Pellicoro A, van den Heuvel FAJ, Geuken M, Moshage H, Jansen PLM, Faber KN. 2006. Human and rat bile acid-CoA:amino acid *N*-acyltransferase are liver-specific peroxisomal enzymes: implications for intracellular bile salt transport. Hepatology 45(2):340-8.

Peng Y, Weisman LS. 2008. The cyclin-dependent kinase, Cdk1, directly regulates vacuole inheritance. Dev Cell 15(3):478-85. doi:10.1016/j.devcel.2008.07.007.

Pfeiffer BD, Jenett A, Hammonds AS, Ngo TT, Misra S, *et al.* 2008. Tools for neuroanatomy and neurogenetics in *Drosophila*. Proc Natl Acad Sci USA 105:9715–9720.

Platta HW, El Magraoui F, Schlee D, Grunau S, Girzalsky W, Erdmann R. 2007. Ubiquitination of the peroxisomal import receptor Pex5p is required for its recycling. J Cell Biol 177(2):197-204.

Platta HW, Grunau S, Rosenkranz K, Girzalsky W, Erdmann R. 2004. Functional role of the AAA peroxins in dislocation of the cycling PTS1 receptor back to the cytosol. Nat Cell Biol 7(8):817-22. doi:10.1038/ncb1281.

Poodry CA, Schneiderman HA. 1970. The ultrastructure of the developing leg of *Drosophila melanogaster*. Roux Arch Dev Biol 166:1-44.

Powers SK, Jackson MJ. 2008. Exercise-induced oxidative stress: cellular mechanisms and impact on muscle force production. Physiol Rev 88:1243–1276.

Prelich G. 2012. Gene overexpression: uses, mechanisms and interpretation. Genetics 190(3):841–854. doi:10.1534/genetics.111.136911.

Prokopenko SN, Brumby A, O'Keefe L, Prior L, He Y, Saint R, Bellen HJ. 1999. A putative exchange factor for rho1 GTPase is required for initiation of cytokinesis in *Drosophila*. Genes Dev 13(17):2301-14.

Purdue PE, Yang X, Lazarow PB. 1998. Pex18p and Pex21p, a novel pair of related Peroxins essential for peroxisomal targeting by the PTS2 pathway. J Cell Biol 143(7):1859-69.

Purdue PE, Zhang JW, Skoneczny M, Lazarow PB. 1997. Rhizomelic chondrodysplasia punctata is caused by deficiency of human *PEX7*, a homologue of the yeast PTS2 receptor. Nat Genet 15:381-4.

Quinn LM, Herr A, McGarry TJ, Richardson H. 2001. The *Drosophila* Geminin homolog: roles for Geminin in limiting DNA replication, in anaphase and in neurogenesis. Genes Dev 15(20):2741-54.

Rachubinski RA, Fujiki Y, Mortensen RM, Lazarow PB. 1984. Acyl-CoA oxidase and hydratase-dehydrogenase, two enzymes of the peroxisomal β-oxidation system, are synthesized on free polysomes of clofibrate-treated rat liver. J Cell Biol 99:2241-46.

Radford SJ, Jang JK, McKim KS. 2012. The chromosomal passenger complex is required for meiotic acentrosomal spindle assembly and chromosome biorientation. Genetics 192(2):417-29.

Ramos-Lewis W, Page-McCaw A. 2019. Basement membrane mechanics shape development: lesson from the fly. Matrix Biol 75-76:72-81. doi:10.1016/j.matbio.2018.04.004.

Rand MD, Kearney AL, Dao J, Clason T. 2010. Permeabilization of Drosophila embryos for introduction of small molecules. Insect Biochem Mol Biol 40(11):792-804. doi:10.1016/j.ibmb.2010.07.007.

Rapp S, Saffrich R, Anton M, (...), Just WW. 1996. Microtubule based peroxisome movement. J Cell Sci 109:837-49.

Reddy JK, Azarnoff DL, Hignite CE. 1980. Hypolipidaemic hepatic peroxisome proliferators form a novel class of chemical carcinogens. Nature 283:397-8.

Reid G, Wielinga P, Zelcer N, (...), Borst P. 2003. The human multidrug resistance protein MRP4 functions as a prostaglandin efflux transporter and is inhibited by nonsteroidal anti-inflammatory drugs. Proc Natl Acad Sci USA 100(16):9244-9249. https://doi.org/10.1073/pnas.1033060100.

Reuber BE, Germain-Lee E, Collins CS, (...), Gould SJ. 1997. Mutations in *PEX1* are the most common cause of peroxisome biogenesis disorders. Nat Genet 17:445-8.

Reuter R, Leptin M. 1994. Interacting functions of snail, twist and huckebein during the early development of germ layers in *Drosophila*. Development 120(5):1137-50.

Reyes AC, Koudelka AP, Amyes TL, Richard JP. 2015. Enzyme architecture: optimization of transition state stabilization from a cation-phosphodianion pair. J Am Chem Soc 137(16):5312-5. doi:10.1021/jacs.5b02202.

Rhodin J. 1954. Correlation of ultrastructural organization and function in normal and experimentally changed proximal convoluted tubule cells of the mouse kidney. Thesis. Department of Anatomy, Karolinska Instituet, Stockholm, Sweden.

Rice P, Longden I, Bleasby A. 2000. EMBOSS: the European Molecular Biology Open Software Suite. Trends Genet (6):276-7.

Rizki TM, Rizki RM. 1980. Properties of the larval hemocytes of *Drosophila melanogaster*. Experientia 36:1223-6.

Robertson FW. 1963. The ecological genetics of growth in *Drosophila*. 6. The genetic correlation between the duration of the larval period and body size in relation to larval diet. Genet Res 4:74-92.

Rodrigues TA, Alencastre IS, Francisco T, (...), Azevedo JE. 2014. A PEX7-centered perspective on the peroxisomal targeting signal Type 2-mediated protein import pathway. Mol Cell Biol 34(15):2917–2928. doi:10.1128/MCB.01727-13.

Royou A, Sullivan W, Karess R. 2002. Cortical recruitment of nonmuscle myosin II in early syncytial *Drosophila* embryos: its role in nuclear axial expansion and its regulation by Cdc2 activity. J Cell Biol 158(1):127-37.

Sacksteder KA, Jones JM, South ST, Li X, Liu Y, Gould SJ. 2000. Pex19 binds multiple peroxisomal membrane proteins, is predominantly cytoplasmic, and is required for peroxisome membrane synthesis. J Cell Biol 148 (5):931.

Sang JH. 1949. The ecological determinants of population growth in a *Drosophila* culture. IV. The significance of successive batches of larvae. Physiol Zool 22:202-10.

Santos CX, Tanaka LY, Wosniak J, Laurindo FR. 2009. Mechanisms and implications of reactive oxygen species generation during the unfolded protein response: roles of endoplasmic reticulum oxidoreductases, mitochondrial electron transport, and NADPH oxidase. Antioxid Redox Signal 11:2409–2427.

Savitsky PA, Finkel T. 2002 Redox regulation of Cdc25C. J Biol Chem 277:20535-40. doi:10.1074/jbc.M201589200.

Schmied C, Tomancak P. 2016. Sample preparation and mounting of *Drosophila* embryos for multiview light sheet microscopy. Methods Mol Biol 1478:189-202. doi:10.1007/978-1-4939-6371-3_10.

Schneider I. 1972. Cell lines derived from late embryonic stages of *Drosophila melanogaster*. J Embryol Exp Morphol 27:353–365.

Schrader M, King SJ, Stroh TA, Schroer TA. 2000. Real time imaging reveals a peroxisomal reticulum in living cells. J Cell Sci 113:3663-71.

Schumacher S, Gryzik T, Tannebaum S, Müller HAJ. 2004. The RhoGEF Pebble is required for cell shape changes during cell migration triggered by the *Drosophila* FGF receptor Heartless. Development 131(11):2631-40.

Scott K, Sun Y, Beckingham K, Zuker CS. 1997. Calmodulin regulation of *Drosophila* light-activated channels and receptor function mediates termination of the light response *in vivo*. Cell 91(3):375-83. https://doi.org/10.1016/S0092-8674(00)80421-3.

Sellin J, Wingen C, Gosejacob D, (...), Bülow MH. 2018. Dietary rescue of lipotoxicity-induced mitochondrial damage in Peroxin19 mutants. PLoS Biol 16(6): e2004893. https://doi.org/10.1371/journal.pbio.2004893.

Semotok LJ, Westwood T, Goldman AL, Cooperstock RL, Lipshitz HD. 2008. Chapter 16. Measuring mRNA stability during early *Drosophila* embryogenesis. Methods Enzymol 448:299-334. https://doi.org/10.1016/S0076-6879(08)02616-5.

Shimozawa N, Suzuki Y, Orii T, Moser A, Moser HW, Wanders RJA. 1993. Am J Hum Genet 52:843-4.

Singh I, Lazo O, Contreras M, Stanley W, Hashimoto T. 1991. Rhizomelic chondrodysplasia punctata: biochemical studies of peroxisomes isolated from cultured skin fibroblasts. Arch Bioch Biophys 286(1):277-83.

Singh I, Moser AM, Moser HW, Kishimoto Y. 1984. Adrenoleukodystrophy: impaired oxidation of very long chain fatty acids in white blood cells, cultured skin fibroblasts, and amniocytes. Pediatr Res 18(3):286-90.

Singh R, Manivannan S, Krikken AM, (...), van der Klei IJ. 2019. *Hansenula polymorpha* Pex37 is a peroxisomal membrane protein required for organelle fission and segregation. FEBS J epub ahead of print (6 Nov 2019). doi:10.1111/febs.15123.

Smallhorn M, Murray MJ, Saint R. 2004. The epithelial-mesenchymal transition of the *Drosophila* mesoderm requires the Rho GTP exchange factor Pebble. Development 131(11):2641-51.

Sohal RS, Arnold L, Orr WC. 1990. Effect of age on Superoxide dismutase, Catalase, Glutathione reductase, inorganic peroxides, TBA-reactive material, GSH/GSSG, $NADPH/NADP^+$ and $NADH/NAD^+$ in *Drosophila melanogaster*. Mech Ageing Dev 56:223-35.

Song H, Liu L, Song Z, Ren Y, Li C, Huo J. 2018. P4HA3 is epigenetically activated by Slug in gastric cancer and its deregulation is associated with enhanced metastasis and poor survival. Technol Cancer Res Treat 17:1533033818796485. doi:10.1177/1533033818796485.

Spranger JW, Opitz JM, Bidder U. 1971. Heterogeneity of chondrodysplasia punctata. Hum Genet 11:190-212.

St Johnston, D. 2002. The art and design of genetic screens: *Drosophila melanogaster*. Nat Rev Genet 3:176-88.

St. Jules R, Setlik W, Kennard J, Holztman E. 1990. Peroxisomes in the head of *Drosophila melanogaster*. Exp Eye Res 51:607-17.

Stewart KD, Floyd GL, Mattox KR, Davis ME. 1972. Cytochemical demonstration of a single peroxisome in a filamentous green alga. J Cell Biol 54:431-4.

Summerer S, Hanano A, Utsumi S, Arand M, Schuber F, Blée E. 2002. Stereochemical features of the hydrolysis of 9,10-epoxystearic acid catalysed by plant and mammalian epoxide hydrolases. Biochem J 366:471–480.

Suzuki Y, Shimozawa N, Orii T, Igarashi N, Kono N, Hashimoto T. 1988. Molecular analysis of peroxisomal β-oxidation enzymes in infants with Zellweger syndrome and Zellweger-like syndrome: further heterogeneity of the peroxisomal disorder. Clinica Chimica Acta 172:65-76.

Swaminathan A, Pile LA. 2010. Regulation of cell proliferation and wing development by *Drosophila* SIN3 and String. Mech Develop 127(1-2):96-106. https://doi.org/10.1016/j.mod.2009.10.003.

Swinkels BW, Gould SJ, Bodnar AG, Rachubinski RA, Subrumani S. 1991. A novel, cleavable peroxisome targeting signal at the amino-terminus of the rat 3-ketoacyl-CoA thiolase. EMBO J 10(11):3255-62.

Tamura S, Matsumoto N, Takeba R, Fujiki Y. 2014. AAA peroxins and their recruiter Pex26p modulate the interactions of peroxins involved in peroxisomal protein import. J Biol Chem 289(35):24336-46. doi:10.1074/jbc.M114.588038.

Tamura S, Yasutake S, Matsumoto N, Fujiki Y. 2006. Dynamic and functional assembly of the AAA peroxins, Pex1p and Pex6p, and their membrane receptor Pex26p. J Biol Chem 281(38):27693-704.

Tan C, Stronach B, Perrimon N. 2003. Roles of myosin phosphatase during *Drosophila* development. Development 130:671-81. doi:10.1242/dev.00298.

Thomson JF and Moss EM. 1955. The intracellular distribution of a bound acid phosphatase of rat liver as studied by gradient centrifugation. Arch Biochem Biophys 61:456-460.

Tian Y, Morissey EE. 2012. Importance of myocyte-nonmyocyte interactions in cardiac development and disease. Circ Res 110:1023–1034.

Titorenko TI, Smith JL, Szilard RK, Rachubinski RA. 1998. Pex20p of the yeast *Yarrowia lipolytica* is required for the oligomerization of thiolase in the cytosol and for its targeting to the peroxisome. J Cell Biol 142(2):403-20.

Titorenko V, Rachubinski R. 1998. Mutants of the yeast *Yarrowia lipolytica* defective in protein exit from the endoplasmic reticulum are also defective in peroxisome biogenesis. Mol Cell Biol 18:2789-2803.

Tolbert NE, Oeser A, Kisaki T, Hageman RH, Yamazaki RK. 1968. Peroxisomes from spinach leaves containing enzymes related to glycolate metabolism. J Biol Chem 243(19):5179-84.

Tolbert NE, Oeser A, Yamazaki RK, Hageman RH, Kisaki T. 1969. A survey of plants for leaf peroxisomes. Plant Physiol 44(1):135-47.

Tolwinski NS. 2017. Introduction: *Drosophila* - A model system for developmental biology. J Dev Biol 5(9). doi:10.3390/jdb5030009.

Tootle TL, Spradling AC. 2008. *Drosophila* Pxt: a cyclooxygenase-like facilitator of follicle maturation. Development 135(5):839-47. doi:10.1242/dev.017590.

Tseng AK, Hariharan IK. 2002. An overexpression screen in *Drosophila* for genes that restrict growth or cell-cycle progression in the developing eye. Genetics 162(1):229-43.

Ui K, Ueda R, Miyake T. 1987. Cell lines from imaginal discs of *Drosophila melanogaster*. In Vitro Cell Dev Biol 23:707–711.

Urquhart AJ, Kennedy D, Gould SJ, Crane DI. 2000. Interaction of Pex5p, the type 1 peroxisome targeting signal receptor, with the peroxisomal membrane proteins Pex14p and Pex13p. J Biol Chem 275(6):4127-36.

van Impel A, Schumacher S, Draga M, Herz HM, Großhans J, Müller HA. 2009. Regulation of the Rac GTPase pathway by the multifunctional Rho GEF Pebble is essential for mesoderm migration in the *Drosophila* gastrula. Development 136(5):813-22.

van Veldhoven PP, Croes K, Asselberghs S, Herdewijn P, Mannaerts GP. 1996. Peroxisomal β-oxidation of 2-methyl-branched acyl-CoA esters: stereospecific recognition of the 2*S*-methyl compounds by trihydroxycoprostanoyl-CoA oxidase and pristanoyl-CoA oxidase. FEBS Letters 288:80-84.

Vasquez CG, Tworoger M, Martin AC. 2014. Dynamic myosin phosphorylation regulates contractile pulses and tissue integrity during epithelial morphogenesis. J Cell Biol 206(3):435-50.

Venken KJ, He Y, Hoskins RA, Bellen HJ. 2006. P[acman]: a BAC transgenic platform for targeted insertion of large DNA fragments in *D. melanogaster*. Science 314: 747–1751.

Venken KJ, Schulze KL, Haelterman NA, Pan H, He Y, *et al*. 2011. MiMIC: a highly versatile transposon insertion resource for engineering *Drosophila melanogaster* genes. Nat Methods 8:737–743.

Vernì F, Somma MP, Gunsalus KC, (...), Gatti M. 2004. Feo, the *Drosophila* homolog of PRC1, is required for central-spindle formation and cytokinesis. Curr Biol 14(17):1569-75.

Volk T, VijayRaghavan K. 1994. A central role for epidermal segment border cells in the induction of muscle patterning in the Drosophila embryo. Development 120(1):59-70.

Walter KM, Schönenberger MJ, Trötzmüller M, (...), KovacsWJ. 2014. Hif-2α promotes degradation of mammalian peroxisomes by selective autophagy. Cell Metabolism 20(5):882-97.

Walton PA, Hill PE, Subramani S. 1995. Import of stably-folded proteins into peroxisomes. Mol Biol Cell 6:675-83.

Wang H, Brust-Mascher I, Scholey JM. 2015. The microtubule cross-linker Feo controls the midzone stability, motor composition, and elongation of the anaphase B spindle in *Drosophila* embryos. Mol Biol Cell 26(8):1452-62.

Wangler MF, Chao Y, Bayat V, (...), Bellen HJ. 2017. Peroxisomal biogenesis is genetically and biochemically linked to carbohydrate metabolism in Drosophila and mouse. PLoS Genet 13(6):e1006825. https://doi.org/10.1371/journal.pgen.1006825.

Warren DS, Morell JC, Moser HW, Valle D, Gould SJ. 1998. Identification of *PEX10*, the gene defective in complementation group 7 of the peroxisome-biogenesis disorders. Am J Hum Genet 63:347-59.

Weigert A, von Knethen A, Fuhrmann D, Dehne N, Brüne B. 2018. Redox-signals and macrophage biology. Mol Aspects Med 63:70-87.

Wilk R, Murthy S, Yan H, Krause HM. 2010. In situ hybridization: fruit fly embryos and tissues. Current Protocols Essential Laboratory Techniques (2010) 9.3.1-24.

Wilmes AC, Klinke N, Rotstein B, Meyer H, Paululat A. 2018. Biosynthesis and assembly of the Collagen IV-like protein Pericardin in *Drosophila melanogaster*. Biology Open 7: bio030361. doi:10.1242/bio.030361.

Winter CG, Wang B, Ballew A, (...), Luo L. 2001. *Drosophila* Rho-associated Kinase (Drok) links Frizzled-mediated planar cell polarity signaling to the actin cytoskeleton. Cell 105(1):81-91. doi:10.1016/s0092-8674(01)00298-7.

Wojitas K, Slepecky N, von Kalm L, Sullivan D. 1997. Flight muscle function in *Drosophila* requires colocalization of glycolytic enzymes. Mol Biol Cell 8:1665-75.

Xue Z, Ren M, Wu M, Dai J, Rong YS, Gao G. 2014. Efficient gene knock-out and knock-in with transgenic Cas9 in *Drosophila*. G3 (Bethesda) 4(5): 925–929. doi:10.1534/g3.114.010496.

Zhang JW, Lazarow PB. 1995. *PEB1* (*PAS7*) in *Saccharomyces cerevisiae* encodes a hydrophilic, intra-peroxisomal protein that is a member of the WD repeat family and is essential for the import of thiolase into peroxisomes. J Cell Biol 129(1):65-80.

Zhou B, Yang L, Li S, (...), Han JJ. 2012. Midlife gene expressions identify modulators of aging through dietary interventions. Proc Natl Acad Sci USA 109(19):E1201-9. doi:10.1073/pnas.1119304109.

Zhu PP, Patterson A, Stadler J, Seeburg DP, Sheng M, Blackstone C. 2004. Intra- and intermolecular domain interactions of the C-terminal GTPase effector domain of the multimeric dynamin-like GTPase Drp1. J Biol Chem 279:35967-74. doi:10.1074/jbc. M404105200.

Zirin J, Hu Y, Liu L, (...), Perrimon N. 2020. Large-scale transgenic *Drosophila* resource collections for loss- and gain-of-function studies. Genetics 214:755-67. doi: https://doi.org/10.1534/genetics.119.302964.

Zoeller RA, Raetz CRH. 1986. Isolation of animal cell mutants deficient in plasmalogen biosynthesis and peroxisome assembly. Proc Natl Acad Sci USA 83:5170-4.